**UNIVERSITÀ DEGLI STUDI DI PAVIA**

**DOTTORATO IN SCIENZE CHIMICHE E FARMACEUTICHE**

**XXXII CICLO**

**Coordinatore: Chiar.mo Prof. Mauro Freccero**

# *PHYSICAL-CHEMICAL CHARACTERIZATION OF POLYSACCHARIDES AND THEIR INTERACTION WITH PROTEINS*


**Tutori**

**Chiar.mo Prof. Giuseppe Zanoni**

**Dott.ssa Sabrina Bertini**

**Tesi di Dottorato di**

**Giulia RISI**


**a.a. 2018- 2019**

# Contents

# List of abbreviations

| | |
|---|---|
| 2-O-SULFATED-L-IDURONIC ACID | IdoA2S |
| 6-SULFTATED-N-ACETYLATED α-D-GLUCOSAMINE | αDGlcNAc(6S) |
| ACETYLATED DOMAIN | NA |
| ACTIVATED PROTEIN C | APC |
| ACTIVE PRINCIPLE INGREDIENT | API |
| ADENINE | A |
| ANTITHROMBIN (III) | AT(III) |
| β-D-GALACTOSAMINE-N-ACETYLATE-4-SULFATE | GalNAc4S |
| BINDING SITES | N sites |
| BOVINE SPONGIFORM ENCEPHALOPATHY | BSE |
| CAPACITY OF BINDIG | ΔCp |
| CHRONIC VENOUS DISEASE | CVD |
| CO-FACTOR II | HCII |
| COEFFICIENT OF VARIATION | CV |
| CYTOSINE | C |
| DALTON | Da |
| DEFIBROTIDE | DFT |
| DERJAGUIN, VERWEY, LANDAU AND OVERBEEK THEORY | DVLO theory |
| DERMATAN SULFATE | DeS |
| DIFFUSION COEFFICIENT | D |
| DIRECT THROMBIN INHIBITORS | DTI |
| DISSOCIATION CONSTANT | Kd |
| DYNAMIC LIGHT SCATTERING | DLS |
| ENDOTHELIAL CELLS | EC |
| ENTHALPY | ΔH |
| ENTHROPY | ΔS |
| EQUILIBRIUM BINDING CONSTANT | Ka |
| EUROPEAN PHARMACOPOEIA | Ph. Eur. |
| EXTRACELLULAR MATRIX | ECM |
| FACTOR XA | fXa |
| FAST-MOVING HEPARIN | Fm-Hep |
| FOOD AND DRUGS ADMINISTRATION | FDA |
| FREE GIBB'S ENERGY | ΔG |
| GEL PERMEATION CHROMATOGRAPHY | GPC |
| GLUCURONIC ACID | GlcA |
| GLYCOSAMINOGLYCAN | GAG |
| GUANINE | G |
| HAEMATOPOIETIC STEM CELLS TRANSPLANTATION | HSCT |
| HANK'S BALANCED SALT SOLUTION | HBSS |
| HEPARIN | Hep |
| HEPARIN-INDUCED THROMBOCYTOPENIA | HIT |

| | |
|---|---|
| HIGH PERFORMANCE LIQUID CHROMATOGRAPHY | HPLC |
| HIGH PERFORMANCE SIZE EXCLUSION CHROMATOGRAPHY TRIPLE DETECTOR ARRAY | HP-SEC-TDA |
| HYDRODYNAMIC RADIUS | Rh |
| IDURONIC ACID | IdoA |
| IMMUNE COMPLEX | IC |
| IMMUNOGLOBULING | IgG |
| INTRINSIC VISCOSITY | [η] |
| ISOTHERMAL TITRATION CALORIMETRY | ITC |
| LIGHT SCATTERING | LS |
| LOW ANGLE LIGHT SCATTERING | LALS |
| LOW MOLECULAR WEIGHT HEPARIN | LMWH |
| MOLECULAR WEIGHT AT THE PEAK | Mp |
| MULTI-ANGLE LIGHT SCATTERING | MALS |
| N,3,6-SULFTATED α-D-GLUCOSAMINE | αDGlcNS(3S,6S) |
| N-ACETYL-D-GLUCOSAMINE | GlcNAc |
| N-SULFATED-D-GLUCOSAMINE | GlcNS |
| NUCLEAR MAGNETIC RESONANCE | NMR |
| NUMBER-AVERAGE MOLECULAR WEIGHT | Mn |
| OVER-SULFATED CHRONDROITIN SULFATE | OSCS |
| PARTIAL THROMBOPLASTIN TIME | aPTT |
| PHOTODIODE ARRAY DETECTOR | PDA |
| PHOTON CORRELATION SPECTROSCOPY | PCS |
| PLATELET FACTOR 4 | PF4 |
| POLYDISPERSIONE INDEX | Mw/Mn |
| PROTEIN C INHIBITOR | PCI |
| PROTEIN/DFT RATIO | PDR |
| PROTEIN/GAG RATIO | PGR |
| PROTEIN/HEPARIN RATIO | PHR |
| PROTHROMBIN TIME | PT |
| REACTIVE CENTER LOOP | RCL |
| REFERENCE STANDARD | RS |
| REFRACTIVE INDEX | RI |
| REFRACTIVE INDEX INCREMENT | dn/dc |
| RIGHT-ANGLE LIGHT SCATTERING | RALS |
| SIZE EXCLUSION CHROMATOGRAPHY | SEC |
| SMALL SIZE COMPLEX | SC |
| STOICHIOMETRY | n |
| SULFATED DOMANI | NS |
| SULFATION DEGREE | DS |
| SULODEXIDE | SLDX |
| THROMBIN TIME | TT |
| THYMINE | T |
| TISSUE FACTOR PATHWAY INHIBITOR | TFPI |

| | |
|---|---|
| TRIPLE DETECTOR ARRAY | TDA |
| ULTRALARGE COMPLEX | ULC |
| ULTRAVIOLET | UV |
| UNFRACTIONATED HEPARIN | UFH |
| UNITED STATES PHARMACOPOEIA | USP |
| VAN DER WAALS ATTRACTION | VA |
| VENO-OCCLUSIVE DISEASE | VOD |
| VENOUS THROMBOEMBOLIC DISORDER | VTE |
| VISCOMETER DIFFERENTIAL PRESSURE | DP |
| VISCOMETER INLET PRESSURE | IP |
| WEIGHT FRACTION | Wt. Fr. |
| WEIGHT-AVERAGE MOLECULAR WEIGHT | Mw |
| WORLD HEALTH ORGANIZATION | WHO |
| Z-AVERAGE MOLECULAR WEIGHT | Mz |
| ZETA POTENTIAL | Zp |

# 1. General background

## 1.1. Glycosaminoglycans (GAGs)

GAGs are a family linear polysaccharides consisting of repetitive disaccharide units composed by a hexosamine (D-glucosamine or D-galactosamine) and an uronic acid sugar (D-glucuronic acid, L-iduronic) or a D-galactose, linked by glycoside linkages[1]. On the basis of the amino sugar present in their chains, GAGs can be classified as glucosaminoglycans (heparin, heparan sulfate, hyaluronic acid and keratan sulfate) or galactosaminoglycans (chondroitin sulfate and dermatan sulfate).

Each GAG is characterized by the prevalent disaccharide repetitive unit, but each single chain generally contains differently sulfated or acetylated amino sugar or uronic acid. In, the GAGs family main and variable repetitive units are reported.

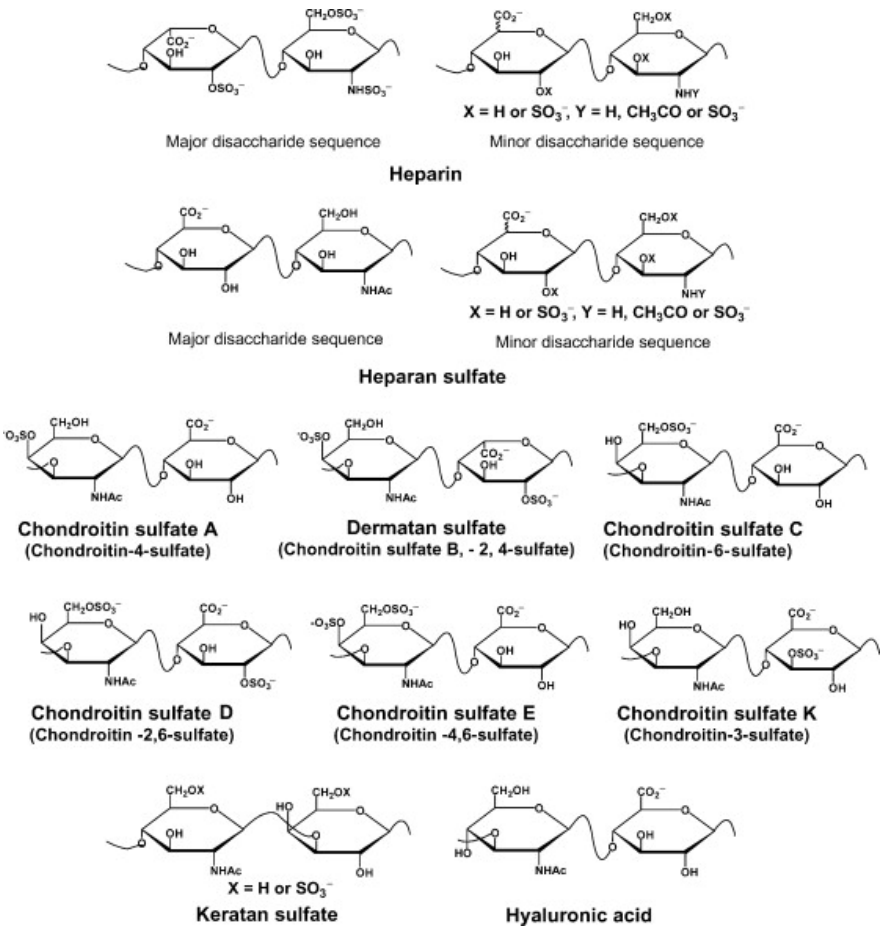


**Figure 1.1.1 GAGs repetitive units' structures.**

The structural heterogeneity of GAGs and their high negative charge density allow these compounds to easily interact with proteins, and in fact most of the biological and pharmacological activities of GAGs are mediated by their ability in binding proteins such as growth factors, enzymes, morphogens, cell adhesion proteins and cytokines[1].

## 1.2. Heparin: a highly sulfated polysaccharide

Heparin, first discovered by Jay McLean in 1916[2], is a member of the GAGs family, and it is one of the principal pharmaceutical agents used in the treatment and prevention of blood clots or thrombi, and consequently finds widespread application in surgery, in the treatment of heart attacks, in preventing of surface contact-induced clotting during blood dialysis and as coating material for a range of medical devices.

Pharmaceutical heparin is obtained almost exclusively from porcine intestinal mucosa, one pig gut yielding in the order of one heparin dose; although there is a predominant repeating unit and many similarities between batches, each heparin sample is composed of numerous polysaccharide chains that have distinct sequences and lengths. Despite this variability, porcine intestinal mucosa heparin remains a reliable and very widely used anticoagulant.

### 1.2.1. Heparin structure

Heparin has the highest negative charge density of any known biological macromolecule thanks to the high content of negatively charged sulphated and carboxylic groups. In Figure 1.2.1, a schematic representation of the structure of heparin is reported.

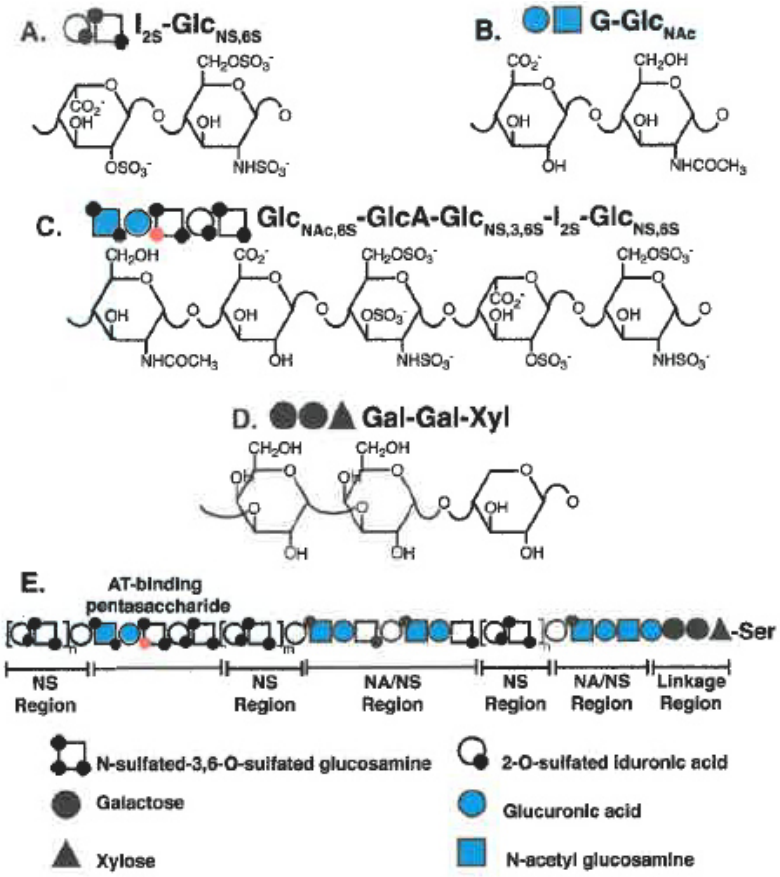


**Figure 1.2.1 The structure of heparin[3].**

Heparin share a basic chemical structure consisting of N-acetyl-D-glucosamine (GlcNAc) and glucuronic acid (GlcA) units, partly modified by epimerization of GlcA to iduronic acid (IdoA) and by sulphation at different positions of mainly GlcNAc and IdoA residues (N-sulphated-D-glucosamine, GlcNS and 2-O-sulphated a-L-iduronic acid, IdoA2S respectively, see Figure 1.2.1, panels A and B)[4]; these residues are assembled in two main disaccharide repetitive units, that are essentially assembled in order to form a prevalently sulphated domain (NS) and one prevalently acetylated (NA). Moreover, a mixed NA/NS domain is found (see Figure 1.2.1, panel E), obtaining more complex sequences, the most significant of which is a pentasaccharide sequence -GlcNAc,6S-G-GlcNS,3S,6S-I2S-ANS,6S- (AGA*IA, see Figure 1.2.1, panel C) that exhibit high affinity for the serpin Antithrombin (III) (AT(III)). The extension of this sequence can produce binding sites that have a greater affinity for AT(III) than the canonical pentasaccharide[5]. As the AGAI*A sequence in a heparin molecule binds to AT(III), it induces local conformational changes which improve the fit between protein and ligand; in turn, further conformational changes propagate through the protein structure, eventually leading

to expulsion of the reactive center loop (RCL)[6]. This loop contains the apparent protease substrate sequence, and its expulsion increases its exposure to the protease. On interaction with the protease (thrombin, for example) active site, the loop is cleaved, and thrombin is trapped by a covalent linkage. At this point, the RCL is incorporated as an extra strand into a beta sheet, pulling with it the thrombin, to the opposite end of the antithrombin molecule, both inactivating the thrombin and disrupting its structure[7].

Another unsulfated sequence is the linkage region, located at the reducing end of the polymer, the site of attachment through a serine residue to the peptide core of the original proteoglycan (see Figure 1.2.1, panel D)[8].

Further minor features, strictly arising from the purification process and not related to the biosynthesis of heparin, can be present in commercial drug. Oxidation under alkaline conditions, which is used to produce a material without colour that does not cause fever on administration, may also induce oxidation at the reducing end of the carbohydrate[9,10].

### 1.2.2. Heparin biosynthesis

Heparin is mainly found in mast cells, where it is synthetized and it can interacts with proteins or inflammatory mediators; the studies of its biosynthesis started with Jeremiah Silbert's work on how mast cell granule fraction incorporated radioactively labeled UDP-sugars into a polysaccharide that was degradable with heparinase[11].

The biosynthesis of heparin occurs primarily in the endoplasmic reticulum and Golgi apparatus of mast cells[12], and it starts with the formation of the so called linkage region attached to a serine residue on a core protein, followed by the addition of D-glucuronic acid (1→4) N-acetyl-D-glucosamine disaccharide units (Figure 1.2.2).

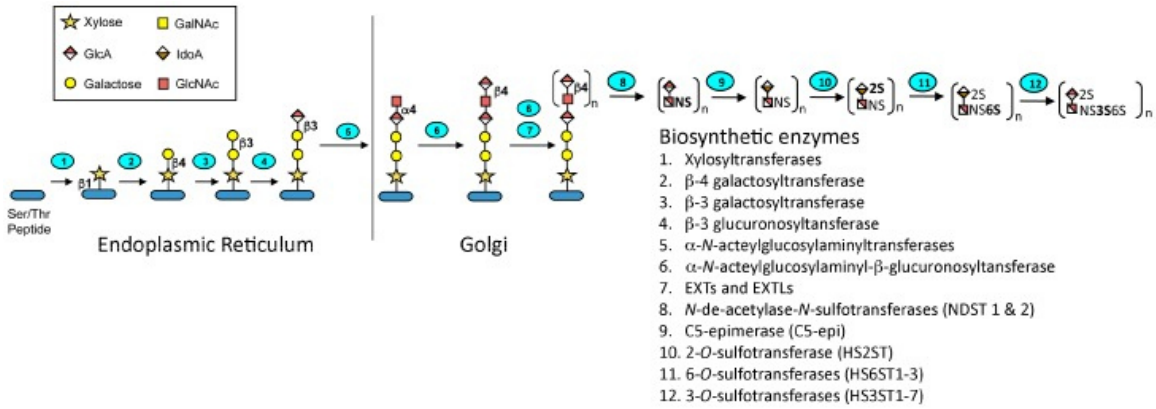


**Figure 1.2.2 Heparin biosynthesis.[13]**

The linkage region synthesis is catalyzed by four enzymes that add the individual monosaccharide the growing chain, first the attachment of xylose (Xyl) followed by a stepwise transfer of two galactose (Gal) and one glucuronic acid (GlcA) residues[14]; the enzymes implicated in this initialization are, in order, a xylosyltransferase, which exists in two isomeric forms, a galactosyltransferase, type I and type II, and glucuronyltransferase, that has only one form[15–17]. Then, the elongation continues with the addition of a N-acetyl-D-glucosamine (GlcNAc), followed by the addition of alternating glucuronate and N-acetyl-glucosamine residues[14]. The elongation of the chain leads to the formation of a polysaccharide with a molecular weight of 60-100 kDa, whereas, the range of the commercial API lies between 15-20 kDa.

The biosynthesis is mediated by a total of 12 enzymes involved in sulfonation and epimerization processes (listed in Figure 1.2.2), and thanks to the isoforms of these enzymes, heparin results as a heterogeneous polysaccharide. The degree of sulfation and the localization of the sulfate residues determines heparin final spectrum of activity; upon mast cell degranulation, peptidoglycan heparin is transformed to the GAG heparin through the action of proteases and β-endo glucuronidase.

The substrate specificity of the various enzyme varies according to the organ and the animal species, but the causes of these differences are not yet known[4].

### 1.2.3. Source of heparin

The original tissue from which heparin was extracted was dog liver, but this source was deemed unsuitable for large-scale production. The use of bovine liver, and then of bovine lung, allowed more of drug to be produced, which was first marketed in 1939 as a pharmaceutical product in USA.

Bovine lung continued as a source of heparin until the mid-1950s, when porcine and bovine intestinal mucosa were introduced as alternative sources, porcine mucosal heparin was subsequently found to be a cleaner and less expensive source tissue, requiring fewer steps in the extraction and purification processes than bovine lung heparin[18,19].

The appearance of the Bovine Spongiform Encephalopathy (BSE) in Europe in the 1990s and the concerns of prion contamination decreased the worldwide production and use of bovine heparin drastically, owing to fears of "mad cow disease", and of ovine heparin, following concerns of over scrapie[20]. The production of bovine heparin in currently restricted to South America and some Islamic countries, while the ovine heparin is confined almost exclusively to laboratory studies, but the US Food and Drugs Administration (FDA) is investigating the possibility of introduction of heparin sodium from bovine intestinal mucosa (bovine mucosal heparin) into the US market[21].

Heparin derived from different animal sources or different organs of the same animal contains a number of subtle structural features. Notably, bovine lung heparin contains much more of the trisulfated disaccharide I2S-ANS,6S than porcine mucosal one, while bovine mucosal heparin exhibits lower sulfation at the 6-O position of the glucosamine residues than either bovine lung or porcine mucosal heparins, as well as more sulfation at the 2-O position of the glucuronic acid residue[22–24].

Finally, recent works have demonstrated the existence of different AT(III)-binding pentasaccharide variants with diverse non-reducing reducing end extensions; their molecular ratios provide further fingerprints of the structural diversity among heparins of different origins[5,23–27].

### 1.2.4. The anticoagulant mechanism of heparin

Heparin exerts its anticoagulant activity mainly thanks to its ability to bind and to enhance the inhibitory activity of the plasma protein antithrombin (AT(III)), member of the serpins' family, against several serine proteases of the coagulation system, most importantly factors IIa (thrombin), Xa and IXa[28]. Protein proteinase inhibitors of the serpin superfamily play a critical role in regulating proteinases in diverse physiologic processes such as development, wound healing and the immune response; the family name is an acronym for serine proteinase inhibitor, but it is now well established that serpins inhibit proteinases of both the serine and cysteine mechanistic classes[29–31].

In vivo, free flowing of blood depends on the balance of pro-coagulant and anticoagulant processes. A complex network of serine proteases, acting in an amplification cascade, converts pro-enzymes to their active form (see Figure 1.2.3)

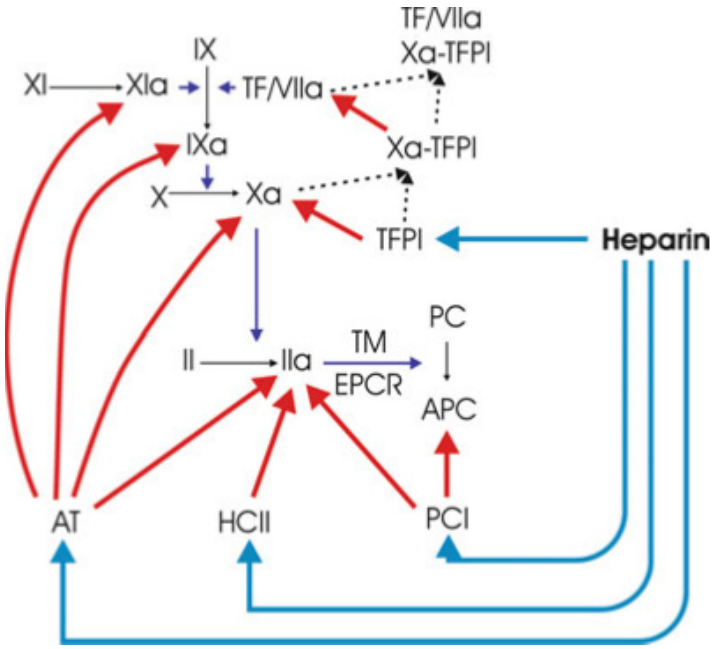


**Figure 1.2.3 Iteraction of heparin with the natural coagulation system**[28]

This coagulation cascade is activated when there is an injury to the vasculature, so that the serine proteases are exposed to pro-coagulant stimuli such as tissue factor and collagen. Several natural or endogenous anticoagulant proteins, which include AT(III), heparin co-factor II (HCII), protein C inhibitor (PCI) and tissue factor pathway inhibitor (TFPI), are also in place to regulate the formation of thrombin[28]. These inhibitors are found at a higher total concentration than the proteases and under normal physiological condition act to keep the clot local to the wound by mopping up any proteases straying into the rest of the vasculature.

AT(III) is best known as the major heparin co-factor in the inhibition of the coagulation proteases, particularly factors Xa and IIa; nowadays, it is well-known that antithrombin binds with high affinity to a specific, unusual pentasaccharide sequence in heparin composed by 6-sulftated-N-acetylated α-D-glucosamine (αDGlcNAc(6S)), β-D-glucuronic acid (βDGlcA), N,3,6-sulftated α-D-glucosamine (αDGlcNS(3S,6S)), αL-iduronic acid (αLIdoA) and N,6-sulfated α-D-glucosamine (αDGlcNS(6S)), also called AGA*IA; the structure of this sequence is showed in Figure 1.2.4.

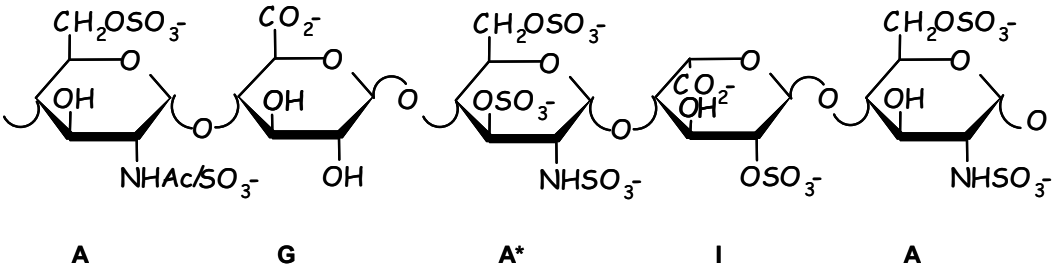


**Figure 1.2.4 AT(III) heparin binding site**

As the high-affinity pentasaccharide sequence in a heparin molecule binds to antithrombin, it induces local conformational changes which improve the fit between protein and ligand; in turn, further conformational changes propagate through the protein structure, eventually leading to expulsion of the reactive centre loop (RCL); this loop contains the apparent protease substrate sequence, and its expulsion increases its exposure to the protease[6]. On interaction with the protease (thrombin, for example) active site, the loop is cleaved, and thrombin is trapped by a covalent linkage. At this point, the RCL is incorporated as an extra strand into a beta sheet, pulling with it the thrombin, to the opposite end of the antithrombin molecule, both inactivating the thrombin and disrupting its structure[7]. The same mechanism is valid for factor Xa (fXa), but there are substantial differences between the way thrombin and fXa engage with heparin activated antithrombin, as was initially indicated by detailed kinetic studies[32]. In fact, it has been found that fXa interacts with antithrombin not only through the RCL, but in addition at a specific exosite. This direct protein–protein interaction is the basis for the specificity of antithrombin for fXa[33]. Thrombin does not bind to the same exosite; instead it binds, rather non-specifically, to the same heparin molecule as is bound to antithrombin. This extra interaction means that a heparin molecule needs to be long enough to reach both proteins; in practice, this needs a chain of about 13 monosaccharide units attached at the non-reducing end of the AT-binding pentasaccharide sequence[28].

Apart from factors Xa and IIa, fIXa is a very important contributor; it binds to the same exosite of antithrombin, though in a somewhat different orientation, and as for fXa the heparin-induced unfolding of the reactive loop exposes the exosite as well as presenting the pseudo-substrate to the enzyme's active site[34].

Factor XIa, a less significant contributor to the anticoagulant action of heparin/antithrombin is structurally different from other coagulation proteases; heparin accelerates the inhibition of fXIa by both antithrombin and protein C inhibitor, and though heparin binding to the enzyme is involved, this

seems to be more complex than is the case for other coagulation proteases and is not only a straightforward template mechanism[35].

In addition to antithrombin, Heparin Cofactor II is a single chain glycoprotein that is a member of the serine protease inhibitor family, with structural similarities to antithrombin[36]. In coagulation heparin cofactor II selectively inhibits thrombin by formation of a stoichiometric 1:1 covalent bimolecular complex in the absence or presence of heparin. The binding of heparin to heparin cofactor II is analogous to heparin and antithrombin binding, and both serpins have similarities in their reactive site peptide structure[37,38].

Protein C is a vitamin K-dependent factor, which is activated by thrombin, forming the so-called Activated protein C (APC), which acts as an anticoagulant by inactivating factors Va and VIIIa in the presence of a co-factor (protein S), and, when complexed with endothelial protein C receptor, elicits a cytoprotective effect through modulation of expression of genes related to anti-inflammatory and anti-apoptotic pathways[39]. The activity of APC is mainly regulated by protein C inhibitor (PCI), an inhibitor from the serpin family, and heparin can influence PCI activity not only by potentiation of antithrombin inhibition of thrombin, but also through its interaction with PCI. It is interesting that the inhibition of thrombin would lead to a decrease in activation of protein C, thereby limiting the inactivation of fVa and fVIIIa. In addition, heparin has been shown to inhibit the inactivation of factor Va by APC[40].

Tissue factor pathway inhibitor is a pleiotropic serine protease inhibitor. Apart from being the main physiological inhibitor of the extrinsic coagulation pathway, it also has important influence in lipid metabolism, innate immunity and angiogenesis[41]. It has high affinity for heparin, essential for the expression of its anticoagulant activity; binding and fXa inhibition studies of heparin oligosaccharides and recombinant TFPI indicated that a dodecasaccharide is the minimum sugar chain length that will enhance the inhibitory activity of TFPI and that saccharide units greater than an octadecasaccharide are needed to achieve full potentiation, as observed with unfractionated heparin[42].

### 1.3. Low Molecular Weight Heparins (LMWHs)

The Low Molecular Weight Heparins (LMWHs), derived from heparin through different depolymerization processes, possess several therapeutic advantages and reduced side effects compared to heparin, maintaining substantially similar monosaccharide composition and oligosaccharide

sequences to heparin[43]. Owing to their lower molecular weight compared to the parent heparins, LMWHs can claim a more predictable pharmacological profile, better bioavailability and longer half-life[44]. The structural heterogeneity that is biosynthetically imprinted, as well as the introduction of additional chemical diversity induced by the depolymerization process, make their structure even more complex than that of heparin[45].

### 1.3.1. Production of LMWHs

Three major strategies are used to prepare LMWHs, and these are depolymerization by chemical deamination and β-elimination, either enzymatically or chemically[45]. In Figure 1.3.1, a schematic view of the reactions involved in the LMWHs preparation with the name assumed by the related process, is reported.

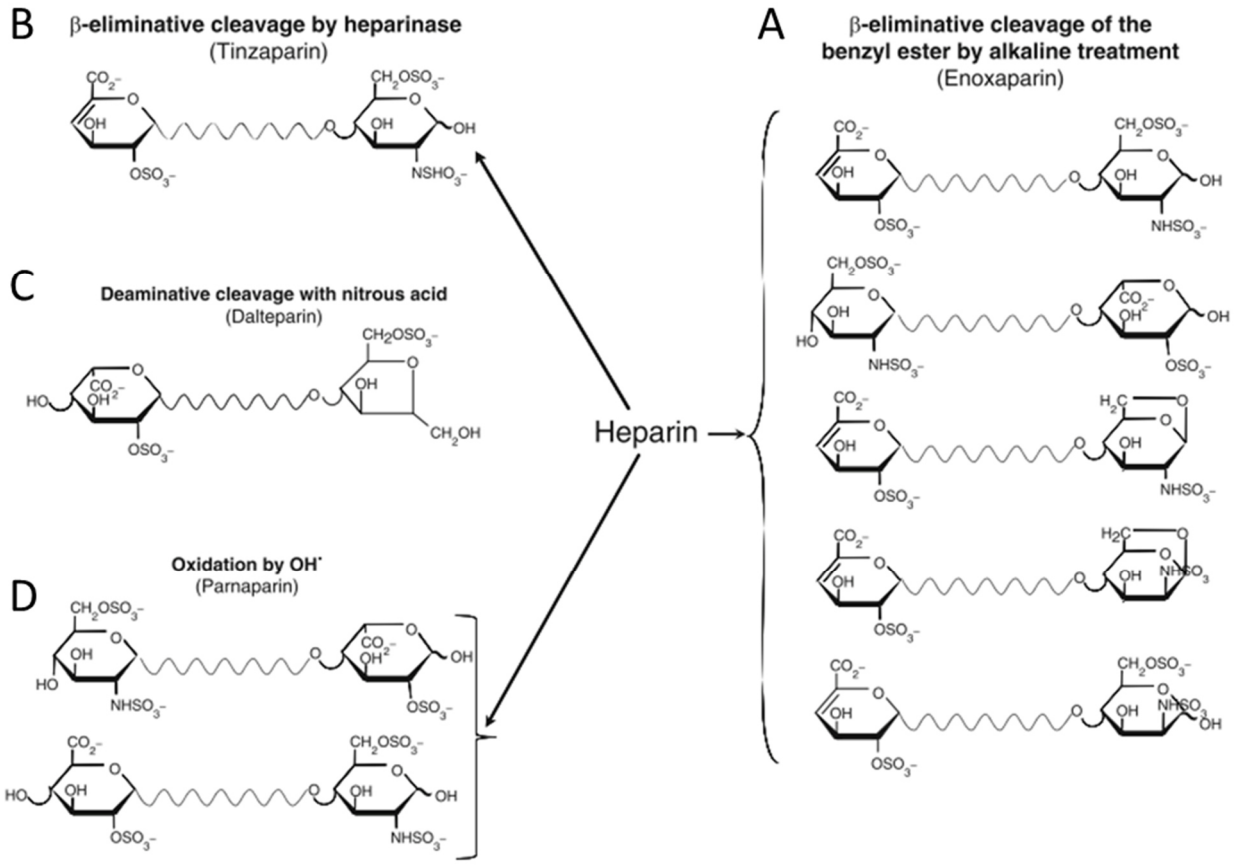


**Figure 1.3.1 Summary of the various methods used to produce LMWHs.**[45]

The chemical β-eliminative method to produce enoxaparin (A) is based on cleavage, in alkaline medium, of the benzyl ester of heparin, which is formed by treatment of the heparin benzethonium salt with benzyl chloride[46]. Under these conditions, β-elimination generates an unsaturated uronate residue at the non-reducing end and an N-sulfo-glucosamine at the reducing end. Similarly, in enzymatic depolymerization (B), the action of heparinase I generates an unsaturated uronate residue at the nonreducing position. However, this residue is mostly 2-O-sulfated due to the preference of the enzyme for the –GlcNNS–IdoA2S– sequence[47].

Heparin undergoes nitrosylation at the amino group of N-sulfo-glucosamine (C); the unstable N-nitroso-sulfonamide residues rearranged to generate a carbocation in C2 and the subsequent ring-contraction and hydrolysis of the adjacent glycosidic bond generate an anhydromannose residue, that is stabilized by reduction with $NaBH_4$ to form a terminal anhydromannitol residue[48].

Heparin can also be oxidatively depolymerized using oxygen radicals generated by different methods such as hydrogen peroxide or ionizing g-irradiation (D)[49–51]. More specifically, in the case of parnaparin, hydrogen peroxide is decomposed in a water solution in the presence of catalytic amount of a transition metal of a low oxidation number (copper II). The strongly electrophilic hydroxyl radical generated by the process easily abstracts hydrogen from alcohols, ethers, and amides, inducing fragmentation of sugar residues and the consequent depolymerization of the chain. This cleavage generates oligomers with both even and odd number of residues[52,53].

### 1.3.2. Structural differences between LMWHs

In principle, LMWHs should differ from their parent heparin only by their molecular weight, which is usually about one third of that of the original UFH. The internal structure of LMWHs should essentially be the same as that of the original UFH in terms of monosaccharide composition, substitution pattern, and oligosaccharide sequence[45]. Even under the assumption that depolymerization processes did not modify the internal structure, procedures involved in the manufacturing of LMWHs (see Figure 1.3.1) cause some structural modifications of the monosaccharidic units at the site of cleavage and are characteristic of each depolymerization procedure. Other differences, regarding the percentage of constituent saccharides and their sulfation pattern, can also be related to both the process and the structural features of the parent UFH used for the LMWH preparation[54].

### 1.3.3. LMWHs *vs* UFH

In contrast to UFH, LMWHs have a lower affinity to bind plasma proteins, endothelial cells (ECs) and macrophages. This difference in binding profile explains the pharmacokinetic variances observed between LMWHs and UFH. The binding of UFH to plasma proteins reduces its anticoagulant activity, which combined with the variations in plasma concentration of heparin-binding proteins, is reflected in its unpredictable anticoagulant response[55].

The main advantages in using LMWHs in respect to the UFH are listed in Table 1.3.1.

**Table 1.3.1 Comparison between UFH and LMWH**

| UFH | LMWHs |
|---|---|
| ○ Higher plasma protein binding | ○ Lower plasma protein binding |
| ○ Lower bioavailability | ○ Higher bioavailability |
| ○ Administered in hospital as continuous infusion by healthcare professional | ○ Easy administration (subcutaneous) directly by patients |
| ○ Need monitoring and dosing adjustments | ○ No monitoring requirements, with fixed or weight-based dosing |
| ○ Require 5-7 days in hospital | ○ No hospitalization requirements |
| ○ Risk of thrombocytopenia and osteoporosis | ○ Decreased risk of adverse events |
| ○ Cheap, but not cost-effective | ○ Demonstrated pharmacoeconomic benefits |

LMWHs exhibit improved subcutaneous bioavailability, lower protein binding, variable number of AT(III) binding sites, variable GAG content, variable anti-serine protease activities, variable potency in releasing tissue factor pathway inhibitor and variable levels of vascular EC binding kinetics[56–59]. For these reasons, over the last decades LMWHs have increasingly replaced UFH in the prevention and treatment of venous thromboembolic disorders (VTE). Randomized clinical trials have demonstrated that individual LMWHs used at optimized dosages are at least as effective as UFH, and probably safer[43]. The convenient once or twice daily subcutaneous dosing regimen without the need for monitoring, has encouraged the wide use of LMWHs; it is well established that different LMWHs vary in their physical and chemical properties due to the differences in their manufacturing methods and these variances corresponds to variances in their pharmacodynamic and pharmacokinetic characteristic[57]. The World Health Organization (WHO) and the USA Food and Drugs Administration (FDA) regard LMWHs as individual drugs that cannot be used interchangeably[57].

Bioavailability of LMWHs after administration is greater than UFH and was determined to be between approximately 87-98%; UFH, by contrast, has a bioavailability only of 15-25% approximately[55]. LMWHs have biological $t_{1/2}$ (based on anti-Xa clearance) nearly double that of UFH, and it is between about 100 and 360 min, depending on the administration (if intravenous or subcutaneous); the anti-Xa activity persists longer than AT(III) activity, which reflects the faster clearance of UFH[60].

LMWH, in doses based on patient weight, needs no monitoring, thanks to its better bioavailability, longer plasma $t_{1/2}$ and more predictable anticoagulant response in comparison with UFH; though LMWHs are more expensive than UFH, both a pilot study and pharmacoeconomic studies in pediatric patients found that their subcutaneous administration reduce the number of necessary laboratory assays, nursing hours and phlebotomy time[61].

### 1.4. Heparin therapy side effects

All the adverse effects of heparins are related to their wide variety of biological activities, with bleeding being the most important safety issue, resulting directly from the potency of heparin as an anticoagulant[62]. This anticoagulant activity is mainly caused by heparin molecules with high affinity to antithrombin AT(III), which amount to only 30–50% of UFH and less than 20% of LMWHs[63]. The incidence of bleeding under heparin therapy is hard to define, as it depends on numerous parameters including the indication, dosage, method, and duration of heparin application, the clinical study design and definition of bleeding, patient characteristics and determinants of bleeding such as type of surgery and co-medication.

Nonbleeding complications as well as other beneficial activities are caused by binding of heparin molecules to proteins other than AT and cells, whereby the structural requirements for many of such interactions are unknown[64]. Generally, the binding tendency of the negatively charged heparin molecules increases with their chain length. As is known with UFH, competing binding partners may even interfere with the high-affinity binding to AT and thus reduce the anticoagulant effect[65]. These so-called “nonspecific bindings” are much less pronounced with LMWHs, which results not only in improved effect-based pharmacokinetics, but also may explain their reduced risk of nonbleeding complications.

Nonbleeding complications must be regarded in terms of their incidence and severity[66]. The prime example for a major adverse effect of UFH is immune heparin-induced thrombocytopenia (HIT). HIT is an uncommon but potentially life-threatening complication so that it has to be considered in every patient treated with UFH. HIT typically occurs in the second week of heparin therapy. Antibody-mediated platelet activation and consequent thrombin generation result in a fundamental paradox: despite thrombocytopenia induced by an anticoagulant, the major clinical effect in HIT is a substantially enhanced risk for venous and/or arterial thrombosis[67].

Osteoporosis is a systemic skeletal disease characterized by low bone mass and micro-architectural deterioration resulting in increased bone fragility and a consequent increase in fracture risk[68]; it represents the most common serious side effect of long-term use of UFH[69]. Osteoporosis should be monitored in all pregnant or elderly patients who require long-term heparin anticoagulation (e.g., 1–2 weeks or longer), although it might be reversible.

In recent years, the most frequent unwanted side effects of heparins were reported to be cutaneous delayed-type hypersensitivity reactions[70]. Traditionally, three types of cutaneous reactions were distinguished[71]: urticarial lesions (immediate hypersensitivity reactions); erythematous papules and plaques (delayed-type hypersensitivity reactions); skin necrosis (most serious dermal reactions). Typically, skin lesions develop >5 days following subcutaneous administration and occur at the sites of heparin injection, although some reports have implicated skin necrosis at sites remote from heparin injection[71]. Although they are usually not life-threatening, they need attention, since they impair the compliance of the patients and may lead to discontinuation of important anticoagulant therapy. Minor elevations of potassium levels or liver transaminases occur often as well, but they are of little clinical relevance in most patients. In these cases, routine monitoring of potassium levels is not necessary.

# 2. Objectives of the thesis

The present PhD work has two main and quite different objectives: the first one to provide and improve adequate molecular weight distribution evaluation methods for polysaccharides and their mixtures, the second one to elucidates more in depth the interaction between a particular chemokine protein called Platelet Factor 4 (PF4) and different polyelectrolytes.

Polysaccharides are heterogeneous and polydisperse compounds, and a correct and reliable molecular weight distribution evaluation is of fundamental importance as it is one of the main parameters that determines their biological functions or applications. Regulatory Entities as the United States Pharmacopoeia (USP) or the European Pharmacopoeia (Ph. Eur.) provide methods for its evaluation that vary on the basis of the compound under investigations, and in the particular case of heparin, all of these "monographs" use Size Exclusion Chromatography technique (SEC, see Chapter 3.1.3), associated to the so-called "Conventional Calibration", that will be elucidated more in detail further (see Chapter 3.1.6); one of the main drawbacks of this kind of calibrations is that they are relative, so if it is not always easy to achieve the correct set of standards, and in this sense the use of a "Light Scattering Calibration" (see Chapter 3.1.5) could provide some advantages.

The importance of Heparin/PF4 interaction characterization relies in the fact that from it a complex is formed, gaining to one of the worst side effect of the heparin therapy, called Heparin-Induced Thrombocytopenia (HIT, see Chapter 4.1), a thrombotic disorder that in some cases leads to the death of the patient. A prompt and rapid recognition of HIT so is fundamental, with a consequent immediate cessation of the heparin therapy, followed by the initiation of an alternative anticoagulant non-heparin therapy. In this sense, the use of GAGs mixtures as the Sulodexide (SLDX, Chapter 4.4), or completely different polymers, like the Defibrotide (DFT, Chapter 5) can be valid options in the HIT management. Moreover, the setup of chemical-physical methods suitable for evaluating the complex heparin/PF4, like the Photon Correlation Spectroscopy (PCS), the Zeta Potential evaluation techniques or the Isothermal Titration Calorimetry (ITC, see Chapter 4.2) could be useful for modulating not only the dosage of heparin but also for evaluating different PF4/compounds interaction.

# 3. Chromatographic characterization of GAGs

## 3.1. Molecular weight and its distribution determination

One of the most fundamental parameters that characterize a macromolecule complex like a polysaccharide is its molecular weight or relative molecular mass principally because of four basic properties:

- They are polydisperse, that is consist of species of different molecular weight;
- They are highly non-ideal in the thermodynamic sense, which means firstly that they have a high thermodynamic exclusion volume resulting from large asymmetry of high solvent affinity and secondly that they have a polyelectrolyte behavior;
- They have a conformation in solution that is difficult to define or determine with precision;
- Some polysaccharides self-associate forming aggregates, particularly at higher solute concentrations.

Indeed, a single determination of an average molecular weight or its distribution requires a research project of some difficulty and duration. These difficulties are unfortunate since knowledge of the molecular weights of polysaccharides is in general of fundamental importance for the understanding of their biotechnological applications and their role in living systems.

### 3.1.1. Heterogeneity and Polydispersion

Polysaccharides are heterogeneous substances, and by heterogeneity means any deviation from single molecular weight behavior of a polysaccharide preparation, no matter what the cause of the variation may be[72].

The molecular weight heterogeneity of polysaccharides can be described by several types of average molecular weights, and the principals are the number average (Mn), the weight average (Mw) and the Z-average (Mz), which are described by the following formulas:

$$Mn = \frac{\sum n_i M_i}{\sum n_i}$$

$$Mw = \frac{\sum n_i M_i^2}{\sum n_i M_i}$$

$$Mz = \frac{\sum n_i M_i^3}{\sum n_i M_i^2}$$

where $n_i$ is the number of components of an ensemble macromolecules characterized by a molecular weight $M_i$[73].

Polydispersion is in many cases reported as the ratio Mw/Mn, and is often referred to as "polydispersion index" by commercial manufacturers of polysaccharides[74]. Its value can be estimated from Gel Permeation Chromatography (GPC) or from absolute methods for molecular weight determination and can provide a useful rule of thumb as to whether the material is "polydisperse" (Mw/Mn ≥1.6) or "monodisperse" (Mw/Mn ≤1.1) but should never be substituted for the characterization of the whole molecular weight distribution.

### 3.1.2. Concentration measurement

Determination of weight concentrations precisely is not easy for polysaccharides; errors can largely be minimized in sedimentation velocity or diffusion coefficient determination through "serial dilution" extrapolation to zero concentration, although it will affect the evaluation of other parameters like the refractive index increment (dn/dc), determined from the slope of a refractive index vs concentration curve[74].

The correction for moisture content in polysaccharides is most frequently done by drying the sample in a dessicator until a constant weight is achieved, although in many cases samples are strongly hygroscopic. A given determination of the molecular weight for a polysaccharide preparation has therefore a rather uncertainty associated to the concentration determination. The use of detectors like UV or refractive index (RI) detectors, with an adequate calibration, is very useful for the correct determination of samples' concentration[75].

### 3.1.3. Gel Permeation Chromatography

Among the techniques available to provide information about the whole molecular weight distribution, calibrated Gel Permeation Chromatography (GPC) has been the most popular in the field of polysaccharides[74]. When the stationary phase in the column is carefully selected and when

adequate calibration methods and data handling procedures are applied, this approach has the potential of resolving the “true” molecular weight distribution.

In GPC, components migrate through the column matrix with different velocities, and consequently elute at different times after injection (see Figure 3.1.1).

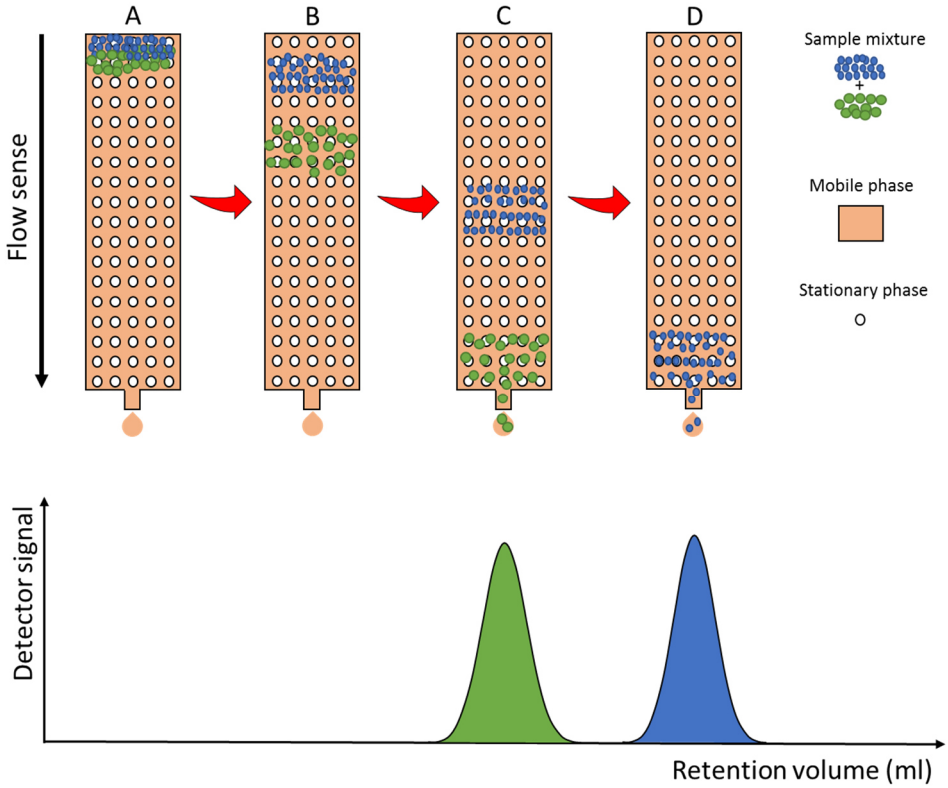


**Figure 3.1.1 GPC elution principle**

The difference in migration after samples injection (Figure 3.1.1, A) velocities occurs due to retention of the molecules by the stationary phase; ideally, it depends on the hydrodynamic volume ($v_h$) of the molecules relative to the accessible pore volume for the given $v_h$. For molecular species with $v_h$ in excess of the largest available pore size of the stationary phase, the separation is due to the steric exclusion of the polymer molecules from the particle walls. As a result, the molecules with the higher $v_h$, that are not retained in the stationary phase’s pores, tend to be faster than the smaller ones, so the two species will separate during the elution (Figure 3.1.1, B).

Polymers ideally elute as a sharp peak at an elution volume determined by its characteristic migration velocity (Figure 3.1.1, C and D); in practice this is not observed due to different broadening

mechanisms. This implies that the chromatographic profile elutes with a Gaussian bell-shape where the maximum of the peak represents the most probable molecular weight and its width its distribution.

### 3.1.4. Detectors for GPC

Typical detectors used are refractive index detectors (RI), ultraviolet (UV), or light scattering detectors (LSD), and each of these detectors has its advantages and disadvantages.

RI is the most common detector for the GPC technique; it is based on the deflection of a beam of light as it passes through a dual compartment flow cell[76]. The deflection of the beam is measured by two photodiodes in a differential circuit. One side of the cell compartment contains the reference solvent of refractive index $n_0$, which is static during the measurement process. The other side contains the sample solution, i.e. the column eluent, having refractive index n. The beam is refracted at the liquid-glass interfaces that separate the two compartments and also at the liquid-glass interface on the exit wall, and again at the glass-air interface on the exit wall.

UV detectors are used for both natural (peptides, proteins) and synthetic macromolecules[77]. Detection at one specific wavelength is often fully sufficient and the majority of applications can therefore be run with single wavelength UV–vis detectors. Dual wavelength detection can be applied in protein analysis to additionally quantitate the amount of protein in the solution. The peptide bonds absorb at around 205 nm. Detection at 214 nm and 280 nm allows more detail to be obtained as UV–vis absorbance between different proteins varies strongly at 280 nm and is related to the actual content of tyrosine, tryptophan, and cysteine.

Photodiode array detectors (PDAs or DADs), which can scan a selectable range of wavelengths, are quite common in HPLC. However, there is only a limited number of applications in GPC/SEC where this functionality is required. In those applications spectra are used to identify oligomeric species, for example, in wood resins or polymer additives. Additional concentration detectors (RIs) are often used to obtain the molar mass distribution results simultaneously to the spectral information. Sometimes the PDA/DAD scan functionality is used to determine a wavelength that can later be used for the specific detection. However, in all cases of UV–vis detection, users should verify upfront that all analyte components can be detected. UV–vis detection alone has a high risk of undetected

components because many macromolecules do not exhibit any chromophores. The verification can be done with the additional use of an RI detector.

### 3.1.5. GPC coupled with a Triple Detector Array (TDA)

Triple Detection GPC/SEC is a well-established technique for the accurate and complete characterization of macromolecules. One of the advantages of a triple detector array (TDA) assembly is that chromatographic calibrations are not necessary[78]. The three detector employed in this technique are a RI or a PDA (described in section 3.1.4), a Light Scattering and a Viscometer, that will described next. The angular dissymmetry in the scattered intensity of light is accounted for by using the combined measurements of intrinsic viscosity and 90° light scattering intensity. The viscometer detector is also useful for determining the size of molecules in solution and particularly of small polymer molecules for which scattering dissymmetry is not observable. The molecular size can then be related to the secondary structure of a polymer, either in terms of chain stiffness or conformation.

#### 3.1.5.1. Static Light Scattering theory

When a solution is illuminated with a beam of light at wavelength $\lambda$, the polymer chains will scatter light in direct proportion to their weight-average molecular mass and, moreover, the angular dependence of the scattered light at low angles can be related to the "hydrodynamic radius" (Rh)[74].
The advantages of using a light scattering (LS) detector in GPC/SEC are well documented, but in summary the LS detector allows the direct measurement of the sample molecular weight without recourse to calibration of the elution volume of the columns with a series of standards (conventional calibration).
There are three types of LS detectors commercially available, right-angle light scattering (RALS, measuring at 90°), low-angle light scattering (LALS, measuring at <10°) and multi-angle light scattering (MALS, measuring at 2 or more angles typically 20-160°).
The principles of the triple detection calculations, once molecular weight is determined at each data slice by RALS, MALS or LALS, is identical. The only difference is in the accuracy of the molecular weight value depending on its origin.

In 1871, Lord Rayleigh published the theory of the scattering of light by free and independent moving gaseous particles much smaller than the light λ[79]. For a small particle in the limit of infinite dilution, the ratio of the intensities between unpolarized incident light (I) and scattered light ($I_s$) is:

$$\frac{I}{I_s} = \frac{2\pi^2 n_0^2 (dn/dc)^2 (1 + cos^2\theta)}{N_A \lambda^4 r^2} cM_w$$

where $n_0$ is the refractive index of the solvent, dn/dc is the specific refractive index increment of the solute-solvent system, Θ is the angle of observation, $N_A$ is the Avogadro number, λ is the wavelength of incident light and r is the distance between the sample and the detector. Simplifying:

$$R_\theta = KcM_w$$

where $R_\Theta$ is called the Rayleigh ratio, and it corresponds to the signal obtained by the detector.
For larger molecules there will be more than one point in each molecule that will scatter light, making the angular dependence more complex.
In general, the light scattering theory is valid for polyelectrolytes if neutral salts are added to the system, for example in the mobile phase. However, some precautions specific to the light scattering system should be taken. When determining dn/dc of a polyelectrolyte, this should be done in the same salt system as used in the GPC experiment; moreover, measurements of the difference in the refractive index of the polyelectrolytes and the solvent should be carried out at constant chemical potential of both the polyelectrolyte and the salt molecules. This means that the polyelectrolyte solutions must be extensively dialyzed against the solvent or, if the sample is solid, dissolved in the same solvent used for GPC experiment.

#### 3.1.5.2. Viscometer

Intrinsic viscosity is a measure of the molecular density of a polymer molecule. A low intrinsic viscosity represents a compact, dense molecule, while a high intrinsic viscosity represents a larger more open molecular structure. The structure of a molecule at a given molecular weight will affect that molecule's contribution to the viscosity of the solution by a given amount, assuming no

interaction between it and other molecules. Measurement of solution viscosity as sample concentration changes at low concentrations is then a way to calculate the intrinsic viscosity of a sample. The viscometer achieves this by measuring the viscosity of the sample solution at concentrations assumed to be low enough to avoid interaction between the sample molecules.

The most common viscometer design is the 4-capillary bridge design invented by Haney (Figure 3.1.2)[80].

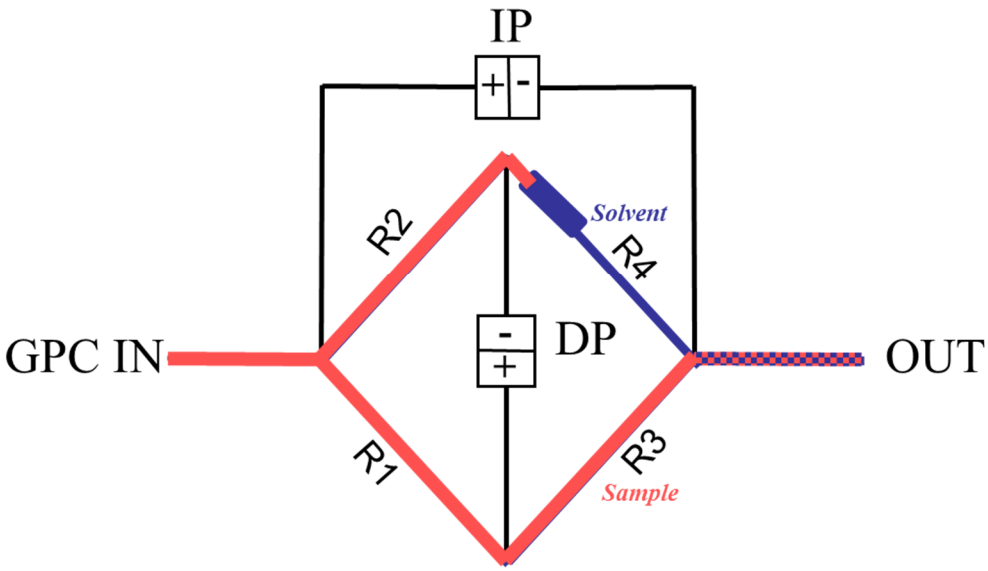


**Figure 3.1.2 Capillary viscometer**

Four capillary tubes R1–R4 with internal diameters of approximately 0.25 mm are arranged in a balanced bridge configuration, analogous to the Wheatstone bridge common in electrical circuits. Differential pressure transducers measure the pressure difference DP (differential pressure) across the midpoint of the bridge and the pressure difference IP (inlet pressure) from inlet to outlet. A delay volume is inserted in the circuit before capillary R4, in order to provide a reference flow of solvent through R4 during elution of the polymer sample. The requirements of the delay volume are: It must have internal volume larger than the net elution volume of the GPC column. The flow resistance must be negligible compared to the capillary resistances.

The capillary tubes are chosen so that the flow resistances are as equal as possible. In this case, the DP output signal will be nearly zero and most of the pump pulsations will be cancelled out in the differential bridge measurement. DP will respond to the viscosity of the sample as it elutes from the GPC. The first peak corresponds to the sample as it elutes into capillaries R1, R2 and R3, while solvent

flows through capillary R4. The second, negative peak is the breakthrough in the delay volume. At this point in time, R4 contains the sample and R1, R2 and R3 contain solvent. The breakthrough peak is not required for the calculation and is simply an artefact of the measurement. The position of this artefact peak can be simply controlled by the size of the delay volume and the length of the analytical run so that it does not interfere with the analytical peak and is fully eluted before the next sample.

The earliest use of the viscometer detector was for Universal Calibration, a column calibration method of determining molecular weight distribution that does not require the standards and samples to have identical structures (see next paragraph).

### 3.1.6. Calibration with Standards

An experimental elution profile obtained from a concentration sensitive detector can be converted to a molecular weight distribution when the system is properly calibrated; the earliest attempts were based on calibration procedures where standards, either synthetic polymers or dextrans, were utilized.

Calibration using “narrow standards”, that are monodisperse certified substances characterized by sharp chromatographic profiles, is also called the “Conventional narrow standard calibration” or “peak-position method” technique, and it is considered a relative calibration because the molecular weights obtained are strictly related to the calibrant. In other words, the sample injected that eluted at the same retention volume of the standard is supposed to have the same molecular weight distribution. After running the series of narrow standards, a polynomial fit is then performed, (usually third or fifth order), and the resulting log M vs. retention time (or volume) calibration curve is plotted. (see Figure 3.1.3).

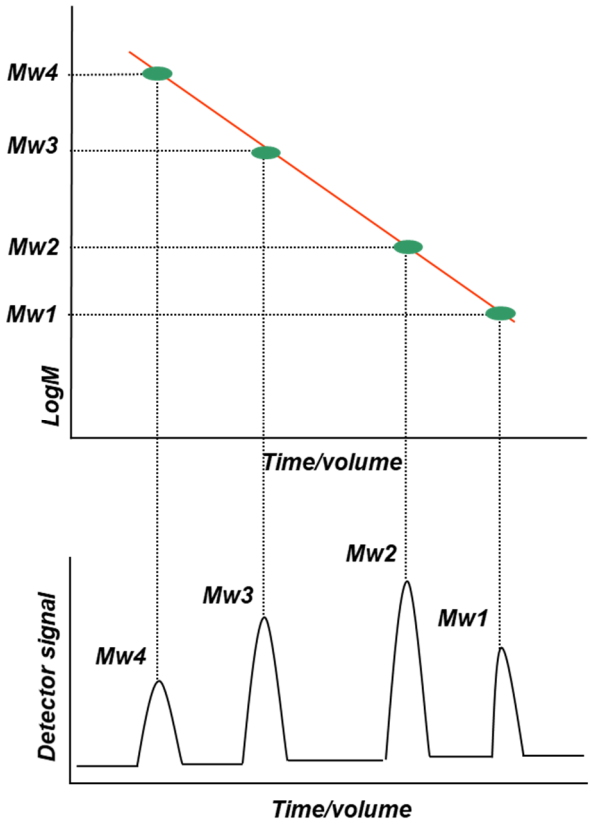


**Figure 3.1.3 Narrow standards set calibration curve.**

There are a few narrow standards available for organic GPC, such as poly(methylmethacrylates), polyisoprenes, polybutadienes, poly(THF), but certainly polystyrene is the major narrow standard used for organic GPC analysis. In the case of aqueous GPC, poly(ethylene oxides) are the most widely used, along with poly(ethylene glycols) for low molecular weight, and the pullulans, which are polysaccharides based on triose structures. The peak position method is considered as one of the best methods to obtain calibration equations[81]. The experimental limitations in applying the peak-position offline calibration method are mainly in the experimental uncertainty in the molecular weight and peak position determination of the standards. Error propagation to the M averages of unknown sample have been studied using computer generated data, and show that the relative error is larger the higher the molecular weight moment[81].

Calibration using "broad molecular weight standards", that are very polydisperse certified substances with precisely quantified molecular weight fractions and large chromatographic profiles, is a relative calibration as well as the narrow standards one. Broad standard can be purchased from a variety of different vendors, and the standard should be well characterized, i.e. the number, weight,

and possibly viscosity average molecular weights have been determined by alternative methods. The advantage to this is being able to use a polymer that has the same structure as the unknown samples being analysed day in and day out. The resulting calibration curve will consist of the data points for each average molecular weight ($Mw_i$) vs the volume or retention time (Figure 3.1.4).

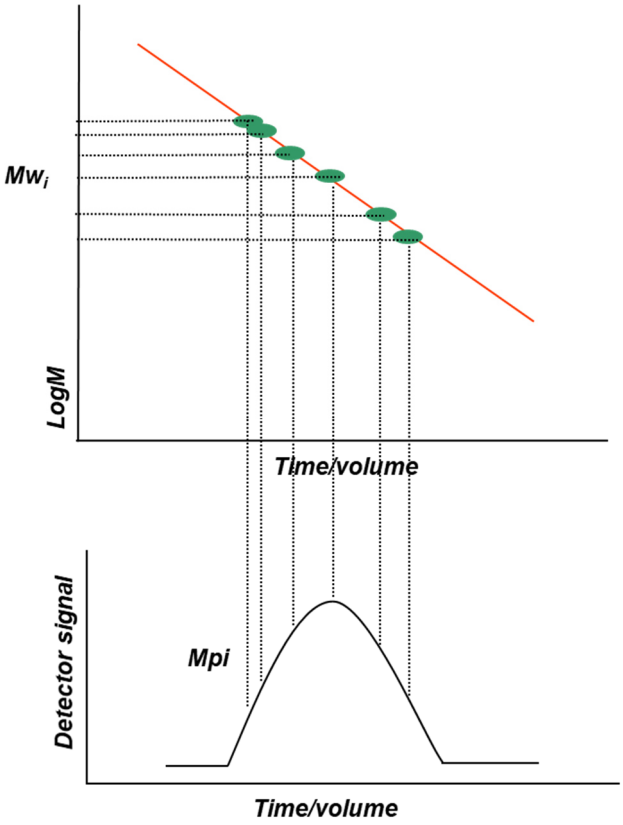


**Figure 3.1.4 Broad standard calibration curve**

The concept of Universal Calibration was introduced by Benoit, et. al. in 1967[82]. Instead of plotting the log molecular weight of a series of narrow standards vs. retention, the log of the product of the intrinsic viscosity [η] and Mw is plotted vs. retention (Figure 3.1.5).

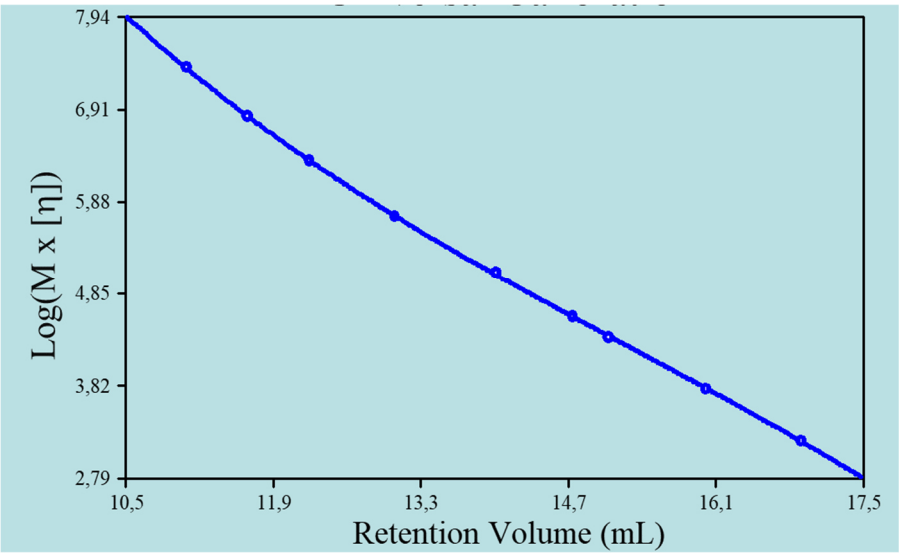


**Figure 3.1.5 Universal calibration plot**

The [η]Mw product is related to the hydrodynamic volume. Benoit found that plotting a series of hydrodynamic volume values for a variety of narrow standards resulted in a singular calibration curve. In other words, all of the points fit the same curve. Once this "Universal" calibration has been established, any random coil polymer can be run in the appropriate solvent, and the molecular weight determined based on the Universal curve. After establishing the Universal curve, we can also plot the log of the intrinsic viscosity vs. the log of the molecular weight for the narrow standards. This plot is called the viscosity law plot, or, the Mark-Houwink plot, that is showed in Figure 3.1.6 with the related equation.

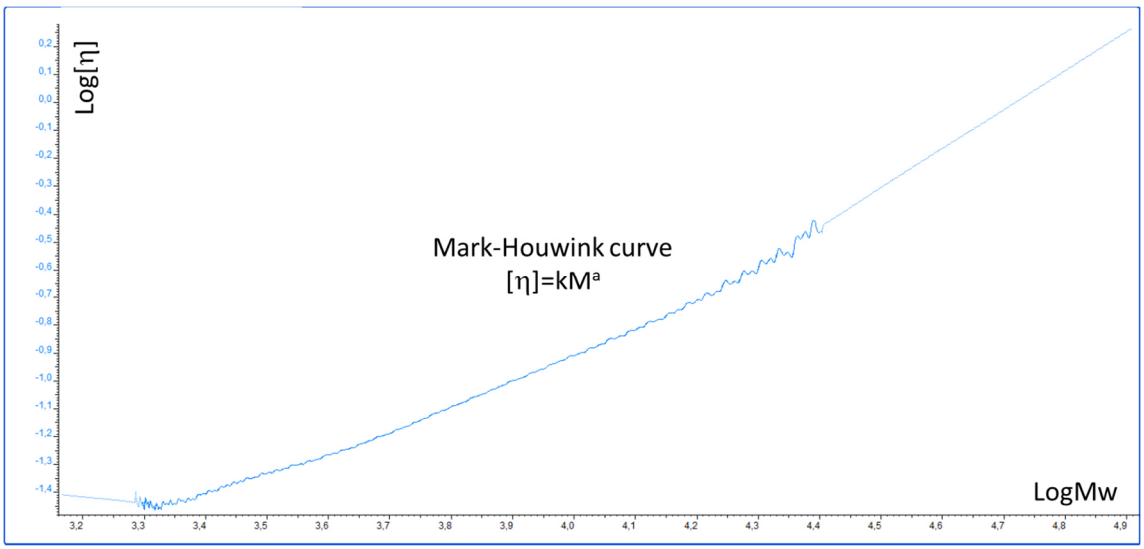


**Figure 3.1.6 Mark-Houwink plot**

This Universal Calibration concept has wide applicability, especially for random coil type polymers, which represents the majority of polymers being analysed today.

### 3.1.7. Selection of column type and material

Manufacturers of commercial column material provide separation ranges for their different products mainly in terms of separation ranges valid for globular proteins or dextrans[74]. It is well documented that most polysaccharides have more extended conformations than the highly flexible and branched dextran molecules, and certainly more extended than the compact globular proteins. The hydrodynamic volume of the stiffer polysaccharides is therefore larger than the corresponding molecular weight of dextrans, and so the separation is expected to differ. It is a necessary requirement that the molecular weight range in the sample is within the separation range for the column material to be able to separate on molecular weight and thereby obtain the molecular weight distribution.
Based on the principle of universal calibration, separation ranges for different column materials have been converted from those of dextrans to other polysaccharides and became narrower the stiffer the polysaccharide.
A proper determination of the void volume, i.e. the elution volume for totally excluded polysaccharides, using a very high molecular weight preparation, and the total volume, using a very low molecular weight compound, is necessary to ensure that the chosen column is able to resolve the molecular weight distribution of interest. By combining different columns in series it is possible to improve the linearity of the separation range and the effective separation range when the pore size distributions of the two columns are properly adjusted each other[83]. This will, firstly, diminish the resolution and, secondly, not increase the upper resolution limit of column with the largest resolution limit, that is one of the limiting factors in characterization using GPC of high molecular weight polysaccharides.
The selection of the column material is in many cases balanced by the two mutually excluding aims of having the highest possible resolution and a wide as possible separation range. Typical GPC stationary phases are either silica-based or polymer-based, and the polarity of the stationary phase should be similar to the polarity of the sample and solvent to ensure a pure size-based separation and to suppress undesired interactions. Silica-based columns, thanks to their high resolving power, are suitable for the separation of monodisperse biopolymers such as proteins and nucleic acids;

they can feature low adsorption and well-defined pore size distribution and generally speaking they can be considered the leading GPC columns in bioanalysis. Polymeric-based columns are packed with hydrophilic, rigid polymethacrylate beads. They are commonly used for the separation of synthetic water-soluble polymers because they exhibit a much larger separation range, better linearity of calibration curves, and less adsorption than the silica-based one; polymeric-based columns have demonstrated good results for small peptides (<1,000 Da), protein aggregates, DNA fragments, and viruses.

## 3.2. Molecular weight characterization of Bovine and Porcine Heparin samples: chromatographic conditions comparison.

### 3.2.1. Introduction

As already mentioned before, heparin is a linear polysaccharide consisting of GlcNAc and GlcA units, partly modified by IdoA and by sulfation at different positions of mainly GlcNAc and IdoA residues[4]. It exerts anticoagulant properties and can be obtained in commercial quantities as a "crude" from intestinal mucosa (cow, pig, and sheep) and lung (cow). Until the late 1980s and early 1990s, when cases of Bovine Spongiform Encephalopathy (BSE) were reported in United Kingdom and other countries, bovine heparin products were widely used together with those extracted from porcine intestine, but their removal from the market increased the demand for porcine heparin[84]. Currently, porcine intestine is the primary source of heparin worldwide, and the only one for enoxaparin[85]; in addition, more of the 50 % of porcine heparin production derives form only one country[21]. In late 2007 and early 2008, a cluster of "allergic type" adverse effects in patients receiving Heparin Sodium Injection occurred in the United States and in some countries in Europe, an event known as the Global Heparin Crisis; the main reason that leads to heparin contamination was the presence of the semisynthetic over-sulfated chondroitin sulfate (OSCS), an inexpensive adulterant with anticoagulant activity[86]. After the global crisis, arises the strong interest from regulatory agencies in broadening the source of heparin, particularly in the reintroduction of bovine deriving drugs already licensed for use in several countries in the world.

The different tissues and/or species sources lead to different heparin degrees of sulfation and acetylation, molecular weight, and anticoagulant activity[5,23,87–89]. The chemical conditions under which

heparins are isolated can also result in structural modifications and altered functional characteristics of the final product, but this correlation is not completely clear[90]. It is known, however, that specific activities of bovine and porcine heparins are considerably different; in e.g., the potency of bovine heparins is typically 30–50% less than that of porcine derived heparin[91]. Such differences in activity may complicate the dosing of such drugs and may limit a clinician's ability to interchange different heparins.

As a therapeutic agent, heparin may be characterized by several physical-chemical techniques as osmosis, static or dynamic light scattering or viscometry (not described here), including chromatographic methods for the measurement of molecular weight, spectroscopic techniques, separation methods for whole polysaccharides, as well as for oligo and monosaccharides and mass spectrometric methods for mapping and sequence analysis. Focusing the attention on the molecular weight, due to polysaccharide heterogeneous structure this parameter cannot be described by a single number. The measurement of molecular weight for heparin is usually, in fact, based on the experimental estimation of the molecular volume in solution, usually by gel permeation chromatography (GPC) or occasionally by electrophoretic methods[92]. UFH contains a little material below 3.0 and above 100.0 kDa, with a mean between 10.0 and 20.0 kDa depending on the tissue and species of origin and the method of preparation[92]. Actually, the most useful method for the measurement of UFH molecular weight is GPC with some form of light scattering detector[78], a technique that does not require a chromatographic calibration, because the molecular weight distribution obtained is absolute (see section 3.1.5), but most of the pharmacopeial chromatographic assays for the molecular weight distributions of heparin still utilize relative calibrations with an UV or a Refractive Index detector, in which are employed narrow standard calibrants prepared from native heparin by fractionation, or broad standards, polydisperse samples that can be used to determine the relationship between molecular weight and retention time in a specific chromatographic system[93]. This second standard type is used for the identification of heparin sodium in the related USP monograph[94], and the associated calibration curve is generated by inspection of the integrated chromatogram to find the retention time at which the proportions above and below particular molecular weights match the values provided in the table specific to that calibrant. Of course, to ensure a correct resolution of the broad standard chromatogram, the use of silica columns is required, for which the great advantage of high resolution is countered by very short life time and many problems of compatibility

with samples (interactions, pH, and so on); furthermore, conventional calibrations curves are used for relative molecular weight distribution evaluation, so adequate calibration standards are needed.

### 3.2.2. Aim of the work

As fully described in 3.1 section, the molecular weight distribution of polysaccharides, which are very complex and heterogeneous macromolecules, is a fundamental parameter and its determination is of great importance, in order to fully understand their biotechnological applications.

In the context of obtaining consensus molecular weight data to generate proposed acceptance criteria for potency and identification assays, we compare the conventional USP calibration method[94] to a light-scattering method; moreover, an evaluation of silica and polymeric columns chromatographic performances was done[95]. As underlined above, the selection of the column material must be balanced by the need of having the highest possible resolution and a wide as possible separation range; in the present case, the necessity of highly performant columns like the silica-based is not required, but the focus is to obtain acceptable chromatographic profiles sufficient to correctly evaluate the molecular weight distribution.

The study also involved the comparison of heparin sodium of bovine intestinal origin with that of bovine lung and porcine intestinal origin.

### 3.2.3. Materials and methods

#### 3.2.3.1. Samples in analysis

A panel of twenty heparin sodium samples from bovine intestinal mucosa, two from bovine lung and two samples from porcine intestinal mucosa were analysed; in Table 3.2.1, the complete list of the samples, with the assigned Ronzoni code and source, are reported. Moreover, the “USP Heparin Sodium Identification Reference Standard” (USP RS) was analysed as a molecular weight distribution system suitability sample, as reported in the official USP calibration method[94].

**Table 3.2.1 List of analysed samples**

| Ronzoni code | Source |
|---|---|
| G11588 | Bovine Intestine |
| G11589 | Bovine Intestine |
| G11590 | Bovine Intestine |
| G11591 | Bovine Intestine |
| G11592 | Bovine Intestine |
| G11593 | Bovine Intestine |
| G11594 | Bovine Intestine |
| G11595 | Bovine Lung |
| G11596 | Bovine Lung |
| G11597 | Porcine Intestine |
| G11740 | Bovine Intestine |
| G11741 | Bovine Intestine |
| G11742 | Bovine Intestine |
| G11743 | Bovine Intestine |
| G11744 | Bovine Intestine |
| G11745 | Bovine Intestine |
| G11746 | Bovine Intestine |
| G11747 | Bovine Intestine |
| G11748 | Bovine Intestine |
| G11749 | Bovine Intestine |
| G11750 | Bovine Intestine |
| G11751 | Bovine Intestine |
| G11752 | Bovine Intestine |
| G11753 | Porcine Intestine |

### 3.2.3.2. Chromatographic conditions

At this stage, not only the comparison of the different columns material, but also the optimization of the sample resolution was taken into account, and in these terms, polymeric columns with different pore and particle sizes were used, two columns in series, in particular, for polymeric stationary phase TSKG2500PWXL + TSKG3000PWXL and TSKG4000PWXL + TSKG3000PXL were chosen, and

2 x PLS5030 and TSKG4000SWXL + TSKG3000SWXL, both benches preceded by a TSKGel Guard Column SWXL, were selected as silica type. Two different temperatures (30 and 40°C) and two different injection volumes (20 and 100 μl) were also tested, using two mobile phases: 0.1 M ammonium acetate + 0.02 % sodium azide and 0.1 M sodium nitrate + 0.05 % sodium azide; to perform the analysis, a Viscotek TDA model 305, equipped with Refractive Index, Right Angle Light Scattering and Viscometer was used. In Table 3.2.2, the complete list of all the chromatographic conditions tested (at least 12 different methods) are reported.

**Table 3.2.2 Summary of the methods used for chromatographic conditions comparison**

| Method | Column Set* | Mobile Phase | T (C°) | Injection Volume | Detector |
|---|---|---|---|---|---|
| 1 | A | 0.1 M $NH_4Ac$ + 0.02 % $NaN_3$ | 30 °C | 20 μl | Refractive Index |
| 2 | B | 0.1 M $NH_4Ac$ + 0.02 % $NaN_3$ | 30 °C | 100 μl | Light Scattering |
| 3 | C | 0.1 M $NH_4Ac$ + 0.02 % $NaN_3$ | 30 °C | 20 μl | Refractive Index |
| 4 | C | 0.1 M $NaNO_3$ + 0.05 % $NaN_3$ | 30 °C | 20 μl | Refractive Index |
| 5 | C | 0.1 M $NaNO_3$ + 0.05 % $NaN_3$ | 40 °C | 100 μl | Light Scattering |
| 6 | C | 0.1 M $NH_4Ac$ + 0.02 % $NaN_3$ | 30 °C | 100 μl | Light Scattering |
| 7 | C | 0.1 M $NH_4Ac$ + 0.02 % $NaN_3$ | 40 °C | 100 μl | Light Scattering |
| 8 | D | 0.1 M $NH_4Ac$ + 0.02 % $NaN_3$ | 30 °C | 20 μl | Refractive Index |
| 9 | D | 0.1 M $NaNO_3$ + 0.05 % $NaN_3$ | 30 °C | 20 μl | Refractive Index |
| 10 | D | 0.1 M $NaNO_3$ + 0.05 % $NaN_3$ | 40 °C | 100 μl | Light Scattering |
| 11 | D | 0.1 M $NH_4Ac$ + 0.02 % $NaN_3$ | 30 °C | 100 μl | Light Scattering |
| 12 | D | 0.1 M $NH_4Ac$ + 0.02 % $NaN_3$ | 40 °C | 100 μl | Light Scattering |

*TSKG4000SWXL + TSKG3000SWXL = A; 2 x PLS5030 = B; TSKG2500PWXL + TSKG3000PWXL = C; TSKG4000PWXL + TSKG3000PWXL = D

Method number one refers to USP monograph for Heparin Sodium Identification[94]. The differences in columns pore and particle sizes are, instead, reported in
Table 3.2.3.

**Table 3.2.3 Columns specifications**

| Column | Pore size (nm) | Particle size (μm) |
|---|---|---|
| TSKG2500PWXL | < 20 | 7 |
| TSKG3000PWXL | 20 | 7 |
| TSKG4000PWXL | < 50 | 10 |
| TSKG3000SWXL | 25 | 5 |
| TSKG4000SWXL | 45 | 8 |
| PLS5030 | 30 | 5 |

### 3.2.3.3. Samples preparation and analysis

Each sample, including the USP RS, was dissolved at about 5 mg/ml in mobile phase and, after 1 h under stirring, injected in twice; different solutions of samples were prepared for all the 12 different methods. Analysis time was of 50 and 60 minutes for respectively polymeric and silica columns methods.

### 3.2.3.4. Chromatograms acquisition and analysis elaboration

For each sample, the two injections mean results of the weight-average molecular weight (Mw, Da), the percentage of heparin with molecular weight in the range 8000 to 16000 (M8000- 16000), the percentage of heparin with molecular weight in the range 16000 to 24000 (M16000-24000) and the percentage of heparin with molecular weight greater than 24000 (M24000) were measured. For Refractive Index methods, the broad standard USP Heparin Sodium Molecular Weight Calibrant RS was used to perform the chromatographic conventional calibration; instead, the Light Scattering detector does not require a chromatographic calibration, because the molecular weight distribution obtained is absolute[78], and in this case only an instrumental calibration for the determination of the detector constants and for detectors' profiles alignment. For this purpose, a polyethylene oxide (PEO) standard, of known Mw, polydispersity, and intrinsic viscosity was used. When the Light Scattering detector is involved, two different dn/dc values, 0.13 for 0.1 M sodium nitrate + 0.05 % sodium azide as mobile phase, and 0.128 for 0.1 M ammonium acetate + 0.02 % sodium azide as mobile phase were used, both experimentally determined.

The chromatographic profiles were elaborated using suitable GPC software: for methods 1, 5, 6, 7, 10, 11 and 12 Clarity version 6.1 was used, and for methods 2, 3, 4, 8 and 9 OmniSEC version 4.6.2 was used.

### 3.2.4. Results and discussion

Before to start with the analysis of all the 24 heparin panels, the suitability of the conditions selected was tested int terms of comparison of columns sets, of different temperatures (only for polymeric columns) and of different mobile phases.

#### 3.2.4.1. Assessment of chromatographic conditions suitability

At this stage, the chromatographic performances were compared, with the goal of determine whether polymeric columns might have acceptable chromatographic properties in respect of silica-based columns for heparin sodium molecular weight determination. The comparison was made in terms of:

- Resolution quality of the heparin profile and its separation from mobile phase or other salts peak;
- Molecular weight distribution evaluation;
- Temperatures and mobile phases variances (only on polymeric benches, using columns set C).

Chromatographic performances were in-depth investigated using columns sets B, C and D (see Table 3.2.3) and G11588 as a random heparin sample. The bench A was not tested in this sense due to its already known use as recommended column bench by, in e.g., USP.

Starting with the columns performances comparison, 100 μl of about 5 mg/ml solutions of G11588 were injected using Light Scattering detector, instrument temperature of 30°C and ammonium acetate + 0.02 % sodium azide as mobile phase (respectively methods 6, 11 and 2); although typical injection volumes of only 20 μl are sufficient for an adequate chromatographic analysis, higher volumes are needed to obtain good Light Scattering profiles. The resulted chromatographic profiles obtained respectively with polymeric (panels A and B, respectively column sets C and D) and silica columns (panel C), are reported in Figure 3.2.1.

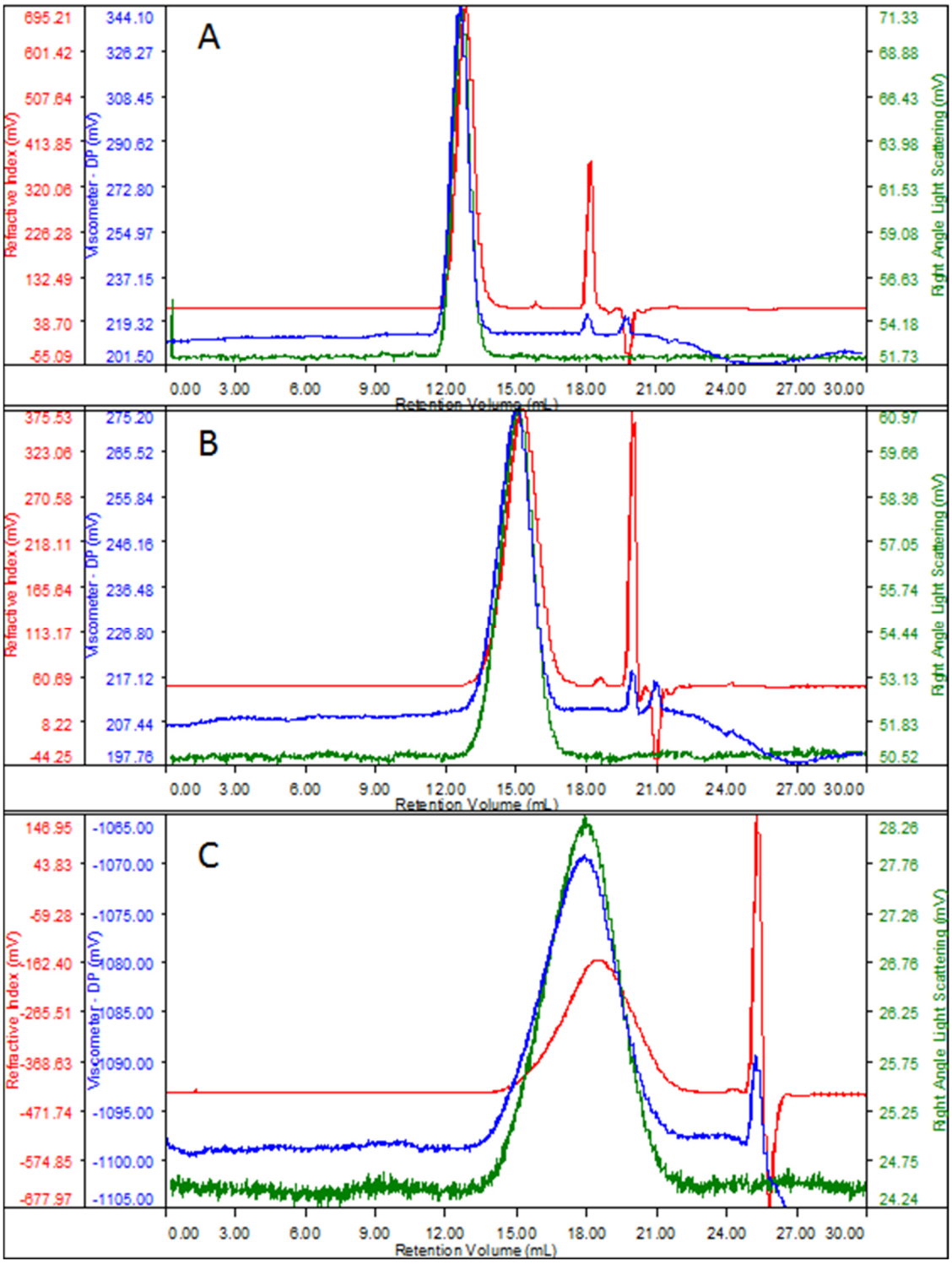


**Figure 3.2.1 Example of heparin chromatograms (G11588) obtained with polymeric columns (TSKG2500PWXL+TSKG3000PWXL and TSKG4000PWXL+TSKG3000PWXL, panels A and B respectively) and silica columns (2xPLS5030, panel C).**

The three panels contain three chromatographic profiles obtained with the response of the three different detectors: red the Refractive Index, blue the Viscometer and green the Right-Angle Light

Scattering; using both columns types, a single peak with the characteristic bell-shape is gained with a good separation from the salts or mobile phase signals that eluted with greater retention times (these secondary profiles are not considered in the molecular weight evaluation), index of the resolution suitability of all the conditions used. The main differences observed are a change in the retention time, mainly due to the different pore and particle sizes of the columns' benches (a consideration that can only be done on sets C and D, due to the presence of a guard column applied on bench B, that of course prolonged elution volume), and the width of the heparin profile, that, as expected, enlarge a lot for the silica type.

On the polymeric columns' retention time difference, as just said, on the set D heparin eluted later and this observation is also correlated to the mobile phase and salts peaks, that maintained quite the same shift to greater retention time; this column bench is the one with the higher pore and particle sizes. Furthermore, heparin set C profile is sharper than D, and this could be an index of less resolution performances of this set. Anyway, none of the two polymeric benches are able to gain the same broad peak as silica column type but for our purpose this fact is not so chief, since the TDA technique has the great advantage of a not-so-high resolution requirement of the sample profile, but only an acceptable separation from mobile phase and other salts. A last consideration is in the Light Scattering detector signal, that is slightly noisier and unstable in panel C than in panels A and B and this could be due to a bleeding phenomenon that was already observed by using silica column types.

The molecular weight distribution resulted from the analysis is reported in Table 3.2.4, in terms of weight-average molecular weight (Mw, Da), number-average molecular weight (Mn, Da) and polydispersion index (Mw/Mn). Results were rounded to the next 100 Da.

**Table 3.2.4 Columns sets performances comparison**

| COLUMNS SET | Mw (Da) | Mn (Da) | Mw/Mn |
|---|---|---|---|
| **C** | 14700 | 12000 | 1.22 |
| **D** | 15100 | 13000 | 1.16 |
| **B** | 16600 | 13500 | 1.23 |

Even though the sharper chromatographic profile, set C Mw/Mn is the same as B one, but with both Mw and Mn quite significantly lower; on the other hand, set D has a slightly less polydisperse but

with quite similar molecular weight values as set B, in particular the Mn one. Overall, at this stage we consider the three chromatographic conditions tested suitable for further investigations.

We then move to test if different temperatures could in some way change the heparin chromatographic profile or its molecular weight distribution. It is, well-known that one of the main difficulty in achieving both high-speed and high-resolution separation in SEC is the slow mass transfer of the large solutes between the interstitial space and the pore space, and in this terms, varying the temperature could be a valuable parameter: as the temperature increases, the mobile phase viscosity decreases, and the analytes diffusivity improves[96]. To check the temperature effect on heparin analysis, the same G11588 was injected at 30°C and 40°C on columns set C (TSKG2500PWXL + TSKG3000PWXL), respectively the USP declared temperature and a condition already known to be suitable for polysaccharides' evaluation[78]; the related chromatographic Refractive Index overlay is reported in Figure 3.2.2, while the molecular weight distribution result is reported in Table 3.2.5.

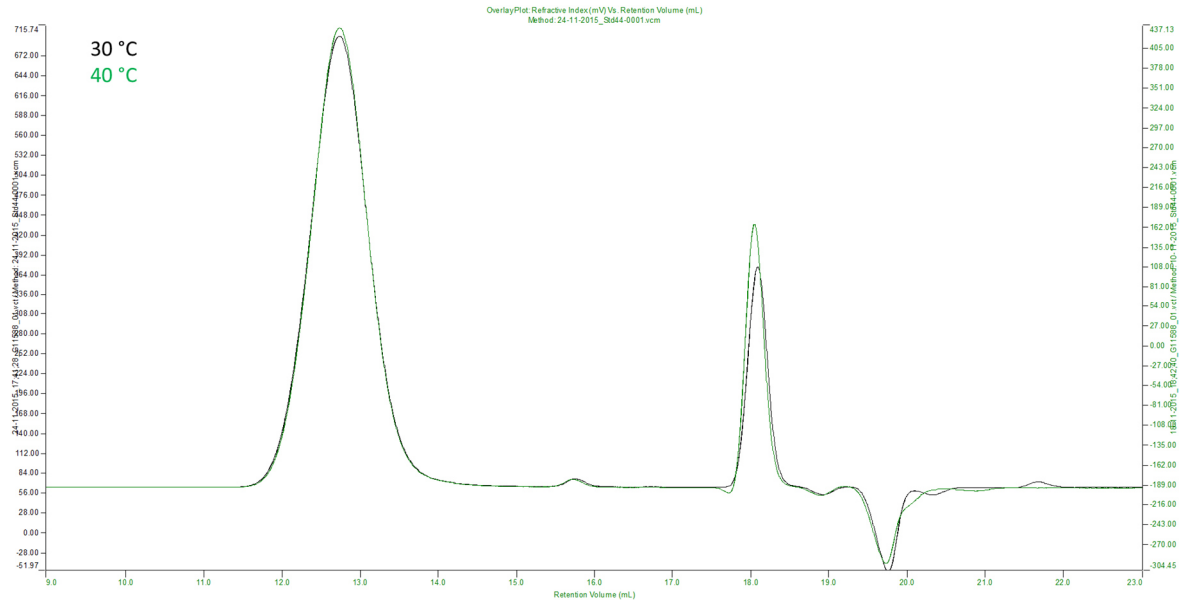


**Figure 3.2.2 Refractive Index overlay of G11588 analysis.**

**Table 3.2.5 Temperatue influence test results obtained by G11588 analysis.**

| TEMPERATURE (°C) | Mw (Da) | Mn (Da) | Mw/Mn |
|---|---|---|---|
| **30** | 14700 | 12000 | 1.22 |
| **40** | 15800 | 12200 | 1.29 |

As it is shown in Figure 3.2.2, neither the heparin elution time nor the chromatographic resolution are affected by the temperature changes, so the two profiles are perfectly overlapped; a very minor

shift of mobile phase was observed, but it is not relevant. On the other hand, a variation in the molecular weight distribution is appreciated, in particular the polydispersion is increased, and this observation is on-line with the what mentioned above on the analytes' diffusivity improvement due to higher temperatures.

Last but not least, two different mobile phases were investigated, in particular the 0.1 M ammonium acetate + 0.02 % sodium azide, that is the one used in the Heparin Sodium Identification USP Monograph, and the 0.1 M sodium nitrate + 0.05 % sodium azide, one of the most used aqueous solution in Ronzoni Institute polysaccharides analysis methods; the two mobile phases are characterized by similar pH (6.8 and 6.9 respectively), but slightly different conductivity (approximately 6.3 and 8.7 mS/cm respectively). The reason in comparing different mobile phases originates from the assumption that any change in its composition strongly influences the hydrodynamic volumes of the solutes and thus affects the conclusions drawn on the solute molecular masses[97]. Again, G11588 was tested on columns set C, and the related chromatographic Refractive Index overlay is reported in Figure 3.2.3, while the molecular weight distribution result is reported in Table 3.2.6.

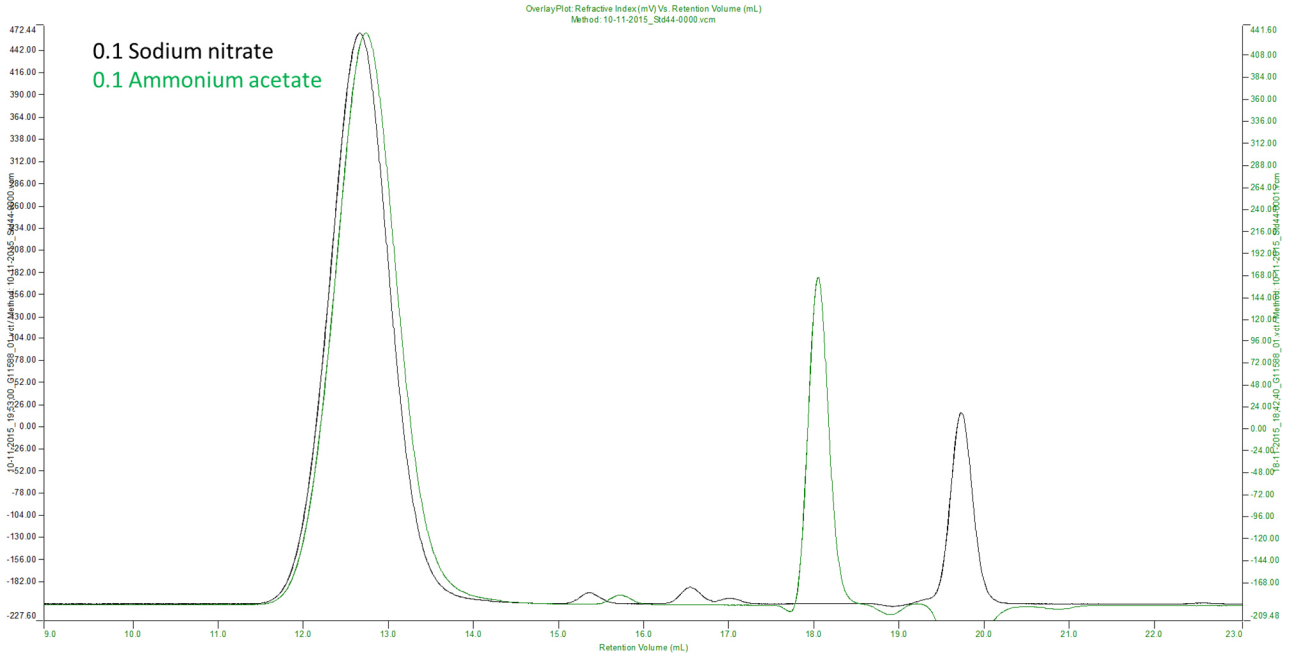


**Figure 3.2.3 Refractive Index overlay of G11588 analysis.**

**Table 3.2.6 Mobile phase influence test results obtained by G11588 analysis.**

| MOBILE PHASE | Mw (Da) | Mn (Da) | Mw/Mn |
|---|---|---|---|
| **0.1 SODIUM NITRATE** | 15500 | 12000 | 1.29 |
| **0.1 AMMONIUM ACETATE** | 15800 | 12200 | 1.29 |

By the results, a slight shift to greater retention times of both heparin and minor salts profiles in 0.1 ammonium acetate was appreciated, and of course different signals for the mobile phase were obtained. It also seems that in this condition the sample peak is slightly broader, particularly on the low molecular chain part, but this is only a qualitative consideration and the polydispersion index, in fact, is the same for both conditions used.

As a final consideration about this first part, all of the chromatographic conditions tested were used for further investigations on the 24-heparins panel, because all of them demonstrated to be suitable for heparin analysis; nonetheless, some variations were observed, and it will be interesting to see if these changes are reproducible or it was just a matter of one sample.

### 3.2.4.2. Comparison of 24 heparins panel

After the assessment of the suitability of the chromatographic conditions used in the present work, all of the heparin samples listed in Table 3.2.1, with the addition of one USP Heparin Sodium Identification RS, were analyzed using different chromatographic conditions (see Table 3.2.2), with the purpose of comparing the conventional USP calibration method to a Light Scattering method. First were performed the analysis with silica columns sets A and B (respectively Methods 1 and 2), and then with polymer column set C (Methods from 3 to 7) and finally with polymer column set D (Methods from 8 to 12). The chromatographic profiles overlay of the USP Heparin Sodium Identification RS is reported in Figure 3.2.4. Once again, its elution peak is always well separated from the mobile phase peak, so all chromatographic conditions tested are suitable for the analysis of this sample. Same results were obtained for the analysis of the other samples (chromatograms not reported).

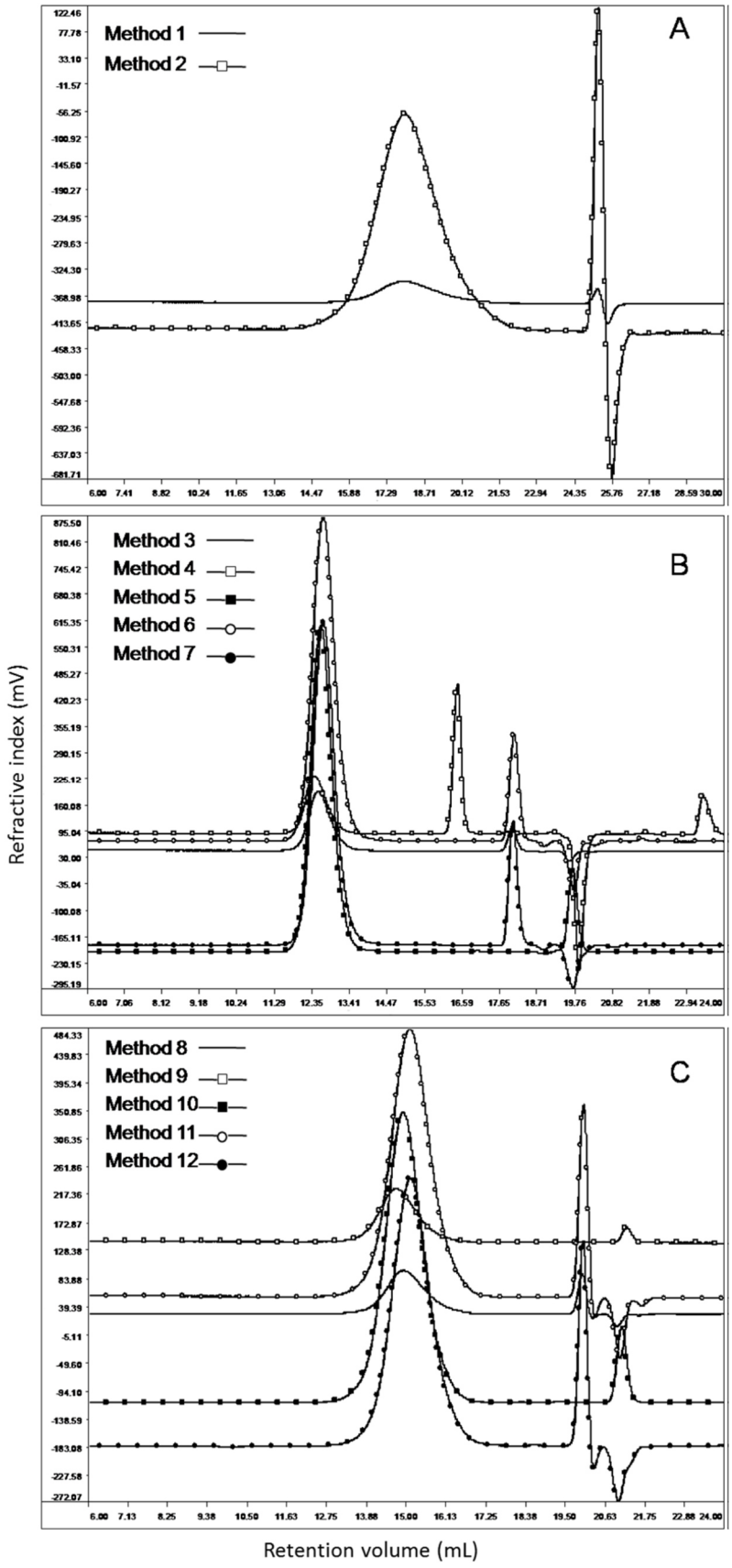


**Figure 3.2.4 USP Heparin Sodium Identification RS Refractive Index profiles overlay.**

After acquisition, data were elaborated using suitable GPC software, as described in 3.2.3; results for weight average molecular weight (Mw, Da) of the heparin samples, percentage of chains above 24 kDa (M24000) and the ratio M8000–16000/M16000–24000 are reported respectively in Table 3.2.7, Table 3.2.8 and Table 3.2.9.

**Table 3.2.7 Weight average molecular weight (Mw) results of heparin samples. (inside the brackets, the standard deviation)**

| | Methods | | | | | | | | | | | |
|---|---|---|---|---|---|---|---|---|---|---|---|---|
| | 1 | 2 | 3 | 4 | 5 | 6 | 7 | 8 | 9 | 10 | 11 | 12 |
| G11588 | 14700 (125) | 16600 (380) | 14700 (8) | 14200 (22) | 15500 (29) | 14700 (8) | 15800 (6) | 14700 (4) | 14600 (1) | 14800 (21) | 15100 (3) | 15300 (0) |
| G11589 | 15600 (146) | 17500 (171) | 15300 (5) | 14700 (15) | 16100 (11) | 15300 (11) | 16400 (28) | 15600 (1) | 15100 (11) | 15300 (14) | 15500 (3) | 15900 (4) |
| G11590 | 15800 (39) | 17700 (80) | 15700 (14) | 15100 (8) | 16300 (13) | 15300 (26) | 16600 (6) | 15700 (1) | 15500 (6) | 15500 (23) | 15700 (3) | 16100 (4) |
| G11591 | 15900 (89) | 17600 (49) | 15400 (27) | 14900 (8) | 16200 (4) | 15400 (20) | 16600 (1) | 15700 (8) | 15400 (1) | 15500 (1) | 15700 (2) | 15900 (1) |
| G11592 | 13800 (278) | 15700 (24) | 14000 (12) | 13600 (41) | 14700 (14) | 14100 (85) | 15000 (15) | 13800 (5) | 13800 (1) | 14100 (1) | 14100 (6) | 14400 (11) |
| G11593 | 14600 (233) | 16600 (76) | 14400 (32) | 14200 (18) | 15600 (16) | 14900 (6) | 15900 (2) | 14600 (1) | 14600 (4) | 14800 (4) | 15000 (1) | 15300 (11) |
| G11594 | 14100 (98) | 15900 (23) | 13900 (27) | 13600 (11) | 14700 (10) | 14000 (17) | 15000 (4) | 14000 (1) | 13900 (1) | 13700 (8) | 14200 (4) | 14300 (2) |
| G11595 | 12800 (127) | 14900 (9) | 12600 (19) | 12600 (38) | 14300 (20) | 13600 (17) | 14500 (7) | 12900 (3) | 12900 (0) | 13600 (9) | 13800 (6) | 14100 (8) |
| G11596 | 13400 (314) | 15500 (226) | 13000 (1) | 12800 (16) | 14600 (4) | 14100 (35) | 14900 (7) | 13300 (5) | 13100 (1) | 14000 (8) | 14300 (4) | 14500 (1) |
| G11597 | 16200 (289) | 18100 (4) | 16000 (44) | 15400 (27) | 16600 (2) | 16100 (32) | 17000 (16) | 16100 (6) | 15800 (7) | 15900 (7) | 16200 (1) | 16600 (4) |
| G11740 | 15800 (37) | N.A. | 15600 (16) | 15500 (27) | 16700 (2) | 16000 (40) | 17100 (3) | 15900 (7) | 16000 (1) | 16000 (3) | 16100 (1) | 16600 (8) |
| G11741 | 15000 (124) | N.A. | 14900 (60) | 14800 (4) | 15800 (6) | 15100 (31) | 16100 (5) | 15100 (3) | 15100 (3) | 15000 (3) | 15300 (4) | 15700 (1) |
| G11742 | 15400 (6) | N.A. | 15200 (4) | 15000 (9) | 16200 (30) | 15600 (3) | 16600 (15) | 15400 (11) | 15300 (0) | 15500 (4) | 15700 (8) | 16100 (1) |
| G11743 | 16300 (3) | N.A. | 16400 (8) | 16000 (2) | 17300 (16) | 16700 (1) | 17700 (4) | 16600 (1) | 16400 12) | 16600 (1) | 16800 (4) | 17100 (1) |
| G11744 | 16200 (13) | N.A. | 16200 (16) | 15900 (6) | 17000 (8) | 16500 (4) | 17500 (4) | 16400 (4) | 16300 (6) | 16400 (4) | 16500 (1) | 17000 (5) |
| G11745 | 20100 (100) | N.A. | 19800 (22) | 19600 (10) | 21100 (20) | 20200 (2) | 21500 (1) | 20600 (5) | 20100 (20) | 20400 (4) | 20600 (5) | 21200 (3) |
| G11746 | 17600 (54) | N.A. | 17600 (4) | 17000 (1) | 18400 (19) | 17800 (35) | 18900 (4) | 17700 (3) | 17600 (4) | 17900 (33) | 17800 (1) | 18400 (1) |
| G11747 | 17700 (93) | N.A. | 17500 (40) | 17100 (8) | 18600 (26) | 18300 (27) | 19100 (1) | 18000 (5) | 17700 (1) | 17900 (23) | 18100 (7) | 18600 (3) |
| G11748 | 17500 (50) | N.A. | 17400 (18) | 17000 (6) | 18400 (12) | 18200 (16) | 18800 (14) | 17800 (8) | 17600 (1) | 17800 (16) | 17900 (5) | 18300 (1) |
| G11749 | 17100 (31) | N.A. | 17000 (66) | 16400 (12) | 18800 (6) | 18500 (27) | 19300 (44) | 17200 (8) | 17100 (10) | 18100 (1) | 18300 (4) | 18900 (4) |
| G11750 | 17900 (80) | N.A. | 18000 (56) | 16900 (1) | 19600 (1) | 19600 (4) | 20300 (3) | 18000 (4) | 17600 (26) | 18900 (6) | 19000 (1) | 19700 (5) |
| G11751 | 19400 (11) | N.A. | 19400 (7) | 18300 (6) | 21200 (16) | 21000 (34) | 21900 (10) | 19700 (5) | 19600 (6) | 20700 (2) | 20500 (0) | 21400 (1) |
| G11752 | 20800 (57) | N.A. | 20600 (13) | 19800 (5) | 23400 (8) | 23100 (8) | 24300 (63) | 21000 (76) | 21100 (5) | 22600 (11) | 22800 (6) | 23600 (1) |
| G11753 | 15600 (13) | N.A. | 15500 (1) | 15200 (8) | 16500 (6) | 16400 (23) | 17100 (4) | 15700 (2) | 15600 (6) | 16100 (1) | 16200 (7) | 16600 (3) |

**Table 3.2.8 Percentage of chains above 24000 Da (M24000) (inside the brackets, the standard deviation)**

| | Methods | | | | | | | | | | | |
|---|---|---|---|---|---|---|---|---|---|---|---|---|
| | 1 | 2 | 3 | 4 | 5 | 6 | 7 | 8 | 9 | 10 | 11 | 12 |
| G11588 | 8.51 (0.51) | 14.61 (0.12) | 8.62 (0.37) | 7.80 (0.08) | 12.57 (0.08) | 9.54 (0.19) | 13.37 (0.11) | 8.78 (0.08) | 8.80 (0.06) | 8.94 (0.21) | 8.44 (0.19) | 10.11 (0.01) |
| G11589 | 10.73 (0.25) | 16.93 (0.22) | 10.18 (0.08) | 9.05 (0.02) | 14.19 (0.13) | 11.03 (0.08) | 15.32 (0.06) | 10.69 (0.18) | 10.15 (0.01) | 10.64 (0.02) | 9.68 (0.06) | 11.79 (0.06) |
| G11590 | 11.17 (0.08) | 18.80 (0.04) | 11.21 (0.05) | 9.59 (0.10) | 14.20 (0.19) | 10.85 (0.16) | 15.42 (0.28) | 11.10 (0.13) | 10.70 (0.03) | 10.70 (0.16) | 10.08 (0.37) | 12.28 (0.15) |
| G11591 | 11.36 (0.18) | 18.37 (0.15) | 10.48 (0.07) | 9.49 (0.03) | 14.27 (0.29) | 11.03 (0.19) | 15.53 (0.03) | 11.12 (0.02) | 10.60 (0.08) | 10.92 (0.21) | 9.83 (0.21) | 12.03 (0.18) |
| G11592 | 7.09 (0.83) | 13.91 (0.06) | 7.72 (0.02) | 6.89 (0.02) | 11.37 (0.08) | 8.49 (0.10) | 12.04 (0.01) | 7.81 (0.04) | 7.60 (0.07) | 8.23 (0.36) | 6.96 (0.11) | 8.75 (0.48) |
| G11593 | 8.44 (0.38) | 16.28 (0.06) | 8.64 (0.06) | 8.19 (0.13) | 12.96 (0.15) | 9.91 (0.07) | 14.08 (0.07) | 9.37 (0.02) | 9.18 (0.22) | 9.56 (0.13) | 8.95 (0.23) | 10.43 (0.11) |
| G11594 | 8.04 (0.12) | 14.08 (0.11) | 8.09 (0.08) | 7.39 (0.03) | 11.70 (0.21) | 8.74 (0.11) | 12.52 (0.16) | 8.51 (0.04) | 8.17 (0.08) | 8.11 (0.00) | 7.95 (0.25) | 9.29 (0.05) |
| G11595 | 6.75 (0.33) | 14.68 (0.25) | 6.21 (0.02) | 6.26 (0.16) | 12.36 (0.06) | 9.73 (0.04) | 13.16 (0.01) | 7.27 (0.04) | 7.23 (0.00) | 9.14 (0.26) | 8.91 (0.33) | 10.53 (0.71) |
| G11596 | 7.87 (0.49) | 15.70 (0.13) | 6.88 (0.02) | 6.98 (0.08) | 13.52 (0.10) | 11.36 (0.36) | 14.54 (0.01) | 8.23 (0.09) | 7.84 (0.02) | 10.83 (0.21) | 10.92 (0.09) | 12.10 (0.16) |
| G11597 | 9.80 (0.44) | 16.91 (0.09) | 10.08 (0.28) | 8.49 (0.28) | 13.71 (0.40) | 9.21 (0.23) | 15.38 (0.16) | 9.38 (0.04) | 8.26 (0.08) | 7.36 (0.01) | 7.04 (0.18) | 8.91 (0.25) |
| G11740 | 11.03 (0.01) | N.A. | 10.77 (0.02) | 10.55 (0.11) | 15.76 (0.09) | 12.30 (0.16) | 17.02 (0.17) | 11.66 (0.08) | 11.57 (0.16) | 12.03 (0.18) | 11.41 (0.28) | 13.60 (0.16) |
| G11741 | 8.27 (0.35) | N.A. | 8.26 (0.19) | 8.05 (0.04) | 12.84 (0.06) | 9.62 (0.13) | 13.79 (0.43) | 8.82 (0.02) | 8.74 (0.11) | 8.47 (0.11) | 8.38 (0.04) | 10.08 (0.25) |
| G11742 | 9.15 (0.11) | N.A. | 8.94 (0.01) | 8.72 (0.04) | 13.77 (0.05) | 10.49 (0.17) | 14.90 (0.05) | 9.80 (0.04) | 9.46 (0.06) | 9.40 (0.19) | 9.55 (0.30) | 11.26 (0.21) |
| G11743 | 11.32 0.01) | N.A. | 11.80 (0.10) | 10.89 (0.00) | 16.30 (0.22) | 12.06 (0.08) | 17.68 (0.19) | 12.31 (0.04) | 11.72 (0.10) | 11.54 (0.18) | 10.72 (0.01) | 12.72 (0.22) |
| G11744 | 10.97 (0.00) | N.A. | 11.20 (0.02) | 10.31 (0.11) | 15.52 (0.13) | 11.63 (0.23) | 17.09 (0.23) | 11.71 (0.01) | 11.50 (0.04) | 10.78 (0.23) | 10.07 (0.21) | 12.15 (0.25) |
| G11745 | 23.85 (0.10) | N.A. | 23.38 (0.07) | 22.40 (0.11) | 29.07 (0.78) | 24.08 (0.52) | 30.58 (0.19) | 26.13 (0.06) | 24.82 (0.05) | 25.26 (0.24) | 23.90 (0.16) | 27.55 (0.13) |
| G11746 | 15.45 (0.05) | N.A. | 15.63 (0.19) | 14.10 (0.02) | 19.33 (0.13) | 15.67 (0.01) | 21.45 (0.16) | 15.98 (0.04) | 16.16 (0.64) | 15.40 (0.12) | 14.22 (0.04) | 17.09 (0.13) |
| G11747 | 15.69 (0.06) | N.A. | 15.26 (0.23) | 14.19 (0.10) | 20.26 (0.05) | 17.63 (0.14) | 21.73 (0.07) | 16.88 (0.08) | 16.05 (0.04) | 15.60 (0.12) | 14.77 (0.01) | 17.45 (0.28) |
| G11748 | 15.50 (0.11) | N.A. | 15.32 (0.08) | 14.22 (0.08) | 20.13 (0.05) | 17.96 (0.01) | 21.50 (0.00) | 16.65 (0.03) | 16.01 (0.02) | 16.00 (0.19) | 15.01 (0.12) | 17.70 (0.11) |
| G11749 | 16.05 (0.01) | N.A. | 15.94 (0.24) | 14.35 (0.01) | 23.23 (0.36) | 21.15 (0.29) | 24.09 (0.02) | 17.00 (0.06) | 16.57 (0.01) | 19.71 (0.26) | 19.80 (0.11) | 21.59 (0.09) |
| G11750 | 18.35 (0.14) | N.A. | 18.95 (0.04) | 15.88 (0.13) | 25.28 (0.12) | 24.55 (0.08) | 26.97 (0.05) | 19.36 (0.10) | 18.49 (0.06) | 22.51 (0.07) | 22.29 (0.19) | 24.63 (0.09) |
| G11751 | 22.55 (22.55) | N.A. | 23.02 (0.52) | 19.82 (0.09) | 29.54 (0.44) | 28.00 (0.66) | 31.24 (0.03) | 24.09 (0.00) | 23.53 (0.02) | 27.18 (0.14) | 26.57 (0.36) | 29.11 (0.05) |
| G11752 | 26.26 (0.14) | N.A. | 26.11 (0.06) | 23.61 (0.04) | 34.90 (0.35) | 33.63 (0.63) | 36.14 (0.02) | 28.10 (0.16) | 27.66 (0.03) | 31.86 (0.18) | 32.28 (0.33) | 34.30 (0.08) |
| G11753 | 8.15 (0.08) | N.A. | 8.89 (0.05) | 8.22 (0.28) | 12.85 (0.96) | 10.66 (0.62) | 15.34 (0.01) | 8.64 (0.02) | 8.24 (0.13) | 7.93 (0.42) | 6.68 (0.24) | 9.48 (0.13) |

**Table 3.2.9 Ratio between percentage of chains between 8000-16000 and 16000-24000 Da. Inside the brackets the standard deviations are reported**

| | Methods | | | | | | | | | | | |
|---|---|---|---|---|---|---|---|---|---|---|---|---|
| | 1 | 2 | 3 | 4 | 5 | 6 | 7 | 8 | 9 | 10 | 11 | 12 |
| G11588 | 3.10 (0.65) | 1.60 (0.00) | 2.44 (0.14) | 2.78 (0.03) | 2.09 (0.02) | 2.29 (0.01) | 1.97 (0.00) | 2.63 (0.02) | 2.68 (0.01) | 2.19 (0.01) | 2.30 (0.02) | 1.93 (0.00) |
| G11589 | 2.78 (0.79) | 1.50 (0.03) | 2.35 (0.02) | 2.52 (0.01) | 1.80 (0.00) | 2.13 (0.00) | 1.85 (0.00) | 2.32 (0.05) | 2.43 (0.01) | 1.99 (0.01) | 1.97 (0.03) | 1.79 (0.01) |
| G11590 | 2.66 (0.88) | 1.49 (0.00) | 2.16 (0.01) | 2.39 (0.02) | 1.77 (0.02) | 2.06 (0.00) | 1.78 (0.01) | 2.22 (0.01) | 2.30 (0.00) | 1.92 (0.00) | 1.83 (0.01) | 1.68 (0.00) |
| G11591 | 2.64 (0.96) | 1.24 (0.00) | 2.28 (0.00) | 2.42 (0.00) | 1.78 (0.01) | 1.97 (0.00) | 1.78 (0.00) | 2.22 (0.02) | 2.32 (0.00) | 1.85 (0.01) | 1.84 (0.00) | 1.73 (0.00) |
| G11592 | 3.55 (0.93) | 1.71 (0.02) | 2.83 (0.01) | 3.09 (0.00) | 2.17 (0.00) | 2.31 (0.03) | 2.16 (0.01) | 2.98 (0.01) | 3.08 (0.01) | 2.44 (0.01) | 2.50 (0.01) | 2.24 (0.01) |
| G11593 | 3.18 (0.94) | 1.54 (0.01) | 2.70 (0.03) | 2.79 (0.05) | 1.97 (0.00) | 2.19 (0.00) | 1.93 (0.00) | 2.65 (0.03) | 2.75 (0.00) | 2.17 (0.00) | 2.18 (0.01) | 1.97 (0.01) |
| G11594 | 3.68 (1.04) | 1.59 (0.04) | 2.99 (0.02) | 3.19 (0.01) | 2.17 (0.00) | 2.34 (0.01) | 2.09 (0.01) | 3.10 (0.00) | 3.20 (0.01) | 2.57 (0.01) | 2.55 (0.00) | 2.27 (0.00) |
| G11595 | 4.04 (1.16) | 1.85 (0.07) | 3.63 (0.01) | 3.59 (0.01) | 2.14 (0.01) | 2.14 (0.00) | 2.11 (0.00) | 3.36 (0.00) | 3.40 (0.00) | 2.25 (0.01) | 2.24 (0.01) | 2.13 (0.00) |
| G11596 | 3.85 (1.17) | 1.85 (0.00) | 3.51 (0.01) | 3.47 (0.02) | 2.15 (0.01) | 2.10 (0.02) | 2.10 (0.00) | 3.23 (0.00) | 3.27 (0.00) | 2.18 (0.01) | 2.18 (0.01) | 2.08 (0.00) |
| G11597 | 1.85 (1.16) | 1.03 (0.01) | 1.72 (0.04) | 1.94 (0.04) | 1.49 (0.03) | 1.57 (0.00) | 1.52 (0.02) | 1.71 (0.00) | 1.78 (0.00) | 1.32 (0.01) | 1.30 (0.02) | 1.13 (0.04) |
| G11740 | 2.45 (1.06) | N.A. | 2.31 (0.01) | 2.35 (0.02) | 1.88 (0.01) | 2.03 (0.00) | 1.85 (0.03) | 2.28 (0.01) | 2.33 (0.00) | 2.01 (0.01) | 1.96 (0.03) | 1.76 (0.00) |
| G11741 | 2.69 (0.87) | N.A. | 2.51 (0.04) | 2.58 (0.01) | 2.08 (0.01) | 2.45 (0.00) | 2.02 (0.01) | 2.51 (0.00) | 2.53 (0.01) | 2.48 (0.01) | 2.33 (0.01) | 2.00 (0.02) |
| G11742 | 2.59 (0.66) | N.A. | 2.44 (0.02) | 2.46 (0.01) | 1.99 (0.00) | 2.28 (0.01) | 1.95 (0.00) | 2.37 (0.00) | 2.44 (0.01) | 2.14 (0.01) | 2.24 (0.01) | 1.92 (0.02) |
| G11743 | 1.99 (0.70) | N.A. | 1.83 (0.03) | 1.94 (0.04) | 1.71 (0.01) | 1.80 (0.02) | 1.71 (0.00) | 1.77 (0.00) | 1.84 (0.01) | 1.65 (0.01) | 1.56 (0.01) | 1.41 (0.01) |
| G11744 | 2.08 (0.71) | N.A. | 1.94 (0.01) | 2.03 (0.03) | 1.70 (0.02) | 1.84 (0.02) | 1.78 (0.00) | 1.85 (0.00) | 1.93 (0.00) | 1.67 (0.00) | 1.65 (0.02) | 1.40 (0.03) |
| G11745 | 1.21 (0.68) | N.A. | 1.14 (0.00) | 1.20 (0.00) | 1.04 (0.49) | 0.87 (0.04) | 1.08 (0.12) | 1.03 (0.01) | 1.06 (0.01) | 0.81 (0.26) | 0.64 (0.17) | 0.69 (0.07) |
| G11746 | 1.67 (0.57) | N.A. | 1.54 (0.02) | 1.67 (0.01) | 1.32 (0.05) | 1.46 (0.03) | 1.52 (0.07) | 1.49 (0.00) | 1.54 (0.00) | 1.26 (0.00) | 1.18 (0.01) | 1.15 (0.05) |
| G11747 | 1.63 (0.53) | N.A. | 1.57 (0.01) | 1.65 (0.03) | 1.42 (0.01) | 1.30 (0.04) | 1.49 (0.02) | 1.46 (0.01) | 1.50 (0.01) | 1.23 (0.02) | 1.13 (0.00) | 1.08 (0.03) |
| G11748 | 1.78 (0.48) | N.A. | 1.67 (0.01) | 1.76 (0.00) | 1.45 (0.04) | 1.43 (0.02) | 1.50 (0.05) | 1.58 (0.00) | 1.64 (0.01) | 1.35 (0.02) | 1.29 (0.00) | 1.25 (0.02) |
| G11749 | 2.26 (0.57) | N.A. | 2.05 (0.05) | 2.18 (0.00) | 1.67 (0.03) | 1.56 (0.05) | 1.67 (0.03) | 2.04 (0.01) | 2.09 (0.01) | 1.62 (0.09) | 1.65 (0.03) | 1.55 (0.01) |
| G11750 | 2.11 (0.62) | N.A. | 1.84 (0.01) | 2.08 (0.03) | 1.52 (0.03) | 1.48 (0.01) | 1.76 (0.01) | 1.90 (0.00) | 1.96 (0.00) | 1.62 (0.04) | 1.57 (0.01) | 1.52 (0.03) |
| G11751 | 1.76 (0.62) | N.A. | 1.55 (0.05) | 1.73 (0.03) | 1.28 (0.03) | 1.19 (0.16) | 1.54 (0.00) | 1.55 (0.00) | 1.61 (0.01) | 1.28 (0.05) | 1.20 (0.01) | 1.22 (0.05) |
| G11752 | 1.61 (0.61) | N.A. | 1.46 (0.01) | 1.55 (0.01) | 1.18 (0.29) | 1.07 (1.72) | 1.40 (0.02) | 1.41 (0.01) | 1.46 (0.00) | 1.17 (0.38) | 1.10 (0.72) | 1.09 (0.37) |
| G11753 | 1.91 (0.54) | N.A. | 1.85 (0.01) | 1.98 (0.08) | 1.43 (0.00) | 1.46 (0.00) | 1.53 (0.01) | 1.71 (0.00) | 1.86 (0.02) | 1.34 (0.00) | 1.24 (0.01) | 1.14 (0.00) |

In Table 3.2.10, the results summary obtained for USP Heparin Sodium Identification RS sample is reported.

**Table 3.2.10 USP Heparin Sodium Identification RS sample results summary. Inside the brackets, the standard deviations are reported**

| | Methods | | | | | | | | | | | |
|---|---|---|---|---|---|---|---|---|---|---|---|---|
| | 1 | 2 | 3 | 4 | 5 | 6 | 7 | 8 | 9 | 10 | 11 | 12 |
| Mw (Da) | 15800 (195) | 17700 (13) | 15700 (33) | 15200 (33) | 16700 (47) | 16100 (2) | 17000 (15) | 15848 (7) | 15700 (27) | 16000 (21) | 16200 (1) | 16400 (8) |
| M 24000 | 8.80 (0.69) | 16.86 (0.16) | 8.93 (0.08) | 8.17 (0.21) | 13.39 (0.40) | 9.12 (0.18) | 14.79 (0.32) | 8.96 (0.07) | 8.47 (0.12) | 7.93 (0.28) | 6.20 (0.37) | 8.32 (0.20) |
| Ratio | 1.89 (0.04) | 0.99 (0.02) | 1.82 (0.01) | 1.97 (0.05) | 1.49 (0.01) | 1.64 (0.00) | 1.48 (0.01) | 1.72 (0.01) | 1.82 (0.01) | 1.37 (0.00) | 1.24 (0.03) | 1.15 (0.02) |

Methods 1-2 were performed on silica-based columns, respectively TSKG4000SWXL+ TSKG3000SWXL and 2xPLS5030, while methods 3-7 were performed on TSKG2500PWXL+ TSKG3000PWXL and methods 8-12 on TSKG4000PWXL+TSKG3000PWXL.

As reported in Table 3.2.10, the Mw range calculated for the USP Heparin Sodium Identification RS, as measured to assess system suitability, is between 15200 and 17700 Da, with an average value of 16200 Da. As reported by the USP Heparin Sodium Identification monograph[94], the acceptance criteria for the RS test indicate that Mw for this sample should lie within +/−500 Da of the established value of 16000 Da. Results for Methods 2, 4, 5 and 7, respectively 17700, 15200, 16700 and 17000 Da are out of the USP acceptance criteria, but considering all 12 methods Mw results, the Relative Standard Deviation (RSD%) calculated is 4.17 %, an acceptable value taking into account the instrument sensitivity and the different chromatographic conditions tested.

Methods 5 and 7 were acquired at 40 °C with same columns and both gave high molecular weight and of course higher M24000 in comparison with Method 1 (official USP method for the analysis of heparin sodium molecular weight distribution); instead Methods 3, 4 and 6, acquired at 30 °C with the same columns but different calibration, gave lower molecular weight in comparison to 5 and 7 (although Methods 3 and 6 respects USP acceptance criteria). So, it is clear that column set C does not completely have the acceptable chromatographic properties required. The main reason of these differences could be the different particle size between columns sets C and A (both columns of the set C have a particle size of 7 µm, while columns set A have particle sizes of 5 and 8 µm respectively for TSKG3000SWXL and TSKG4000SWXL). Regarding to the columns set B, both molecular weight and ratio M8000–16000/M16000–24000 are out of the acceptance criteria; again, the main problem could be the particle size of the columns set (5 µm). As a conclusion for this first part, it seems that with a chromatographic system in which the particle size is the same for each column used in

series, the correct resolution required is not reached, with the only exception of Method 3 chromatographic conditions, very similar to the USP official method.

Looking at Methods 8 to 12, each of these chromatographic conditions results are within the acceptance criteria; the fact that column set D particle sizes are different (respectively 10 µm for the TSKG4000PWXL and 7 µm TSKG3000PWXL) could be a confirmation that having a single particle size in a column set cannot reach the right resolution required. Particularly remarkable is that the use of a light-scattering detector allows us to reach results comparable with the official USP method for the analysis of heparin sodium.

Taking into account results from the whole set of 24 heparin samples (Table 3.2.9 and Table 3.2.10), a methods comparation for use over a wide range of heparin samples can be achieved. Methods 3, 8 and 9 give results in especially good agreement with Method 1 over the entire range; few values for Mw are more than 500 Da away from the Method 1 value, and few values for M24000 are outside +/−10% of the Method 1 value. Methods 10 and 11 use the same column set as Methods 8 and 9 but with different calibration; in particular in methods 10 and 11, light scattering detector was used, while in 8 and 9, the USP Heparin Sodium Identification relative calibration was performed (refractive index detector), using the proper broad standard calibrant. This calibrant was characterized for use with silica columns specified in the monograph, and it is characterized by the following slice table of mass fraction vs. molecular weight (Table 3.2.11).

**Table 3.2.11 Broad Standard Table for the USP Heparin Sodium Molecular Weight Calibrant RS**

| MW (Da) | % below MW | % above MW |
|---|---|---|
| 6000 | 3.2 | 96.8 |
| 8000 | 10.4 | 89.6 |
| 10000 | 19.8 | 80.2 |
| 12000 | 31.7 | 68.3 |
| 14000 | 43.4 | 56.5 |
| 16000 | 55.5 | 44.5 |
| 18000 | 66.0 | 34.0 |
| 20000 | 74.4 | 25.6 |
| 22000 | 80.3 | 19.7 |
| 24000 | 84.4 | 15.6 |
| 26000 | 87.5 | 12.5 |
| 28000 | 90.1 | 9.9 |
| 32000 | 93.4 | 6.6 |
| 36000 | 95.6 | 4.4 |
| 40000 | 97.0 | 3.0 |

Using the proper GPC software, a calibration curve can be obtained using the percentages of mass fraction vs. molecular weight, which are a property of the calibrant material, theoretically independent of the chromatographic system used. In principle therefore, the broad standard calibrant should be transferable to any SEC column for which the sample is fully included. Methods 10 and 11 give reasonable agreement with Method 1 across most of the range of heparin samples in the panel, but less good agreement than do light-scattering Methods 8 and 9. Transference of this calibration method to column types other than those specified in the monograph cannot be guaranteed, and is particularly poor for column set C in this study (Methods 5, 6 and 7), but appears to work best when used for heparin samples with molecular weight distributions within the current USP acceptance criteria.

Finally, the different source heparin comparison. The two porcine mucosal heparins G11597 and G11753 have average Mw near to 16000 Da, a typical value for heparin sodium as previously

determined and close to the characteristic value of 16000 Da for the USP Heparin Sodium Identification RS[93,94]. They also resulted with an M24000 value of about 10%, and the ratio M8000–16,000/M16,000–24,000 is about 1.5. Two bovine lung heparins G11595 and G11596 have lower molecular weight distribution, outside the acceptable range for heparin sodium at about 13500 Da. This is consistent with values determined for bovine lung heparins dating from the 1950s to the 1990s[98].

For the 20 bovine mucosal heparins, variability between individual samples is like that for porcine heparin before introduction of molecular weight acceptance criteria, as determined previously[93]. Three samples (G11745, G11751 and G11752) have Mw higher than 19000 Da, and the same three samples have more than the USP Heparin sodium Identification monograph limit of M24000 (>20%). G11752, the highest Mw sample analyzed, also has a low value for the ratio M8000–16000/M16000–24000. The observed differences for the heparin panel samples are likely to originate from variant manufacturing protocols, though variations in the source tissues due to climate, nutrition, etc. are also possible[95].

### 3.2.5. Conclusions

This study has two main aims, the first to compare the performance of different chromatographic conditions for the analysis of heparin with the official pharmacopoeial method, and the second one to compare a panel of 22 lots of bovine unfractionated heparins (20 from intestine and 2 from lung) to 2 porcine unfractionated heparins in terms of molecular weight distribution, to demonstrate the similarity of samples deriving from different sources.

The work started with the assessment of the suitability of the selected chromatographic conditions, in terms of good columns set's resolution and temperature or mobile phase changes in both elution time or molecular weight distribution, and for this part a heparin sample was analyzed. The results showed that all the chromatographic conditions tested were able to separate satisfactorily the sample from mobile phase and other salts, although with different resolution performances and with minor changes in elution times; overall, we consider the tests satisfying and all columns benches under investigation suitable for the analysis. Moreover, bearing in mind that one of the focus of this work was to obtain acceptable chromatographic profiles sufficient to correctly evaluate the molecular weight distribution, bypassing the silica-based columns problem of a very short life time and

many problems of compatibility with samples, we can say that the use of polymeric-based columns could be considered an improvement.

Alternative SEC methods for molecular weight analysis of heparin sodium give varying degrees of comparability with the USP monograph method. Use of the USP Heparin Sodium Molecular Weight Calibrant RS with long-lived polymer-based columns gave comparable results with the USP monograph method for samples within the current acceptable range of heparin sodium samples; some methods using polymer-based columns with Light Scattering detection gave good agreement throughout the full range of heparin samples investigated in this study. One of the most critical points in the analysis with Light Scattering detector is the use of the correct dn/dc value, a parameter that is a function not only of the sample but also of the chromatographic conditions, and this is the base of the differences observed in molecular weight distribution results[93]; for this reason, two different dn/dc values were used, as reported in 3.2.3 section, in particular 0.13 for methods involving $NaNO_3$ 0.1 M + 0.05 % $NaN_3$ mobile phase, while 0.128 for methods involving $NH_4Ac$ 0.1 M + 0.02 % $NaN_3$ mobile phase. Both values were previously experimentally calculated in Ronzoni Institute.

Results of the whole 24-heparins panel shows that for samples deriving from bovine intestine the average molecular weight is like those of porcine mucosal heparin samples, but with a wider variation from sample to sample, probably reflecting differences in manufacturing methods for heparin from a single species and tissue source. Some molecular weight values fall outside current USP acceptance criteria for heparin sodium. Bovine lung heparin samples were lower in average molecular weight than mucosal heparin, as has been reported in the past[98].

## 3.3. In-depth molecular weight distribution evaluation of Sulodexide.

### 3.3.1. Introduction

Sulodexide (SLDX) is a heparinoid obtained from porcine mucosa by a patented process[99], described as a highly-purified mixture of 80% fast-moving heparin (Fm-Hep), and 20% dermatan sulfate (DeS); it is presently marketed as a drug in Italy, Spain, Eastern Europe, and in the countries of South America and Asia for the treatment of chronic venous disease (CVD), of venous ulcers and of arterial and cardiovascular disease[100–102]. The Fm-Hep fraction has a mean molecular weight of about 7 kDa,

with properties somewhat closer to those of LMWHs, and compared to UFHs has a lower sulfation degree and a less effect on global coagulation tests and a lower degree of pro-hemorrhagic effects[103]. This fraction confers to SDLX other major differences from UFH, including longer half-life and especially oral bioavailability. Similar to "normal" heparin, Fm-Hep consist in a 1,4-linked repeating disaccharide units containing an uronic acid, mainly α-l-iduronic (IdoA) or β-d-glucuronic (GlcA) acids, and a α-N-acetyl-glucosamine (GlcNAc) or more frequently a α-N-sulfated-glucosamine (GlcNS); the main repetitive units could be O-sulfated in position 2 of the IdoA and in position 6 and/or rarely in position 3 of the glucosamine residue[104].

DeS has a mean molecular weight of 25 kDa and it is composed, as a major disaccharide sequence, of a β-d-galactosamine-N-acetylate-4-sulfate (GalNAc4S), that can be alternatively or additionally sulfated in position 6, and an IdoA, sulfated in minor sequence in position 2; the two residues are joined by β 1,4 or 1,3 linkages[105]. DeS has been demonstrated to inhibit thrombus formation and growth in different experimental models of venous thrombosis, but unfortunately there is a paucity of experimental data available on the effect of DeS on arterial thrombus formation in respect to heparin[106]. However, in a model of arterial thrombosis in rats, the effects of a low and high molecular weight DeS, of SDLX, and of LMWH and UFH, were compared, resulting in an effectiveness of DeS as an inhibitor of arterial thrombosis without inducing bleeding complications[106]. DeS was also clinically active in the prevention of postoperative deep vein thrombosis in humans[107]; moreover, recent evidence highlighted a novel biological action of DeS, namely inhibition of matrix metalloproteinases (MMP), which play a key role in extracellular matrix (ECM) remodeling, thus also conferring protective effects to SLDX against vascular wall damage and inflammation in chronic venous diseases (CVD)[108,109]. More recently, it has also been found that DeS may act as an adjuvant factor for initiating and accelerating wound healing[110].

The coexistence of Fm-Hep, with affinity for antithrombin III (AT), and of DeS, with affinity for heparin cofactor II (HCII), confers to SLDX various biological activities, such as lipasemic, anticoagulant, anti-Xa, HCII, APTT determined against the IV International Standard of Heparin, and antithrombotic activity[104]. Thrombin inhibition by the simultaneous activation of AT and HCII would give to SLDX greater efficacy than heparin in preventing thrombus formation, such that a lower dosage of SLDX can achieve an equivalent antithrombotic effect[111]. SLDX can undergo extensive absorption by the vascular endothelium, and has the great advantage of oral, subcutaneous and intravenous

administration[111]. In preclinical studies, SLDX administered parenterally displays an antithrombotic action similar to that of heparin but associated with fewer alterations of the blood clotting mechanisms and tests, thus being much less conducive to bleeding risk than heparin[112]. When given orally, SDX is associated with minimal changes in classic coagulation tests but maintains a number of important effects on the structure and function of endothelial cells (EC), and the intercellular matrix, including prevention or restoration of the integrity and permeability of EC, counteraction versus chemical, toxic or metabolic EC injury, regulation of EC–blood cell interactions, inhibition of microvascular inflammatory and proliferative changes, and other similar effects, thus allowing oral SDX to be considered as an endothelial-protecting agent[113]. Many clinical studies have demonstrated the safety and efficacy of SLDX, not only for the prophylaxis and treatment of thromboembolic diseases but also for the treatment of diabetic nephropathy[104]. Although SLDX has raised a notable interest as antithrombotic drug only a few structural and biochemical data are available in literature[114].

### 3.3.2. Aim of the work

The aim of the present work was to provide a fine evaluation of the molecular weight distribution of SLDX and of its components, obtained by HP-SEC-TDA technique using a Light Scattering detector[115], and by conventional calibration method with a Refractive Index detector.

### 3.3.3. Materials and methods

#### 3.3.3.1. Samples in analysis

Three different SLDX commercial samples were analyzed, and by enzymatic digestion of one SLDX sample, the single components were isolated; in addition, three mixtures of a Hep fraction and of a DeS fraction in different proportions, were prepared for molecular weight determination methodic comparison. The corresponding Ronzoni codes are reported in Table 3.3.1.

**Table 3.3.1 Samples in analysis**

| Sample type | Ronzoni code |
|---|---|
| SLDX 1 | A5192 |
| SLDX 2 | G10088 |
| SLDX 3 | G12512* |
| Fm-Hep | G12824_A |
| DeS | G12909_Fr1 |
| Heparin fraction | G13066 |
| DeS fraction | G13805_C |
| DeS/Hep mix 1 (7/3 w/w) | G14202 |
| DeS/Hep mix 2 (5/5 w/w) | G14203 |
| DeS/Hep mix 3 (3/7 w/w) | G14204 |

*From this sample, G12824_A and G12909_Fr1 were obtained by enzymatic digestion.

### 3.3.3.2. Enzymatic digestion

Digestion of G12512 with Chondroitinase ABC

100 mg of sample were dissolved in 50 ml of 50 mM Na phosphate/50 mM Na acetate buffer, pH 8 and incubated with 0.7 IU of Chondroitinase ABC for 48 h at 37 °C, added in three times. The digestion was inactivated by boiling for 5 min followed by filtration with a cellulose acetate, 0.2 μm cut-off.

Digestion of G12512 with heparinase III

250 mg of sample were dissolved in 2.5 ml of 2 mM Ca/50 mM Na acetate buffer, pH 7.4 and digested with 4U of Heparinase III for 48 h at 37 °C, then the digestion was inactivated by boiling for 5 min followed by filtration with a cellulose acetate, 0.2 μm cut-off. Then, about 250 mg of sample were dissolved in 50 ml of water and kept in a cold bath and 57 mg of $NaNO_2$ were added. The pH of the solution was corrected to 2 with HCl and after 30 min was readjusted to neutrality with NaOH. Then, 78 mg of NaBH4were added and the pH was corrected to 3 with HCl for ten minutes in a cold bath, then readjusted again to 7.

### 3.3.3.3. Chromatographic conditions

For both methods, a Viscotek TDA model 305 (Malvern Panalytical Instruments, UK), equipped with Refractive Index, Right Angle Light Scattering and Viscometer was used, and chromatograms acquisition/elaboration was performed with the software dedicated OmniSEC version 4.6.2. SLDX samples, the isolated single components and the three Hep/DeS mixture were equally injected at about

5 mg/ml, while the two species fractions for calibration curves construction were injected in a concentration range between 2 and 7 mg/ml for respectively higher and lower molecular weights.

Light Scattering calibration conditions

Chromatographic conditions were set up using TSKG2500PWXL + TSKG3000PWXL columns with an aqueous solution of 0.1 M $NaNO_3$ added with 0.05% $NaN_3$ pre-filtered onto 0.22 μm nylon filter (Millipore), used as mobile phase at a flow rate of 0.6 ml/min and 40 °C; 100 μl of each sample were injected. G12512 was also analyzed using silica columns (TSKG4000SWXL + TSKG3000SWXL columns), for column performance comparison, with an aqueous solution of 0.1 M $NH_4Ac$ added with 0.02% $NaN_3$ pre-filtered on 0.22 μm nylon filter (Millipore) as mobile phase and by maintaining the same operating conditions, with the only exception of instrument temperature (30 °C); the difference was due to silica columns temperature tolerance, that is at least 30 °C. For instrument calibration, a pullulan standard was used (PolyCAL-Pullulan57K standard, Malvern Panalytical Instruments, UK).

Conventional calibration conditions

Chromatographic conditions were set up as for TSKG2500PWXL + TSKG3000PWXL columns configuration reported above; to perform the instrument calibration, a pullulan standard was used (PolyCAL-Pullulan57K standard). The conventional calibration curves were built using at least 5 Hep fractions and 6 DeS fractions, previously obtained at the Ronzoni Institute by size-fractionation of respectively a porcine UFH (G9850) and of G12909_Fr1, which codes and already characterized molecular weights at peak (Mp) are reported in Table 3.3.2.

**Table 3.3.2 Hep/DeS fractions codes for calibration curves construction.**

| Sample type | Ronzoni code | Mp (kDa)* |
|---|---|---|
| DeS fraction | D24 | 38.4 |
| DeS fraction | D30 | 32.5 |
| DeS fraction | G13805_B | 25.5 |
| DeS fraction | G13805_D | 14.5 |
| DeS fraction | G13805_E | 9.4 |
| DeS fraction | G13805_F | 4.9 |
| Hep fraction | G13062 | 40.6 |
| Hep fraction | G13064 | 19.9 |
| Hep fraction | G13065 | 13.8 |
| Hep fraction | G13066 | 9.7 |
| Hep fraction | G13067 | 6.3 |

*Molecular weight reported is the average value of a double injection of each sample.

To assess the suitability of the two calibration curves, G9850 and G12909_Fr1 were injected and analyzed; furthermore, G12512 was analyzed as system suitability sample for Hep/DeS mixture analysis.

### 3.3.4. Results and Discussion

3.3.4.1. SLDX and its components molecular weight distribution evaluation by HP-SEC-TDA technique

SLDX samples molecular weight distribution

Analysis of molecular weight distribution was performed using the equipment reported in Materials and methods section. Chromatographic profiles of three SLDX samples are shown in Figure 3.3.1.

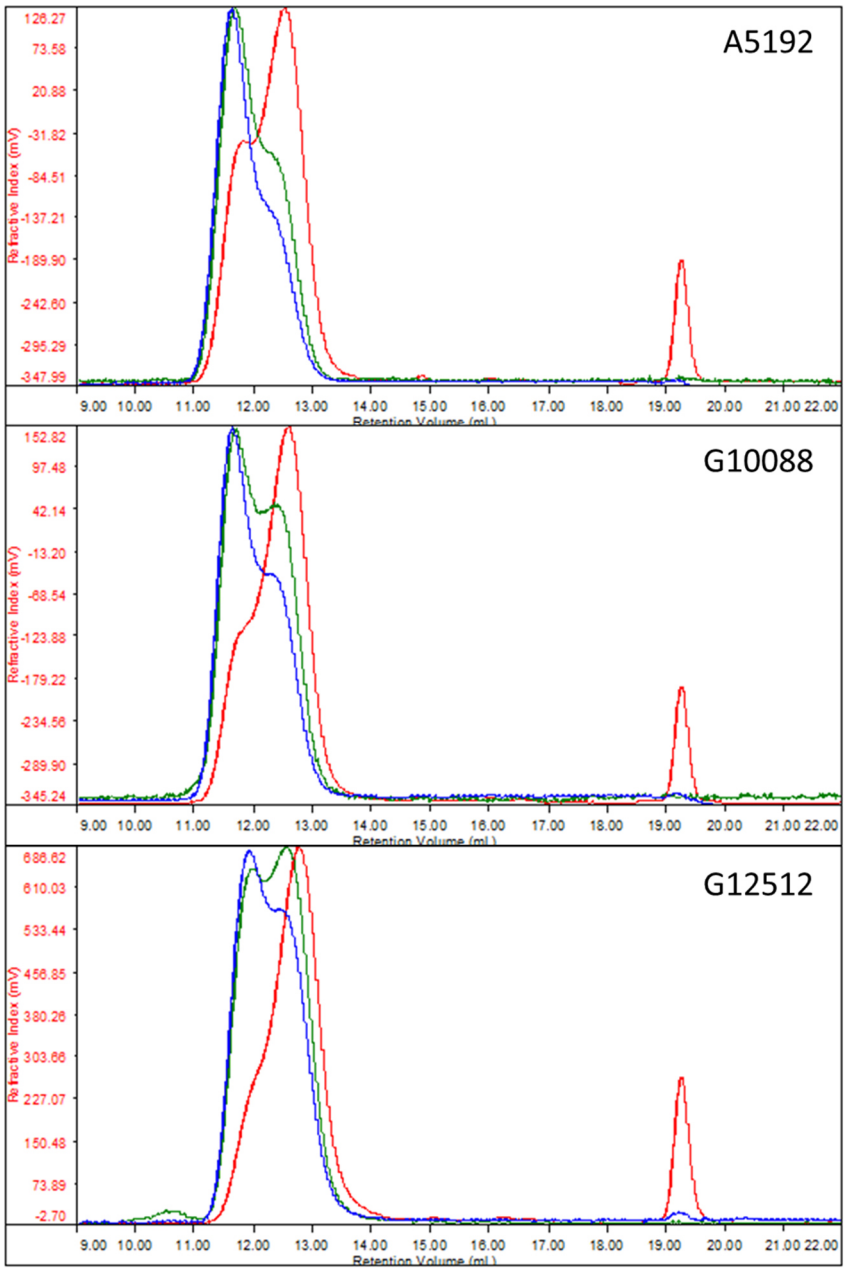


**Figure 3.3.1 SLDX samples chromatographic profile (Red, Refractive Index; green, Light Scattering; blue, Viscometer).**

Chromatograms were elaborated both integrating the whole peak and separating DeS from Fm-Hep profiles. Molecular weight distributions were obtained applying different refractive index increment (dn/dc) values, precisely 0.125[78] to DeS profile and 0.13[95] to Fm-Hep, by using RALS detector and considering the value of concentration determined by Refractive Index. For the whole sample, a dn/dc of 0.129 was used, as a result of a weighted average of the two components weight percentages (approximately 20% of DeS and 80 % of Fm-Hep).

As shown by the chromatographic profiles, each detector reveals two components, the first one attributed to DeS (elution volume at about 11.8 ml), the second one to Fm-Hep (elution volume at about 12.9 ml), which appear differently resolved depending on their molecular dimension and relative amount. At this stage, the attribution was alleged taking into account that the DeS species has a higher molecular weight by literature than the Fm-Hep one[103].

For the whole peak integration, the average results of two analyses, in terms of number average molecular weight (Mn, Da), weight average molecular weight (Mw, Da), polydispersity index (Mw/Mn) and intrinsic viscosity ([η], dl/g) are reported in Table 3.3.3; in the same Table, the percent weight recovery of the whole peak calculated as difference between theoretical and experimental concentration is also reported together with the Mw value of the two components and the percentual amount of separated fractions (Wt. Fr.%); these latter values were estimated as the relative percentage of refractive index areas of DeS or Fm-Hep component vs the whole peak.

**Table 3.3.3 SLDX samples results (inside brackets, the related standard deviations)**

| Sample | Peak | Mw (Da) | Mn (Da) | Mw/Mn | [η] (dl/g) | Wt. Fr. % | Recovery % | Column type |
|---|---|---|---|---|---|---|---|---|
| A5192 | 1 | 28800 (521) | - | - | - | 32.3 | - | Polymeric |
| | 2 | 9200 (270) | - | - | - | 67.7 | - | |
| | Whole peak | 15000 (32) | 9000 (31) | 1.67 | 0.260 | | 92.0 | |
| G10088 | 1 | 27200 (1558) | - | - | - | 25.6 | - | Polymeric |
| | 2 | 8500 (415) | - | - | - | 74.4 | - | |
| | Whole peak | 12900 (2) | 8300 (93) | 1.56 | 0.215 | | 88.3 | |
| G12512 | 1 | 30800 (986) | - | - | - | 19.9 | - | Polymeric |
| | 2 | 9700 (240) | - | - | - | 80.2 | - | |
| | Whole peak | 13500 (37) | 9400 (81) | 1.44 | 0.213 | - | 101.4 | |
| | 1 | 31800 (1238) | - | - | - | 16.9 | - | Silica |
| | 2 | 10600 (204) | - | - | - | 83.1 | - | |
| | Whole peak | 13500 (160) | 10500 (78) | 1.29 | 0.203 | | 92.7 | |

No weight distribution results or [η] were attributed to DeS and Fm-Hep species, due to the great uncertainty in integration of the chromatographic profiles and in fact the related Mw values resulted with quite high standard deviations.

For A5192, peak 1 is clearly detected by all detectors, including refractive index since it is represented for about 30% (see Table 3.3.3), while for G12512 it is revealed as a shoulder due to its lower

content, estimated close to 20%; accordingly, for G10088 the peak 1 elutes as an half-way between a clearly detected peak and a shoulder and in fact its content is approximately 25 %, value quite perfectly averaged compared to the other two. The molecular weight parameters of the two components were determined by separating SLDX profile at about 12 ml, where DeS and Fm-Hep peaks overlap. By considering the whole peaks, the Mw of the three samples ranged from 12.9 to 15.0 kDa, with a polydispersity of 1.44–1.67. Looking at separated peaks, in all samples the heparin component was the smaller one, with a Mw ranging from 8.5 to 9.7 kDa, whereas DeS had a notably higher Mw, ranging from 27.2 to 30.8 kDa. For the whole peak intrinsic viscosity raised mainly with the increase of DeS relative content. Samples recovery are all higher than 88%, value that can be considered acceptable, taking into account the polysaccharide hygroscopicity.

Since G12512 exhibited a very poor resolution of the two GAG components by refractive index detector, it was also analyzed by employing silica gel columns, which are known to have higher resolution performances, and the related chromatographic profile is reported in Figure 3.3.2; the molecular weight distribution results were reported in Table 3.3.3.

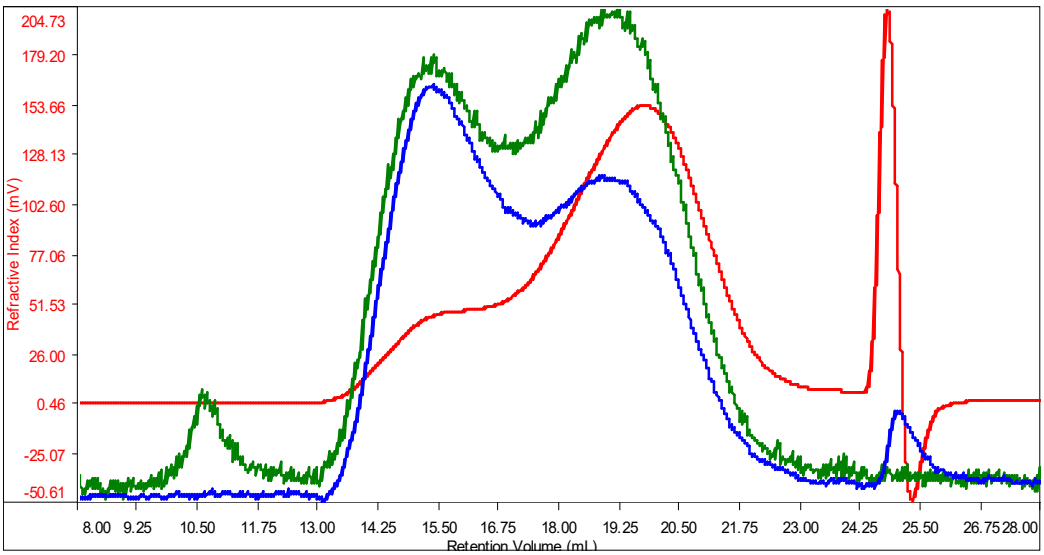


**Figure 3.3.2 G12512 chromatographic profile obtained with silica columns (Red, Refractive Index; green, Light Scattering; blue, Viscometer).**

With such a stationary phase, chromatographic profile of G12512 exhibited a greatly improved separation of DeS and Fm-Hep with all detectors, including refractive index. Nevertheless, molecular weight values turned out to be highly similar to those obtained with polymeric columns, both for whole peak and for separated components. The present results demonstrate that the two

chromatographic conditions are comparable, as reported previously (see section 3.2). Results of the analyses performed in duplicate were very similar each other, proving the reproducibility of the technique.

Isolated components molecular weight results

The isolation of the SLDX components was obtained as reported in 3.3.3 section (see Enzymatic Digestions); for DeS separation, briefly, 250 mg of G12512 were first digested with Heparinase III for 48 h, then filtered after enzyme inactivation. The obtained sample was then treated with nitrous acid and subsequentially reduced with $NaBH_4$, process followed by a chromatographic purification on a TSKHW40 column, obtaining 91.7 mg of G12909_Fr1. The isolation of the Fm-Hep species was obtained treating 100 mg of G12512 with Chondroitinase ABC that was added after three different times (0, 6 and 28 h); again, after the enzyme inactivation, sample was purified on a TSKHW40 column, recovering 79.4 mg of G12824_A. As a final step, it was verified by NMR spectroscopy the nature of the two isolated components, as well as the absence of DeS or Fm-Hep residues in the two different samples.

The evaluation of the molecular weight distributions on isolated G12909_Fr1 and G12824_A was obtained in the same polymeric chromatographic conditions of the SLDX samples; the average results of two injections in terms of number average molecular weight (Mn, Da), weight average molecular weight (Mw, Da), polydispersity (Mw/Mn) and intrinsic viscosity ([μ], dl/g) are reported in Table 3.3.4, while the chromatographic profiles of the two components are reported in Figure 3.3.3, as an overlay with the starting G12512 sample. In this case the same molecular weight parameter showed for the three SLDX were evaluated, since each sample contains only one GAG species.

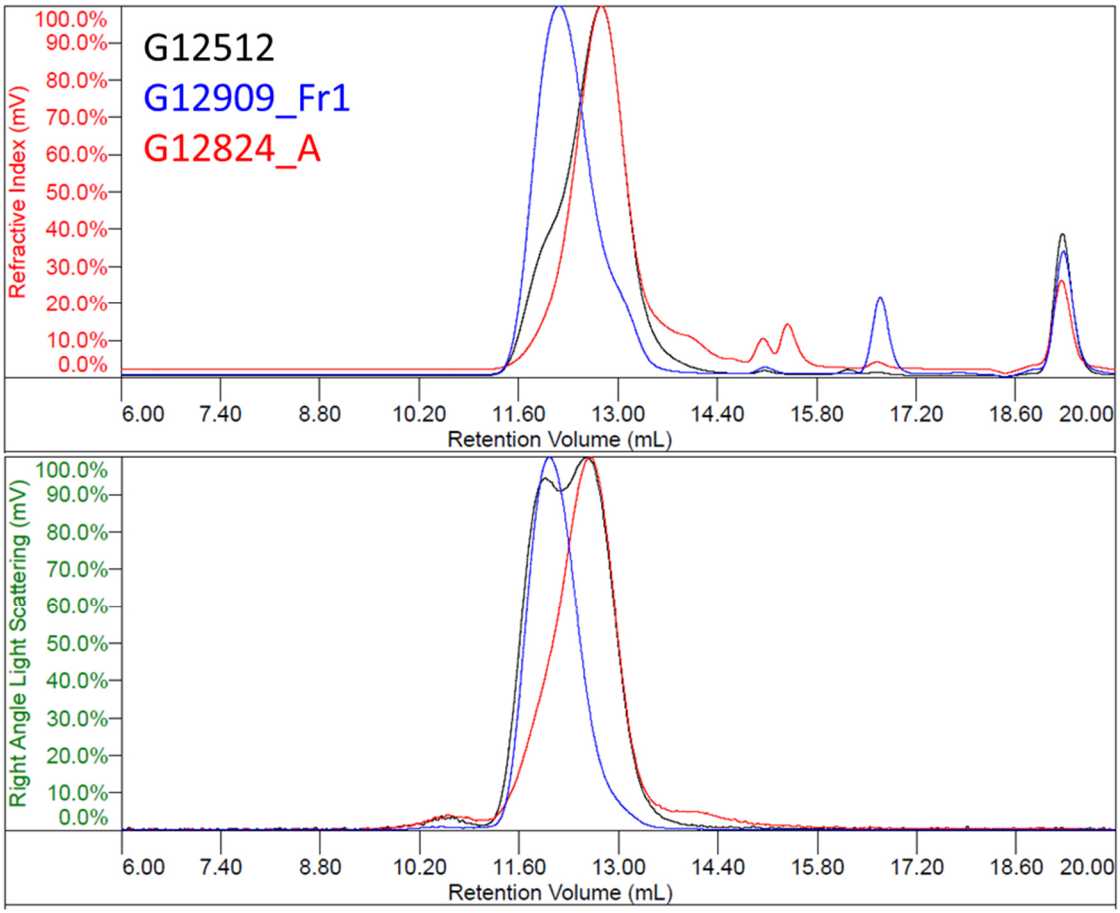


**Figure 3.3.3 Isolated components profiles' overlay with starting G12512.**

**Table 3.3.4 Isolated components molecular weight distribution results.**

| Sample | Mw (Da) | Mn (Da) | Mw/Mn | [η] (dl/g) | Recovery % |
|---|---|---|---|---|---|
| G12909_Fr1 | 21500 | 16900 | 1.28 | 0.403 | 103.2 |
| G12824_A | 10900 | 8300 | 1.32 | 0.147 | 104.0 |

Molecular weight distribution values obtained turned out to be a slightly different from those estimated on the whole mixture, in particular the Mw values of both the components were about the 32% lower and about the 10% higher respectively. This apparent discrepancy is greatly due to peak overlapping of the two components in the SLDX, so that the lowest molecular weight chains of the DeS and the highest molecular weight chains of Fm-Hep are underestimated, influencing the whole distribution; the degree of overlapping phenomenon is clearly visible in Figure 3.3.3, in particular by the Refractive Index chromatograms (upper panel). Also, the viscosity values resulted slightly lower and higher for respectively G12909_Fr1 and G12824_A, due to the correspondent changes in the Mw of the two components.

3.3.4.2. Conventional *vs* absolute molecular weight distribution evaluation of *ad hoc* prepared DeS/Hep mixtures

For polysaccharides that are copolymers or are in mixture like the SLDX, some caution is advised when interpreting the molecular weight distribution obtained by a Light Scattering method, because of the requirement specific dn/dc parameters for the two species, which chromatographic profile could be affected by overlapping phenomena, as shown in the present case. As a result, the Mw obtained could be not completely correct.

To try to overcome to this problem, a conventional calibration method, for which the obtained Mw is only a function of the retention time, was set up and two different relative calibration curves, one for the DeS and one for the Fm-Hep species, were built.

Calibration curves construction and suitability

The Hep and DeS fractions selected (see Table 3.3.2), were analyzed by HP-SEC-TDA technique and used for the relative calibration curves building (third order), that are reported in Figure 3.3.4, while their overlay is reported in Figure 3.3.5.

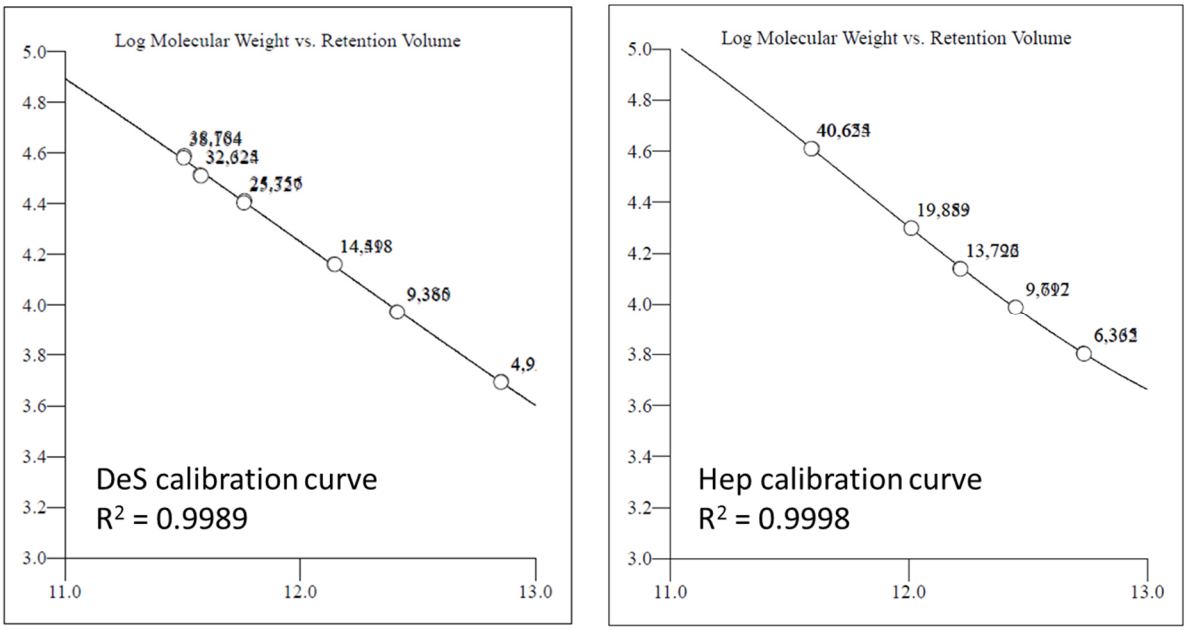


**Figure 3.3.4 Conventional calibration curves results.**

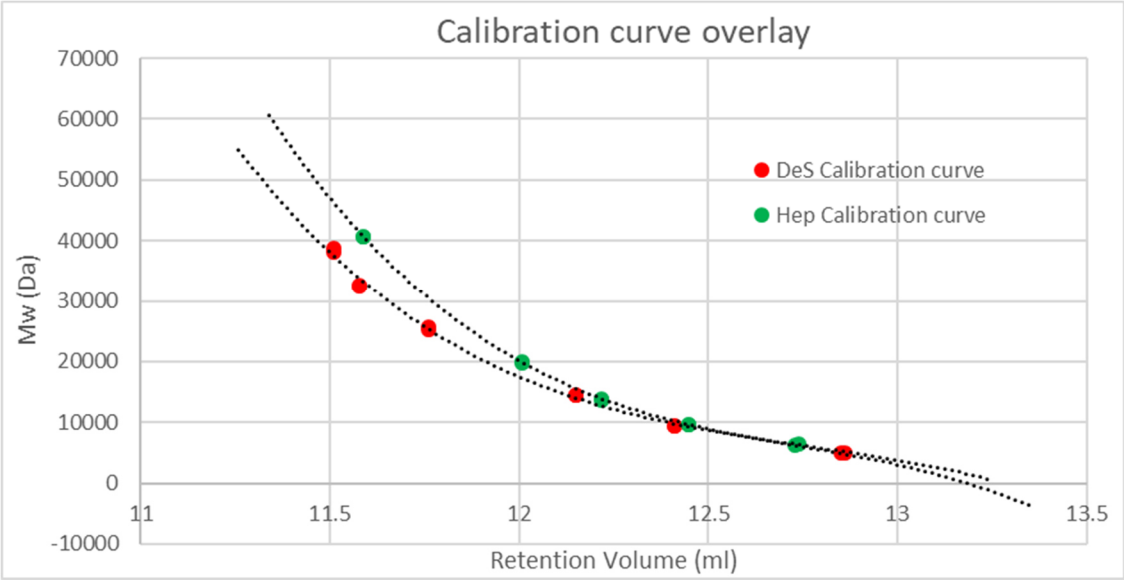


**Figure 3.3.5 Calibration curves overlay**

By the overlay view of the two calibration curves, is highly probable that little conformation difference occur between the two species and in fact it is possible to note that although G13062, a Hep fraction with a Mp of 40.6 kDa, elutes after D24, a DeS fraction with a slightly lower Mp (38.4 kDa), and the same observation can be done for G13066 (Hep, Mp=9.7 kDa) and G13805_E (DeS, Mp=9.4 kDa).

Although a very good result in linearity, as $R^2$ value, was obtained for both the calibration curves, their suitability in correctly determine the molecular weight distribution was tested analyzing the G12909_Fr1 and G9850 for respectively DeS and Hep curves, and the results were compared to the related Light Scattering method (see Table 3.3.5), in terms of weight average molecular weight (Mw, Da), number-average molecular weight (Mn, Da) and polydispersion index (Mw/Mn). Furthermore, the percentual coefficient of variation (CV %) was calculated on Mw value for the two system suitability samples, in order to statistically evaluate the difference in Mw calculation; CV % was evaluated as the standard deviation/average % ratio.

**Table 3.3.5 System suitability results**

| | *Calibration* | *Mw (Da)* | *Mn (Da)* | *Mw/Mn* | *Mw CV %* |
|---|---|---|---|---|---|
| *G12909_Fr1, DeS* | Conventional | 22000 | 13900 | 1.58 | 1.63 |
| | HP-SEC-TDA | 21500 | 16900 | 1.28 | |
| *G9850, Hep* | Conventional | 18200 | 12700 | 1.43 | 0.39 |
| | HP-SEC-TDA | 18100 | 13900 | 1.30 | |

Looking at the results, the main difference was in the Mn value, and of course on the related poly-dispersion index, that is lower for both the conventional calibration calculations, particularly for the DeS sample. This observation is justifiable by the fact that the two detectors used for the molecular weight distributions had different sensitivities due to the low signal-to-noise ratio of, in particular, the Light Scattering detector; this problem is most often encountered on the low molecular weight side when light scattering signals have a lower sensitivity than a concentration-sensitive detector such as the Refractive Index, so with by TDA method the Mn value cannot be determined with great accuracy[116]. On the other hand, the Mw obtained are very similar, reaching in both cases a CV % significantly lower than 5 %, which is a limit under which two values are considered not different[95]. After the suitability assessment of the two calibration curves, the G12512 SLDX sample was injected again and tested to evaluate the capability of the relative method to evaluate the correct molecular weight distribution of the two singular components (integration reported in Figure 3.3.6); the related results are reported in Table 3.3.6, in terms of Mw and CV % calculated as the standard deviation/average % ratio.

**Table 3.3.6 Test on G12512 components results.**

| | Calibration | Mw (Da) | CV % |
|---|---|---|---|
| **DeS** | HP-SEC-TDA | 29200 | 3.08 |
| | Conventional | 30500 | |
| **Hep** | HP-SEC-TDA | 9600 | 1.46 |
| | Conventional | 9800 | |

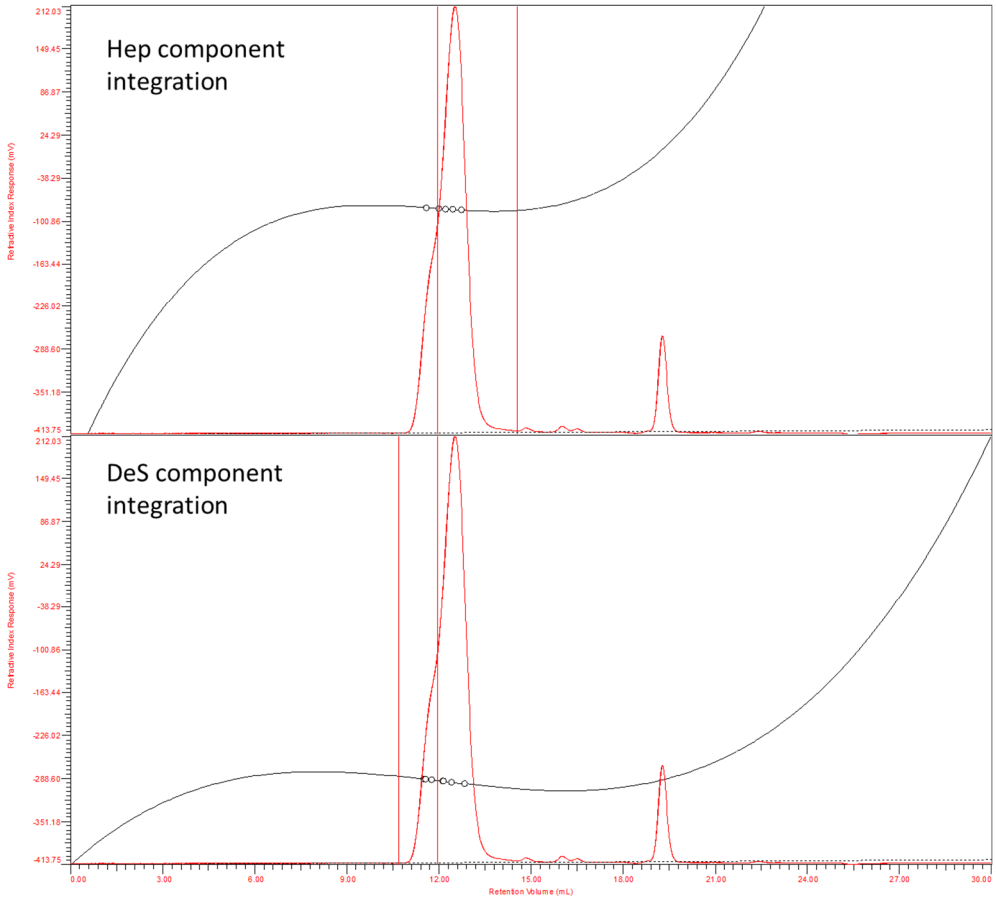


**Figure 3.3.6 Integration of single SLDX components chromatographic profiles, overlayed with the related calibration curves.**

As shown in Figure 3.3.6, the integration of the two single components was obtained "cutting" the SLDX profile in the correspondence of the large shoulder on higher molecular weight chains side, exactly as was done in 3.2.4.2 section; for the molecular weight distribution, then, the conventional curve associated to the related polysaccharidic species was applied, and the results shows that this method is not significantly different from the HP-SEC-TDA one, with CV % values, calculated on the Mw data, clearly lower than 5 %. The major discrepancy from the absolute calibration is found for the DeS component, for which 3.08 CV % was obtained, and in fact looking at its calibration curve it is appreciated that a higher molecular weight point would have been needed; unfortunately, it was not possible to quantitatively separate such a high molecular weight component, but however we considered the evaluation obtained enough for our purpose. On the other hand, the Hep component suffered the same DeS problem and, also in this case, probably the addition of another point in the curve, this time a lower Mw one, would have been resolutive, but as for the DeS species, it was not possible to quantitative obtain the desired Mw Hep fraction.

A final consideration on the data just discussed is about the Mw results obtained by the re-injection of G12512, for which a slight discrepancy between the TDA results obtained is found comparing the single species values reported in Table 3.3.3 and the ones in Table 3.3.6; this observation should be taken as the demonstration of how the chromatographic profile overlay phenomenon of the two SLDX components could influence the final result as of a sort of casual error done in setting the integration limits. In addition, bearing in mind the basic differences of the two methods applied, mainly in terms of how the molecular weight distribution is evaluated, we can at least consider the two conventional calibration curves greatly suitable for further investigation on polysaccharides mixture.

Hep and DeS mixture chromatographic comparison and molecular weight distribution evaluation.

A DeS (G13805_C) and a Hep (G13066) samples of respectively 21100 and 10000 Da, were selected for making *ad hoc* mixtures of them, with the aim of studying the chromatographic changes of the two components in solutions when present at different concentrations. The two samples were chosen for the Mw similarity to isolated components of the SLDX previously investigated.

Three DeS/Hep mixture were created by weighing separately the two components and then collecting them together before the dissolving step. The Ronzoni codes of both starting materials and final samples and the nominal w/w ratio of the two species are reported in Table 3.3.1, while their exact weight (mg) for each mixture is reported in Table 3.3.7.

**Table 3.3.7 Exact weight (mg) of DeS/Hep species in each mixture.**

| | **G14202** | **G14203** | **G14204** |
|---|---|---|---|
| **G13805_C, DeS** | 7.86 mg | 5.55 mg | 3.02 mg |
| **G13066, Hep** | 2.72 mg | 4.58 mg | 6.98 mg |

Samples were injected, and the refractive index overlay of the three samples is reported in Figure 3.3.7.

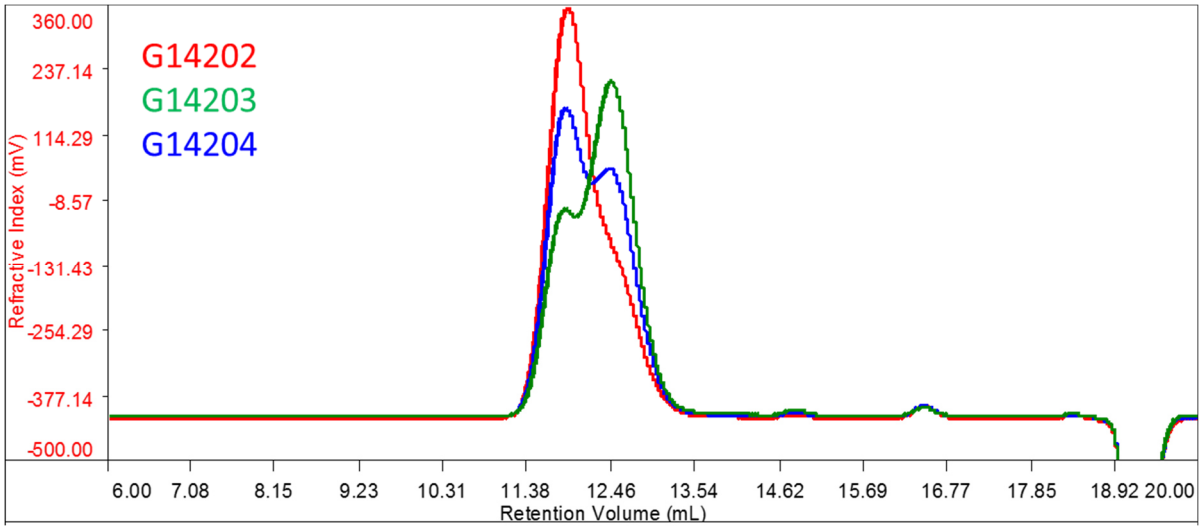


**Figure 3.3.7 DeS/Hep mixture refractive index overlay**

It is appreciable how the sample profile change on the basis of the mixture component, so as the DeS species decrease and the Hep one increase, respectively a lowering and a rising of the related peak can be observed. Anyway, all the three profiles provide a separation of the two species. This consideration is not so clearly achieved, instead, for the light scattering overlay, reported in Figure 3.3.8.

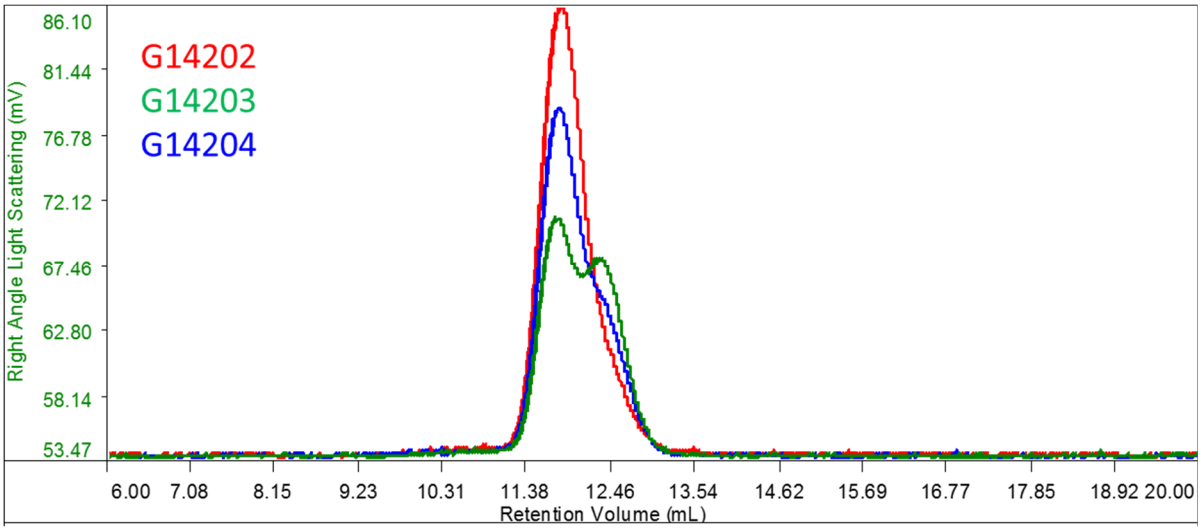


**Figure 3.3.8 DeS/Hep mixture light scattering overlay**

As shown, the decrease of DeS species profile is not directly proportional to the increase of the Hep peak, although the detector scale was normalized, and the concentration of the samples was quite

the same for each injection; moreover, when the Hep component is the minor one (sample G14202) its peak is almost completely overlapped from the DeS one.

The separation of the single components was, so, performed considering both refractive index and light scattering profile, for a better assurance of a correct integration of the two polysaccharides in mixture, and the resulted molecular weight distribution values, in terms of Mw, with the addition of the Mw CV %, is reported in Table 3.3.8. Moreover, the calculated percentual difference on the Mw between G13066 (Hep) or G13805_C (DeS) values and the data obtained by both conventional and absolute calibrations (dMw%) is reported; the exact formula used for this calculation is the following:

$$dMw\% = \frac{std.\,dev.\,(Mw_{st.}; Mw_{calc})}{mean\,(Mw_{st.}; Mw_{calc})} \cdot 100$$

were $Mw_{st}$ is G13066 or G13805_C value and $Mw_{calc}$ is the calculated one. Mw results were rounded to the nearest 100 Da.

**Table 3.3.8 Results on conventional vs absolute molecular weight distribution characterization of DeS/Hep mixtures.**

| Sample | | Calibration | Mw (Da) | dMw% | CV % |
|---|---|---|---|---|---|
| G14202 | DeS | HP-SEC-TDA | 21100 | 0.00 | 2.9 |
| | | Conventional | 22000 | 2.89 | |
| | Hep | HP-SEC-TDA | 9700 | 2.43 | 14.8 |
| | | Conventional | 7800 | 17.22 | |
| G14203 | DeS | HP-SEC-TDA | 21700 | 1.82 | 4.9 |
| | | Conventional | 23200 | 6.76 | |
| | Hep | HP-SEC-TDA | 9600 | 2.58 | 7.2 |
| | | Conventional | 8700 | 9.75 | |
| G14204 | DeS | HP-SEC-TDA | 23300 | 6.84 | 7.0 |
| | | Conventional | 25700 | 13.82 | |
| | Hep | HP-SEC-TDA | 10100 | 0.62 | 2.1 |
| | | Conventional | 9800 | 1.43 | |

By the results, it can be noted that for conventional calibration a tendency to deviate from the starting materials' Mw value was observed, with the very only exception of DeS component in G14202 and of Hep component in G14204; in particular, in the case of the Hep species, the highest variance

is found in sample G14202 (17.22 %) and decreases markedly in G14204 (1.43 %); for DeS, instead, the trend is opposite (respectively 2.89 % and 13.82 % for the two samples). This observation is clearly due the overlap of the elution profiles, that is strongly marked for G14202, sample, as already discussed previously, in particular for the Hep component that eluted with the worst resolution, and this fact leads to the major difference deviation from a starting polysaccharide Mw; indeed, for G13805_C in mixture the widest dMw% is quite lower. This phenomenon flows to the consequent general difficulty in the integration of the two species, creating a possible problem for the use of a conventional calibration method, since it is mainly based on chromatographic resolution and this comment is more evident in the Mw calculation of the Hep component, which is also the one that suffers fairly the profile overlay problem since it appears as a shoulder in the polysaccharides mixtures; not by chance, its dMw % are always higher than the DeS component, with the very only exception of G14204, the sample in which a good resolution was obtained.

On the opposite, apart from the DeS species in G14204, HP-SEC-TDA technique always leads to greatly acceptable Mw values, with CV % significantly low; this means that this calibration does not suffers the problems in the Light Scattering profile resolution, so it is of course the most adequate method for the molecular weight distribution evaluation.

Finally, from the HP-SEC-TDA calibration, the percentual recovery of sample, in terms of % ratio between the theorical concentration and the experimental one, was calculated starting from the weighed singular components reunited for mixtures creations (see Table 3.3.7) and results shows that there is an overestimation and an underestimation in the calculation of the weight percentages calculated respectively by DeS and Hep in the samples G14202 and G14203, and a slight underestimation of DeS in G14204, again due to the overlapping of the chromatographic profiles (see Table 3.3.9).

**Table 3.3.9 Weight percentages calculations**

| | G14202 | G14203 | G14204 |
|---|---|---|---|
| **DeS** | 111.17 | 108.61 | 94.67 |
| **Hep** | 87.46 | 88.59 | 97.35 |

This final consideration is definitely the measure of how the poor resolution of the two components is a problem in the correct evaluation of the molecular weight distribution of polysaccharides mixtures.

### 3.3.5. Conclusions

The goals of this part were the characterization of the molecular weight distribution of three different SLDX samples and of their two components by an absolute calibration method that uses the Light Scattering as the evaluation detector, and an in-depth study of chromatographic methods development for the molecular weight distribution evaluation of polysaccharides in mixture; in particular a conventional calibration and an absolute calibration were taken into account and their results were compared. A first level of investigation, so, was directed to the analysis of the whole drug chromatographic profile, that eluted as a single peak with an evident shoulder on the high molecular weight chains side, corresponding to the DeS species, and a major peak with greater retention time related to the Fm-Hep species. The molecular weight distribution was calculated both integrating the whole profile and "cutting" in the correspondence of the two components separation and results showed a Mw value of whole peak out to be about 13–15 kDa, with a polydispersity of 1.44-1.67, whereas for two singular components ranges of 8.5–9.7 kDa for Hep component, and 27.2 to 30.8 kDa for DeS one, were obtained. Then, isolation of the two species was obtained by selective enzymatic digestions and the individual molecular weight features (roughly 11 kDa for Fm-Hep and 22 kDa for DeS) were obtained. Thanks to the isolation procedure of the two polysaccharides a chromatographic profile overlay of the Fm-Hep on the DeS shoulder was observed, an outcome that leads to variance in the Mw value between the isolated and the in whole drug fraction; in particular, an under- and an overestimation respectively is obtained by the integration of the two species in the whole drug.

The second step was centered on the construction of two different relative calibration curves, one for the Hep and the other for the DeS analysis, by plotting of at least 5 fractions of the two species chromatograms Mw *vs* Retention time. After the evaluation of their suitability, both in terms of linearity and also in terms of correct evaluation of the molecular weight distribution of two system suitability samples (respectively the starting Hep and DeS used for fractions separation), the curves were tested on the G12512 SLDX sample, obtaining quite satisfactorily results in comparison to the TDA results; the CV % calculated on the Mw value resulted from the absolute calibration and the conventional one were indeed very low, index once again of the suitability of the curves. Unfortunately, also in this case the overlay phenomenon was a problem, in particular on the polydispersion index evaluation; anyway, we considered the curves good for study continuing.

Finally, we prepared three DeS/Hep mixtures with different polysaccharides' ratios in order to study how the two species can influence the chromatographic profile and most of all the molecular weight distribution, and we analyzed them using both TDA and conventional calibration methods. The first consideration made was on the chromatographic resolution of the three samples, which underlines how the overlay problem of the two species in mixture leads to underestimation or overestimations of the correct Mw value by above all the conventional method evaluation; in fact, not only the CV % of techniques comparison, but also the calculated difference between the starting material Mw and the experimentally resulted one, demonstrated difficulties in the correct evaluation of the molecular weight distribution by the conventional calibration curves created. Nevertheless, some problems were found also in the calculations with the TDA technique, for which under/overestimations of the recovery % of the fractions in mixture were obtained, index also that some improvements are needed, probably on the chromatographic resolution performances. One try was made, in this sense, using silica columns for G12512 analysis, and due to the very close to polymeric columns results, we did not use that bench for further investigations.

# 4. Characterization of PF4/GAGs complexes

## 4.1. Heparin/PF4 interaction

As mentioned above, the heparin structure is composed of repetitive disaccharidic units, that are ordered at least in three domains: a prevalently sulphated domain (NS-domain), a prevalently acetylated domain (NA-domain) and a mixed one (NS-NA-domain). Of course, at physiological pH, all carboxylic acid and sulphate groups are deprotonated, leading heparin to reach the highest negative charge of any molecule in biology; most of the proteins bind to the NS-domains but the mixed domain, which contribute 20–25% of the polymer chain, also contribute to binding specificity. In view of this negative charge, electrostatic interactions were responsible for the nonspecific binding of proteins, while particular repetitive units sequences in heparin demonstrated a high degree of specificity, and so the heparin-binding to consensus sequences in proteins is a function of the polysaccharide structure, composition and chain length as well as charge[117].

Chemokines are a group of small, cytokine-like proteins with a variety of biological functions including selective recruitment and activation of cells during inflammation, stimulation of leukocyte degranulation and angiogenesis or angiostasis promotion[118–120]. The heparin interactions with chemokines, as well as the interaction with AT(III), described previously, are the best characterized; this interaction has been suggested to play a role in the formation of haptotactic gradients on the surface of endothelial cells and to enhance the local concentration of chemokines in the vicinity of G-protein- coupled receptors[121–123]. Platelet Factor 4 (PF4) is the first member of the chemokine family to be discovered, and it is released from platelets; it exerts several biological properties including hematopoiesis and angiogenesis inhibition, platelet coagulation interference, and host inflammatory response promotion[124]. PF4 exists mainly as a tetramer under physiological conditions and binds to heparin with a very high affinity in a 1:1 ratio[125,126].

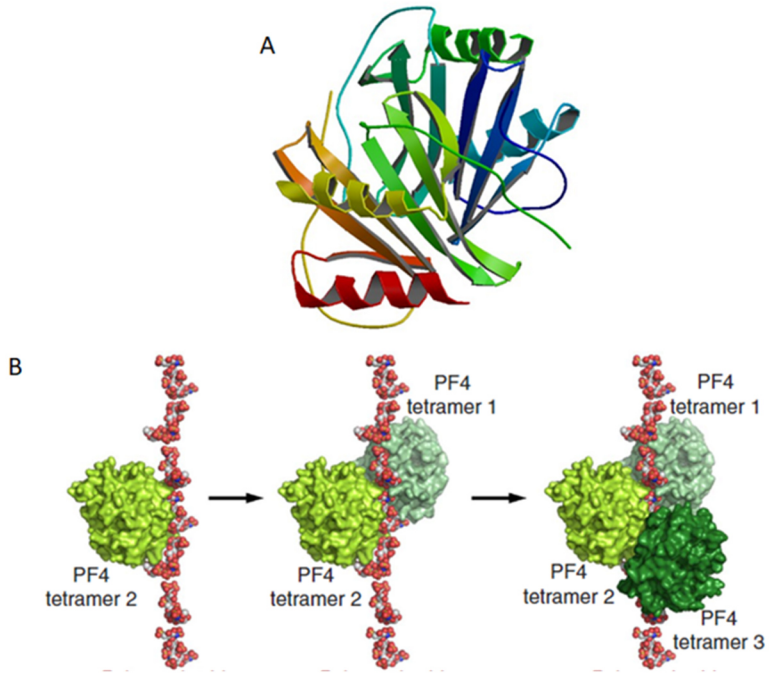


**Figure 4.1.1 A) PF4 tetramer crystal structure[127] and B) PF4 complexed with heparin crystal lattice analysis[128].**

As showed in Figure 4.1.1, panel A, the human PF4 can assume an asymmetric tetrameric configuration; each monomer contains three-stranded antiparallel β-sheets on which an aperiodic N-terminal domain and an amphipathic C-terminal a-helix are folded[127]. The tetrameric structure of PF4 is stabilized not only by salt bridge interactions between dimers AB/CD, but also by the antiparallel β-sheet-like structures in the N termini of dimers AC or BD. Moreover, it has been assumed that the asymmetry of the PF4 tetramer plays a role in heparin binding[129].

Starting from the crystal study of the PF4-Fondaparinux complex, Cai *et al* proposed the Figure 4.1.1 panel B pathway for the formation of the heparin/PF4 complex: heparin first binds to the groove in one PF4 tetramer, and this imparts a local linearized structure on heparin; then, a second PF4 tetramer binding is enhanced. Progression of this process eventuates in the formation of the large antigenic complex in which PF4 tetramers cluster around a semi-rigid linear heparin chain[128]. The authors' presented model is also consistent with previous NMR and site-directed mutagenesis studies[130–132].

It is nowadays well known that PF4 and heparin interactions are exclusively charge dependent; optimal PF4/heparin complex formation occurs when the two compounds are present at certain molar amounts associated with charge neutralization[133–136]. Changes in molar amounts of PF4 or heparin

leading to excess of one component or another results in charge imbalance and increased repulsive forces that affect complex assembly.

The PF4 heparin complex can lead to a dangerous immunologically induced loss of platelets causing a condition called heparin-induced thrombocytopenia (HIT); HIT is the heparin's most clinically relevant non-hemorrhagic complication. It is an immune side effect caused by antibodies that directed recognize the complexes containing heparin and PF4. Although the immune reaction is common (8% to 50%), clinical complications of thrombocytopenia and thrombosis are far less frequent, affecting ~ 0.2% to 3% of patients exposed to the drug in various clinical settings[137,138].

At least, two different HIT types are known, a relatively common nonimmune, clinically harmless type I and a rare immune-mediated, serious HIT-type II. The first type, caused by direct interaction of heparin with the platelet membrane resulting in enhanced platelet aggregation, occurs in approximately 10% of patients treated with heparins, usually within the first few days of treatment[139]. Heparin-induced thrombocytopenia type II, typically occurring 10 to 14 days following the initiation of heparin therapy in about 5% of treated patients, is an adverse immunological effect; in HIT type II, there is the formation PF4/heparin complexes that induce the binding of immunoglobulin G (IgG) antibodies to form immune complexes (ICs) (Figure 4.1.2).

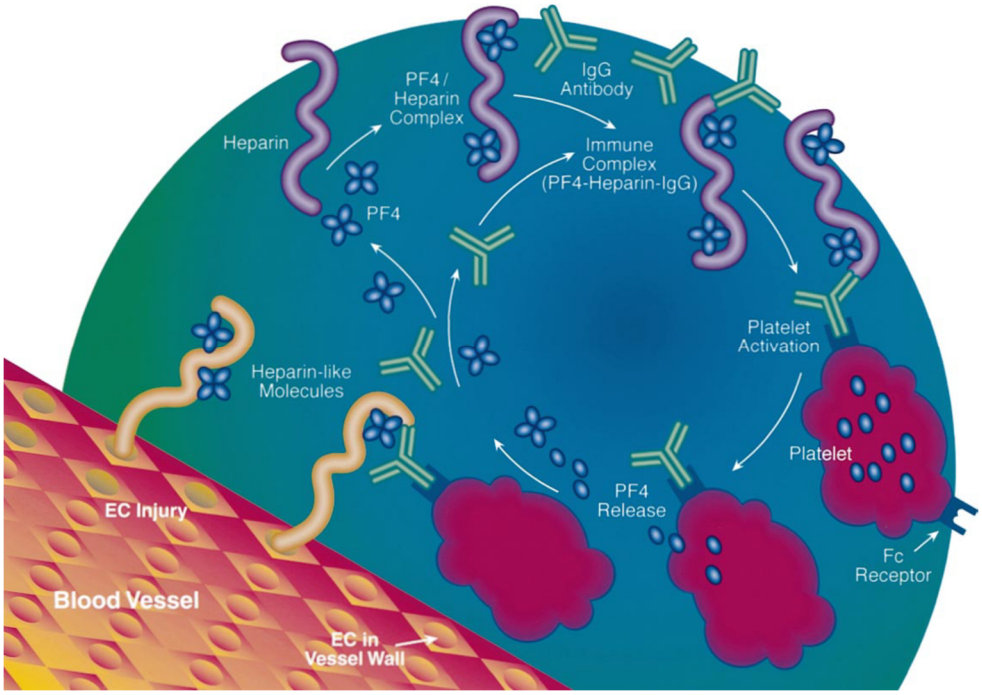


**Figure 4.1.2 HIT Type II mechanism of action**[140]

The IC binding to FcyRIIa receptors on the platelet membrane activates platelets leading to a greater release of PF4, platelet consumption, and the first HIT-type symptoms. The excess of PF4 binds GAGs on endothelial cell membrane to form new PF4 antigens and antibodies causing vascular endothelial injury, leading to thrombi formation and disseminated intravascular coagulation[141]. The antigenicity of the complex depends on the concentration, polydispersion (Pd), sulfation degree (DS), chemical composition, structure of the GAG, and structural and conformational changes of PF4 as suggested by NMR and circular dichroism spectroscopic studies[142,143].

Both HIT types occur more frequently with UFHs than with LMWHs or with the synthetic pentasaccharide, fondaparinux, which does not form antigens with PF4 recognized by HIT antibodies[137,144,145]. UFH and LMWHs produce the same type of PF4 complexes but a different clinical frequency of HIT mainly due to the different sizes and amount of complexes formed. Greinacher et al presented a model for the interaction of LMWH, UFH, and fondaparinux with PF4 taking into account the different plasma concentrations of the GAG anticoagulants[135]. They concluded that smaller PF4/LMWH/IgG complexes crosslink fewer of the platelet FcγRIIa receptors, thereby activating platelets to a lesser degree than the larger PF4/UFH/IgG complexes. This is a likely reason for the reduced breakthrough of HIT-related thrombocytopenia and thrombosis with LMWH treatment among immunized patients.

Asymptomatic patients developing HIT type I in the absence of the heparin-dependent antibody do not require specific treatment. However, it may be difficult to distinguish this condition from early type II; these patients should be closely monitored, and if there is any doubt, heparin should be discontinued[140]. On the contrary, for patients who develop HIT type II the main pinpoint of therapy is the absolute discontinuation of heparin. It is imperative that all potential sources of heparin be avoided, a task that can be difficult given the ubiquity of the drug in the hospital setting. Once heparin is discontinued, the platelet count should begin to increase within 24 to 48 h and reach normal levels by 4 to 5 days[146]. After heparin therapy cessation, clinical management of patients with HIT is with a non–heparin anticoagulant such as a direct thrombin inhibitor or danaparoid followed by a vitamin K antagonist for long-term treatment; alternatively, anti–factor Xa drugs (fondaparinux, rivaroxaban, apixaban) and other non–heparin antithrombotic agents can potentially be used for the treatment of HIT if clinically validated[147].

## 4.2. Biophysical tools for PF4-Heparin complex characterization

In recent years, biophysical tools have gained an important role to complement immunological and functional assays for better understanding the interaction of heparin with PF4[148]. This allowed identification of those features that make PF4 immunogenic (e. g. a certain conformational change induced by the polyanion, a threshold energy of the complexes, the existence of multimeric complexes, a certain number of bonds formed by PF4 with the polyanion) and to characterize the morphology and thermal stability of complexes formed by the protein with polyanions.

In the present work, the PF4/heparin complex characterization was performed by Photon Correlation Spectroscopy (PCS), a very sensitive technique usually used to analyze the size of particles in solution by measuring the Brownian motion and relating this to the size of the particles[136], the Zeta Potential evaluation (Zp), that can be calculated from the particle's electrophoretic mobility in solution and Isothermal Titration Calorimetry (ITC), a method that can provide, with only one experiment, thermodynamic parameters like enthalpy ($\Delta$H), entropy ($\Delta$S), free Gibbs' energy ($\Delta$G), equilibrium binding constant (Ka) and stoichiometry[149]. All the mentioned techniques have been used for studying protein binding to other proteins, peptides, and DNA, but has been challenging for characterizing protein–GAG interactions.

Below, an overview of the principles of the mentioned techniques is reported.

### 4.2.1. Dynamic Light Scattering

Dynamic Light Scattering (DLS), sometimes referred to as Photon Correlation Spectroscopy or Quasi-Elastic Light Scattering, is a technique classically used for measuring the size of particles typically in the sub-micron region, dispersed in a liquid. The sensitivity of some modern systems is such that it can also now be used to measure the size of macromolecules in solution, e.g. proteins[150].

DLS measures Brownian motion and relates this to the size of the particles. Brownian motion is the random movement of particles due to the bombardment by the solvent molecules that surround them. The larger the particle or molecule, the slower the Brownian motion will be. Smaller particles are "kicked" further by the solvent molecules and move more rapidly. An accurately known temperature is necessary for DLS because knowledge of the viscosity is required (because the viscosity of a liquid is related to its temperature). The temperature also needs to be stable, otherwise convection currents in the sample will cause non-random movements that will ruin the correct interpretation

of size. The velocity of the Brownian motion is defined by a property known as the translational diffusion coefficient (D), and the size of a particle is calculated from the translational diffusion coefficient by using the Stokes-Einstein equation:

$$d(H) = \frac{kT}{3\pi\eta D}$$

where d(H) is the hydrodynamic diameter, k the Boltzmann's constant, T the absolute temperature and η the viscosity. Note that the diameter that is measured in DLS is a value that refers to how a particle diffuses within a fluid, so it is referred to as a hydrodynamic diameter. The diameter that is obtained by this technique is the diameter of a sphere that has the same translational diffusion coefficient as the particle. The particle translational diffusion coefficient will depend not only on the size of the particle "core", but also on any surface structure that will affect the diffusion speed, as well as the concentration and type of ions in the medium. Factors that can affect the diffusion speed are discussed in the following sections.

To explain how a DLS works, imagine if a cuvette, containing particles which are stationary, is illuminated by a laser and a frosted glass screen is used to view the sample cell. A classical speckle pattern would be seen (Figure 4.2.1).

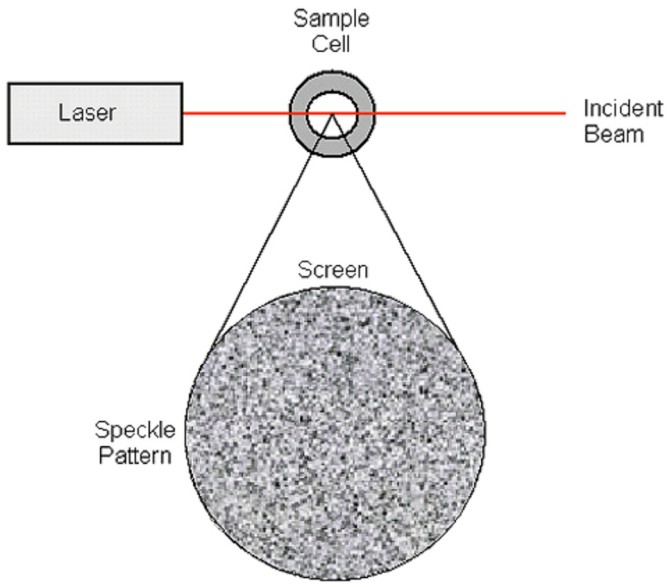


**Figure 4.2.1 Schematic representation of a speckle pattern**[150]

The speckle pattern will be stationary both in speckle size and position because the whole system is stationary. The dark spaces are where the phase additions of the scattered light are mutually destructive and cancel each other out. The bright blobs of light in the speckle pattern are where the light scattered from the particles arrives with the same phase and interfere constructively to form a bright patch. For a system of particles undergoing Brownian motion, a speckle pattern is observed where the position of each speckle is seen to be in constant motion. This is because the phase addition from the moving particles is constantly evolving and forming new patterns. The rate at which these intensity fluctuations occur will depend on the speed, and hence the size of the particles. Figure 4.2.2 schematically illustrates typical intensity fluctuations arising from a dispersion of large particles and a dispersion of small particles. The small particles cause the intensity to fluctuate more rapidly than the large ones.

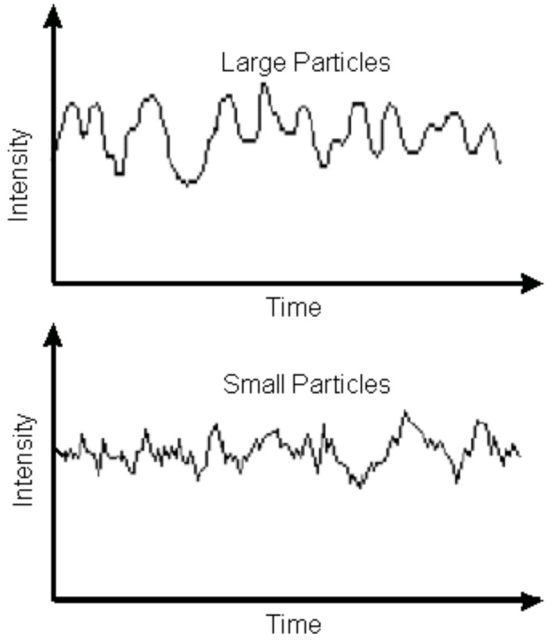


**Figure 4.2.2 Typical intensity fluctuations for large and small particles**[150]

It is possible to directly measure the spectrum of frequencies contained in the intensity fluctuations arising from the Brownian motion of particles, but it is inefficient to do so. The best way is to use a device called a digital autocorrelator, that is basically a signal comparator. It is designed to measure the degree of similarity between two signals, or one signal with itself at varying time intervals. If the

intensity of a signal is compared with itself at time zero, then the two signals will be perfectly correlated.

The important concept of the autocorrelator is that we are not comparing the intensities at discrete times, but comparing the history of the signal, over a significant time, as long as seconds, with the whole signal nanoseconds or microseconds later. This requires a large number of parallel multiplications in real time and is the reason for dedicated hardware for this task. If the particles are large the signal will be changing slowly, and the correlation will persist for a long time (Figure 4.2.3, panel A); if the particles are small and moving rapidly then correlation will reduce more quickly (Figure 4.2.3, panel B). These correlation functions are plotted with time on a log scale to help visualise decay rates that differ by orders of magnitude onto the same scale.

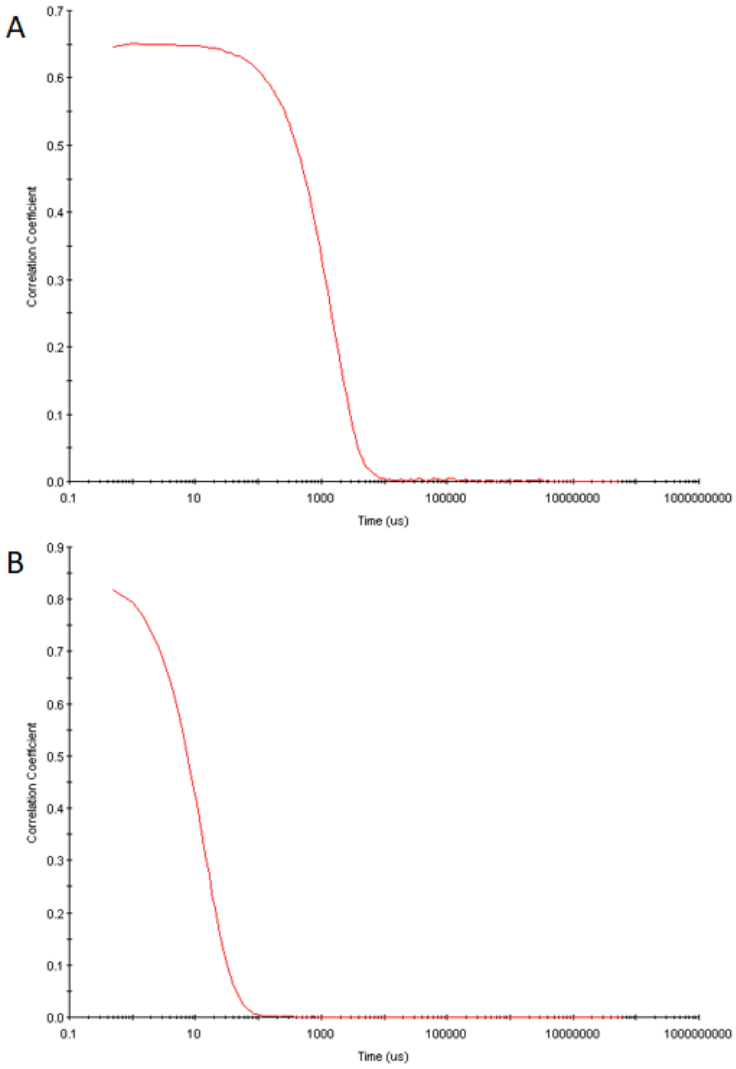


**Figure 4.2.3 Typical correlogram from a sample containing large particles (panel A) or small particles (panel B).**

Size is obtained from the correlation function using various algorithms. There are two fundamentally different approaches that are often taken (1) fit a single exponential to the correlation function to obtain the mean size (z-average diameter) and an estimate of the width of the distribution (polydispersity index), and (2) fit a multiple exponential to the correlation function to obtain the distribution of particle sizes.

### 4.2.2. Zeta Potential evaluation

Zeta potential is a physical property which is exhibited by any particle in suspension, macromolecule or material surface[151]. It can be used to optimize the formulations of suspensions, emulsions and protein solutions, predict interactions with surfaces, and optimize the formation of films and coatings. Knowledge of the zeta potential can reduce the time needed to produce trial formulations. It can also be used as an aid in predicting long-term stability.

In certain circumstances, the particles in a dispersion may adhere to one another and form aggregates of successively increasing size, which may settle out under the influence of gravity. An initially formed aggregate is called a floc and the process of its formation flocculation. The floc may or may not sediment or phase separate. If the aggregate changes to a much denser form, it is said to undergo coagulation. An aggregate usually separates out either by sedimentation (if it is denser than the medium) or by creaming (if it less dense than the medium). The terms flocculation and coagulation have often been used interchangeably. Usually coagulation is irreversible whereas flocculation can be reversed by the process of deflocculation. Figure 4.2.4 schematically represents some of these processes.

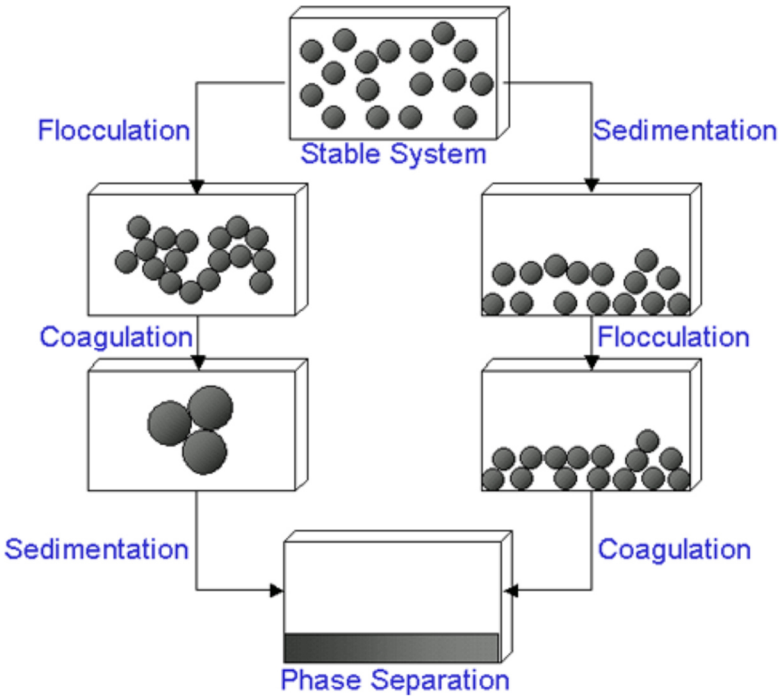


**Figure 4.2.4 Schematic diagram showing various mechanisms where stability may be lost in a colloidal dispersion.[151]**

The scientists Derjaguin, Verwey, Landau and Overbeek developed a theory in the 1940s which dealt with the stability of colloidal systems[152]. DVLO theory suggests that the stability of a colloidal system is determined by the sum of these van der Waals attractive (VA) and electrical double layer repulsive (VR) forces that exist between particles as they approach each other due to the Brownian motion they are undergoing (Figure 4.2.5, panel A).

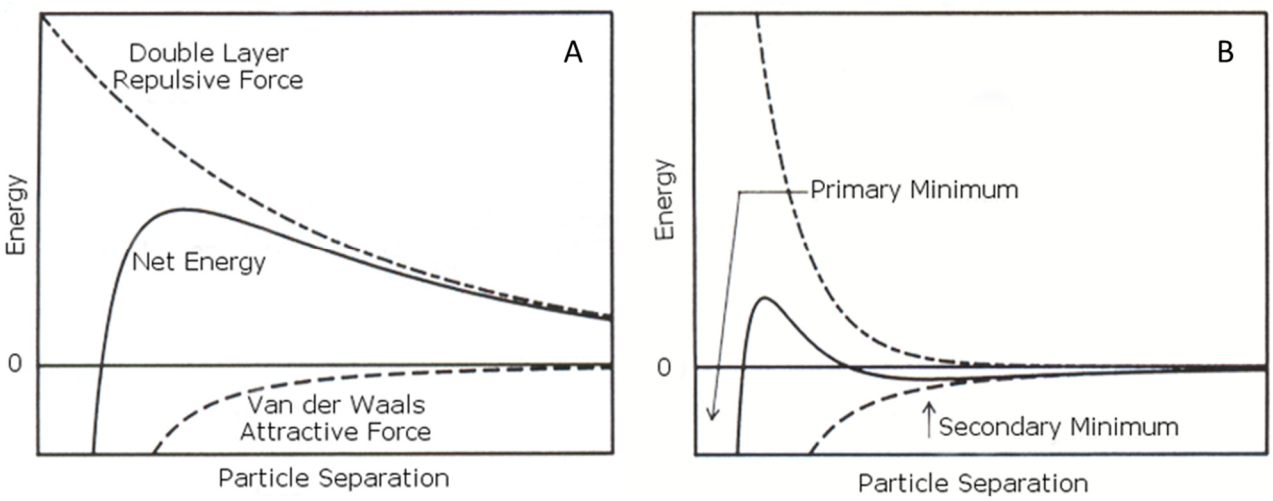


**Figure 4.2.5 A) Schematic diagram of the variation of free energy with particle separation according to DVLO theory. B) Schematic diagram of the variation of free energy with particle separation at higher salt concentrations showing the possibility of a secondary minimum.[151]**

This sum has a peak, and the theory proposes that particles that are initially separated are prevented from approaching each other because of the repulsive force. However, if the particles are forced with sufficient energy to overcome that barrier, for example by increasing the temperature, the attractive force will pull them into contact where they adhere strongly and irreversibly together. Therefore, if the particles have a sufficiently high repulsion, the dispersion will resist flocculation and the colloidal system will be stable. However, if a repulsion mechanism does not exist then flocculation or coagulation will eventually take place. If the zeta potential is reduced (e.g. in high salt concentrations), there is a possibility of a "secondary minimum" being created, where a much weaker and potentially reversible adhesion between particles exists (Figure 4.2.5, panel B). These weak flocs are sufficiently stable not to be broken up by Brownian motion, but may disperse under an externally applied force such as vigorous agitation.

To maintain the colloidal stability, two different ways exist: a steric repulsion or an electrostatic one. Each mechanism has its benefits for particular systems. Steric stabilization is simple, requiring just the addition of a suitable polymer. However, it can be difficult to subsequently flocculate the system if this is required, the polymer can be expensive and in some cases the polymer is undesirable e.g. when a ceramic slip is cast and sintered, the polymer has to be 'burnt out'. This causes shrinkage and can lead to defects. Electrostatic or charge stabilization has the benefits of stabilizing or flocculating a system by simply altering the concentration of ions in the system. This is a reversible process and is potentially inexpensive.

The development of a net charge at the particle surface affects the distribution of ions in the surrounding interfacial region, resulting in an increased concentration of counter ions, ions of opposite charge to that of the particle, close to the surface. Thus, an electrical double layer exists round each particle. The liquid layer surrounding the particle exists as two parts; an inner region (Stern layer) where the ions are strongly bound and an outer (diffuse) region where they are less firmly associated. Within the diffuse layer there is a notional boundary inside which the ions and particles form a stable entity. When a particle moves (e.g. due to gravity), ions within the boundary move it. Those ions beyond the boundary stay with the bulk dispersant. The potential at this boundary (surface of hydrodynamic shear) is the zeta potential (Figure 4.2.6).

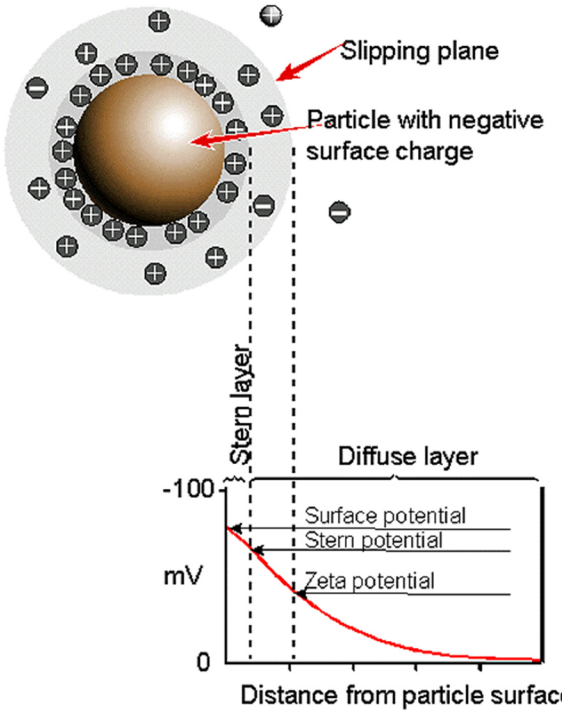


**Figure 4.2.6 Schematic representation of zeta potential.[151]**

The magnitude of the zeta potential gives an indication of the potential stability of the colloidal system. If all the particles in suspension have a large negative or positive zeta potential, then they will tend to repel each other and there will be no tendency for the particles to come together. However, if the particles have low zeta potential values then there will be no force to prevent the particles coming together and flocculating.

The general dividing line between stable and unstable suspensions is generally taken at either +30 or -30 mV. Particles with zeta potentials more positive than +30 mV or more negative than -30 mV are normally considered stable. However, if the particles have a density greater than the dispersant, even though they are dispersed, they will eventually sediment forming a close packed bed.

### 4.2.3. Isothermal Titration Calorimetry

Isothermal Titration Calorimetry (ITC) is the most quantitative means available for measuring the thermodynamic properties of a protein-protein interaction[153]. ITC measures the binding equilibrium directly by determining the heat evolved on association of a ligand with its binding partner. In a single experiment, the values of the binding constant (Ka), the stoichiometry (n), and the enthalpy of binding ($\Delta H_b$) are determined. The free energy and entropy of binding are determined from the

association constant. The temperature dependence of the $\Delta H_b$ parameter, measured by performing the titration at varying temperatures, describes the heat capacity of binding term ($\Delta C_p$).
An ITC instrument consists of two identical cells composed of a highly efficient thermal conducting material (Hasteloy or gold) surrounded by an adiabatic jacket (Figure 4.2.7).

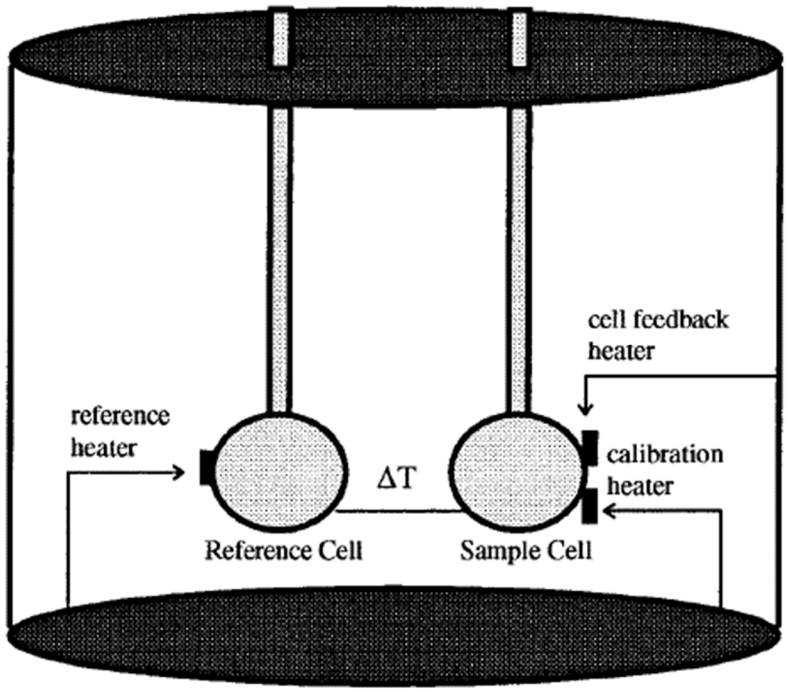


**Figure 4.2.7 Scheme of an adiabatic jacket.[153]**

The jacket is usually cooled by a circulating water bath. Sensitive thermopile/thermocouple circuits detect temperature differences between the two cells and between the cells and the jacket. Heaters located on both cells and the jacket are activated when necessary to maintain identical temperatures between all components. In an ITC experiment, the macromolecule solution is placed in the sample cell. The reference cell contains buffer or water minus the macromolecule. Prior to the injection of the titrant, a constant power is applied to the reference cell. This signal directs the feedback circuit to activate the heater located on the sample cell. This represents the baseline signal. The direct observable measured in an ITC experiment is the time-dependent input of power required to maintain equal temperatures in the sample and reference cell. During the injection of the titrant into the sample cell, heat is taken up or evolved depending on whether the macromolecular

association reaction is endothermic or exothermic. For an exothermic reaction, the temperature in the sample cell will increase, and the feedback power will be deactivated to maintain equal temperatures between the two cells. For endothermic reactions, the reverse will occur, meaning the feedback circuit will increase power to the sample cell to maintain the temperature.

The heat absorbed or evolved during a calorimetric titration is proportional to the fraction of bound ligand. Thus, it is of extreme importance to determine accurately the initial concentrations of both the macromolecule and the ligand. For the initial injections, all or most of the added ligand is bound to the macromolecule, resulting in large endothermic or exothermic signals depending on the nature of the association. As the ligand concentration increases, the macromolecule becomes saturated and subsequently less heat is evolved or absorbed on further addition of titrant. The amount of heat evolved on addition of ligand can be represented by the following equation:

$$Q = \frac{V_0 \Delta H_b [M]_t K_a [L]}{1 + K_a [L]}$$

where $V_0$ is the volume of the cell, $\Delta H_b$ is the enthalpy of binding per mole of ligand, $[M]_t$ is the total macromolecule concentration including bound and free fractions, $K_a$ is the binding constant, and [L] is the free ligand concentration.

## 4.3. Physical-chemical characterization of PF4-Heparin Complexes

### 4.3.1. Introduction

Treatment with heparin or LMWH products can be associated with a potentially fatal adverse event, heparin-induced thrombocytopenia (HIT)[154]. This occurs when the patient produces antibodies to heparin or LMWH in complex with the chemokine platelet factor (PF4), leading to irreversible aggregation and depletion of blood platelets (thrombocytopenia).

Biological and physical-chemical evaluations of the PF4/heparin complex are not at the moment required by entities like the American Food and Drugs Administration (FDA), but of course kindly suggested, in particular FDA expects sponsors of generic enoxaparin products to demonstrate that their manufactured versions do not have any higher risk of these or other dangerous reactions than

Lovenox[155]. The chosen method(s) must be suitable for identifying differences in the /heparin complexes, in e.g. in their sizes or charges, and the development and validation studies that support the suitability of the method(s) selected should be submitted to the application. The results obtained should be confirmed using an orthogonal method, whenever possible.

The size of the PF4/heparin complex is important for the pathogenesis of HIT, and in fact were observed clear differences in the frequency of clinically manifest of HIT depending on the heparin chain length (UFH> LMWH>fondaparinux), and these variances were based on the different sizes and amounts of their respective complexes formed with PF4[135]. The size distribution had been investigated by size exclusion chromatography (SEC) using the radiolabeled protein[134], and it has been shown that the formation of ultralarge complexes (ULCs) and small-size complexes (SC) of UFH and PF4 occurs over a narrow ratio of molar concentrations, and that their relative proportion depends on the amount of heparin present in the solution. In fact, the ULCs were found predominantly for PF4/heparin ratios greater than 1, whereas the SCs are more abundant at ratios lower than 1. In order to overcome the need to radiolabel PF4 and the low sensitivity of HPLC-SEC, the same authors published another study examining the macromolecular complexes formed at distinct protein/heparin ratios using photon correlation spectroscopy (PCS). Suvarna *et al* observed a progressive increase followed by a decrease of PF4 particle size that was a function of the PF4-heparin concentration ratio (PHR).

As mentioned previously, the PF4 heparin interaction is related to electrostatic interaction, in particular to the sulfation degree; for this reason, the evaluation of the complexes surface charge is an important parameter to be evaluated.

### 4.3.2. Aims of the work

While immunological and biochemical methods have been used since the 1990s to characterize the interaction between PF4, polyanions, and anti-PF4/heparin antibodies, biophysical tools have been increasingly applied during the past decade[148]. In this work, we evaluated the formation of complexes between PF4 and heparin of different sources and different molecular weights by PCS and Zp evaluation, useful techniques used for particles in solution characterization, and ITC analysis, a technique widely used for protein-ligand interaction studies; moreover, all the techniques mentioned were already used for PF4/heparin interaction with very good results[156,157].

### 4.3.3. Materials and Methods

#### 4.3.2.1. Samples

The complete list of the research samples under investigation is reported in Table 4.3.1; the weight average molecular weight (Mw, Da) and polydispersion index (Mw/Mn), obtained by HP-SEC-TDA technique, and the sulfation degree, obtained by 2D HSQC NMR experiment are also reported. The three LMWHs are enoxaparins, that where kindly provided from prof. Fareed's research group of the Loyola University of Chicago.

**Table 4.3.1 Samples in analysis.**

| Sample name | Sample type | Mw (Da) | Mw/Mn | DS |
|---|---|---|---|---|
| **G9850** | Porcine UFH | 18100 | 1.30 | 2.4 |
| **G11388** | Bovine UFH | 15900 | 1.52 | 2.8 |
| **G12301** | Ovine UFH | 15100 | 1.32 | 2.7 |
| **G12292** | Porcine LMWH | 4500 | 1.30 | 2.5 |
| **G13152** | Bovine LMWH | 4600 | 1.31 | 2.5 |
| **G13168** | Ovine LMWH | 4400 | 1.28 | 2.7 |

As can be observed, in the present study a considerably higher Mw porcine UFH was used in respect of the same origin samples analysed earlier (see Chapter 3.2); this choice was decided with the idea of having a wide range of molecular weights (and so of chains length) to be tested.

#### 4.3.2.2. PCS and Zeta Potential analysis

Protein dissolution

PF4 was purchased by Cromatec GmbH as 1 mg vials freeze-dried in Hanks' Balanced Salt Solution (HBSS, Sigma Aldrich), and each vial was reconstituted in 1 ml of deionized and filtered $H_2O$, reaching a final 1 mg/ml protein concentration, that corresponds to 32 μM concentration, and a 5 % HBSS total amount. Once solubilized, the protein was left about 2 h under stirring to enhance complete dissolution.

Titration solutions preparation

In order to prepare the different sample solutions, the following scheme was followed:

- 0.2mM each sample (**solution 1**; considering the molecular weight of sample reported in Table 4.3.1)

- 31.6µl solution 1+68.4µl $H_2O$ = 0.0632mM (**solution 2**);
- 31.6µl solution 2+68.4µl $H_2O$ = 0.0200mM (**solution 3**);
- 31.6µl solution 3+68.4µl $H_2O$ = 0.00632mM (**solution 4**);
- 31.6µl solution 4+68.4µl $H_2O$ = 0.00200mM (**solution 5**);

To perform the evaluation of PF4/heparin interaction, titration of protein by the samples was performed at different Protein/Heparin Ratio (PHR), calculated as:

$$\mathbf{PHR=\frac{hPF4\ molar\ concentration}{Heparin\ molar\ concentration}}$$

At least, five PHR were selected for each titration curve, taking into account samples' molecular weight distribution and each PHR solution was prepare starting with the addition of the proper sample amount to the related $H_2O$/HBSS volumes; then, 4 or 40 µl of PF4 was added and analysis was performed at room temperature 60 minutes after mixing for PCS analysis, or 10 minutes after mixing for Zeta Potential analysis, times optimized previoulsy[156]. PHR solutions preparations for respectively PCS and Zp experiments are reported in the following tables.

**Table 4.3.2 G9850 PCS preparation (final reached volume: 80 µl)**

| ***hPF4 mother solution (32 µM)*** | | ***Sample*** | | ***HBSS added*** | ***PHR*** |
|---|---|---|---|---|---|
| *Added volume* | *Final PF4 concentration* | *Added volume* | *Final sample concentration* | | |
| 4µl | 1.6µM | 3.2µl solution 5 | 0.080µM | 73µl | 20.0 |
| 4µl | 1.6µM | 4.0µl solution 5 | 0.100µM | 72µl | 16.0 |
| 4µl | 1.6µM | 5.0µl solution 5 | 0.125µM | 71µl | 12.8 |
| 4µl | 1.6µM | 7.1µl solution 5 | 0.178µM | 69µl | 9.0 |
| 4µl | 1.6µM | 10µl solution 5 | 0.250µM | 66µl | 6.4 |

**Table 4.3.3 G11388 PCS preparation (final reached volume: 80 μl)**

| ***hPF4 mother solution (32 μM)*** | | ***Sample*** | | ***HBSS added*** | ***PHR*** |
|---|---|---|---|---|---|
| *Added volume* | *Final PF4 concentration* | *Added volume* | *Final sample concentration* | | |
| 4μl | 1.6μM | 4.0μl solution 5 | 0.100μM | 72μl | 16.0 |
| 4μl | 1.6μM | 5.0μl solution 5 | 0.125μM | 71μl | 12.8 |
| 4μl | 1.6μM | 10μl solution 5 | 0.250μM | 66μl | 6.4 |
| 4μl | 1.6μM | 6.3μl solution 4 | 0.500μM | 70μl | 3.2 |
| 4μl | 1.6μM | 10.1μl solution 4 | 0.800μM | 66μl | 2.0 |

**Table 4.3.4 G12301 PCS preparation (final reached volume: 80 μl)**

| ***hPF4 mother solution (32 μM)*** | | ***Sample*** | | ***HBSS added*** | ***PHR*** |
|---|---|---|---|---|---|
| *Added volume* | *Final PF4 concentration* | *Added volume* | *Final sample concentration* | | |
| 4μl | 1.6μM | 4.0μl solution 5 | 0.100μM | 72μl | 16.0 |
| 4μl | 1.6μM | 5.0μl solution 5 | 0.125μM | 71μl | 12.8 |
| 4μl | 1.6μM | 7.1μl solution 5 | 0.178μM | 69μl | 9.0 |
| 4μl | 1.6μM | 10μl solution 5 | 0.250μM | 66μl | 6.4 |
| 4μl | 1.6μM | 6.3μl solution 4 | 0.500μM | 70μl | 3.2 |

**Table 4.3.5 LMWHs PCS preparation (final reached volume: 80 μl)**

| ***hPF4 mother solution (32 μM)*** | | ***Sample*** | | ***HBSS added*** | ***PHR*** |
|---|---|---|---|---|---|
| *Added volume* | *Final PF4 concentration* | *Added volume* | *Final sample concentration* | | |
| 4μl | 1.6μM | 10μl solution 5 | 0.250μM | 66μl | 6.4 |
| 4μl | 1.6μM | 5.1μl solution 4 | 0.400μM | 71μl | 4.0 |
| 4μl | 1.6μM | 6.3μl solution 4 | 0.500μM | 70μl | 3.2 |
| 4μl | 1.6μM | 10.1μl solution 4 | 0.800μM | 66μl | 2.0 |
| 4μl | 1.6μM | 5.8μl solution 3 | 1.455μM | 70μl | 1.1 |

**Table 4.3.6 G13062 Zeta Potential preparation (final reached volume: 800 μl)**

| ***hPF4 mother solution (32 μM)*** | | ***Sample*** | | ***HBSS added*** | ***PHR*** |
|---|---|---|---|---|---|
| *Added volume* | *Final PF4 concentration* | *Added volume* | *Final sample concentration* | | |
| 40μl | 1.6μM | 3.2μl solution 3 | 0.080μM | 757μl | 20.0 |
| 40μl | 1.6μM | 4.0μl solution 3 | 0.100μM | 756μl | 16.0 |
| 40μl | 1.6μM | 5.0μl solution 3 | 0.125μM | 755μl | 12.8 |
| 40μl | 1.6μM | 7.1μl solution 3 | 0.178μM | 753μl | 9.0 |
| 40μl | 1.6μM | 10μl solution 3 | 0.250μM | 750μl | 6.4 |

**Table 4.3.7 G11388 Zeta Potential preparation (final reached volume: 800 μl)**

| ***hPF4 mother solution (32 μM)*** | | ***Sample*** | | ***HBSS added*** | ***PHR*** |
|---|---|---|---|---|---|
| *Added volume* | *Final PF4 concentration* | *Added volume* | *Final sample concentration* | | |
| 40μl | 1.6μM | 4.0μl solution 3 | 0.100μM | 756μl | 16.0 |
| 40μl | 1.6μM | 5.0μl solution 3 | 0.125μM | 755μl | 12.8 |
| 40μl | 1.6μM | 10μl solution 3 | 0.250μM | 750μl | 6.4 |
| 40μl | 1.6μM | 6.3μl solution 2 | 0.500μM | 754μl | 3.2 |
| 40μl | 1.6μM | 10.1μl solution 2 | 0.800μM | 750μl | 2.0 |

**Table 4.3.8 G12301 Zeta Potential preparation (final reached volume: 800 μl)**

| ***hPF4 mother solution (32 μM)*** | | ***Sample*** | | ***HBSS added*** | ***PHR*** |
|---|---|---|---|---|---|
| *Added volume* | *Final PF4 concentration* | *Added volume* | *Final sample concentration* | | |
| 40μl | 1.6μM | 4.0μl solution 3 | 0.100μM | 756μl | 16.0 |
| 40μl | 1.6μM | 5.0μl solution 3 | 0.125μM | 755μl | 12.8 |
| 40μl | 1.6μM | 7.1μl solution 3 | 0.178μM | 753μl | 9.0 |
| 40μl | 1.6μM | 10μl solution 3 | 0.250μM | 750μl | 6.4 |
| 40μl | 1.6μM | 6.3μl solution 2 | 0.500μM | 754μl | 3.2 |

**Table 4.3.9 LMWHs Zeta Potential preparation (final reached volume: 800 μl)**

| ***hPF4 mother solution (32 μM)*** | | ***Sample*** | | ***HBSS added*** | ***PHR*** |
|---|---|---|---|---|---|
| *Added volume* | *Final PF4 concentration* | *Added volume* | *Final sample concentration* | | |
| 40μl | 1.6μM | 10μl solution 3 | 0.250μM | 750μl | 6.4 |
| 40μl | 1.6μM | 5.1μl solution 2 | 0.400μM | 755μl | 4.0 |
| 40μl | 1.6μM | 6.3μl solution 2 | 0.500μM | 754μl | 3.2 |
| 40μl | 1.6μM | 10.1μl solution 2 | 0.800μM | 750μl | 2.0 |
| 40μl | 1.6μM | 5.8μl solution 1 | 1.455μM | 754μl | 1.1 |

Data elaboration

Analysis were acquired using a Zetasizer Nano ZS instrument (Malvern Panalytical, UK) with the related dedicated software Zetasizer version 7.12. Data where then exported in Excel for the Z-Average vs PHR plot creation (PCS titration) or further copied in GraphPad software to fit the PHR vs the Zeta Potential and obtaining the Zp=0 PHR, which represents the maximum of aggregation (Zeta Potential titrations).

Instrument set up

- *Size acquisition parameters*

Material: Protein

Dispersant: deionized water

General options: Use dispersant viscosity as sample viscosity

Temperature: 25°C

Equilibration time: 30 secs

Cell: Disposable micro cuvette, for size measurement, minimum volume 40µL (ZEN0040, Malvern Panalytical Instruments Ltd)

Measurement: Angle: 173° Backscatter

Number of runs: 10 runs

Run duration: 10 secs

Number of measurements: 3

Delay between measurements: 5 secs

Position method: Seek for optimum position

Automatic attenuation selection: Yes

Data processing: General purpose (normal resolution)

To obtain the size of complexes in solution, single exponential fitting of correlation function was applied and mean size in terms of z-average radius was obtained.

- Zeta Potential acquisition parameter

Material: Protein

Dispersant: deionized water

Sample viscosity: Use dispersant viscosity as sample viscosity

Model for F(Ka): Smoluchowsky F(Ka) = 1.50

Temperature: 25°C

Equilibration time: 30 secs

Cell: Disposable folded cuvettes for the measurement of Zeta Potential, minimum volume 800 µl (DTS1070, Malvern Panalytical Instruments Ltd)

Measurement: manual (alternately automatic. with number run between 10 to 100)

Number of runs: 10 for every measurement

Number of measurements: 6

Delay between measurement: 5 secs

Automatic attenuation selection: Yes

Automatic voltage selection: Yes

Data processing: Monomodal

#### 4.3.2.3. ITC analysis

PF4 solution preparation

PF4 1 mg per vial was reconstituted in water as reported in section 4.2.2.1; then, it was diluted to 10 μM or 3.75 μM for titrations analysis of UFHs and LMWHs respectively with HBSS. 280μl of PF4 diluted solution were loaded in the instrument sample cell.

Samples preparation

Each heparin sample was first prepared at 0.2 mM in HBSS; then, UFHs were diluted to 50 μM and LMWHs to 75 μM, in HBSS, and each solution was then loaded in the instrument syringe.

Data elaboration

ITC measurements were carried out using a MicroCal PEAQ-ITC (Malvern Instruments), and data were acquired and elaborated with the dedicated MicroCAL PEAQ-ITC Analysis Software version 1.0.0.1259.

Instrument set up

For each experiment, a 60-second delay was followed by the injection of 1 or 2 μL of respectively UFHs and LMWHs, for a total of 19 titration points spaced 240 seconds apart; sample cell was maintained at 25°C under stirring, 1000 rpm. HBSS solution was used as reference buffer and loaded in the instrument reference cell.

### 4.3.4. Results

#### 4.3.3.1. PCS titrations results

Heparin is a polydisperse polysaccharide whose sulfation pattern, average chain length, and molecular weight distribution were found to vary, not only with respect to the source material, organ, and species but also to manufacturing process. In order to study how such variability can affect the aggregation of hPF4, 3 UFHs samples and 3 LMWHs samples derived from different species were studied. These samples exhibit different degrees of sulfation and average molecular weights, as reported in Table 4.3.1. The obtained titrations results are showed in Figure 4.3.1, while data are reported in Table 4.3.10, in which in italic are highlighted the PHR for which the maximum is achieved.

The PCS method employed was already optimized for PF4/heparin interaction in our laboratory, with very good results[156], and further improved, in particular in terms of method validation[158].

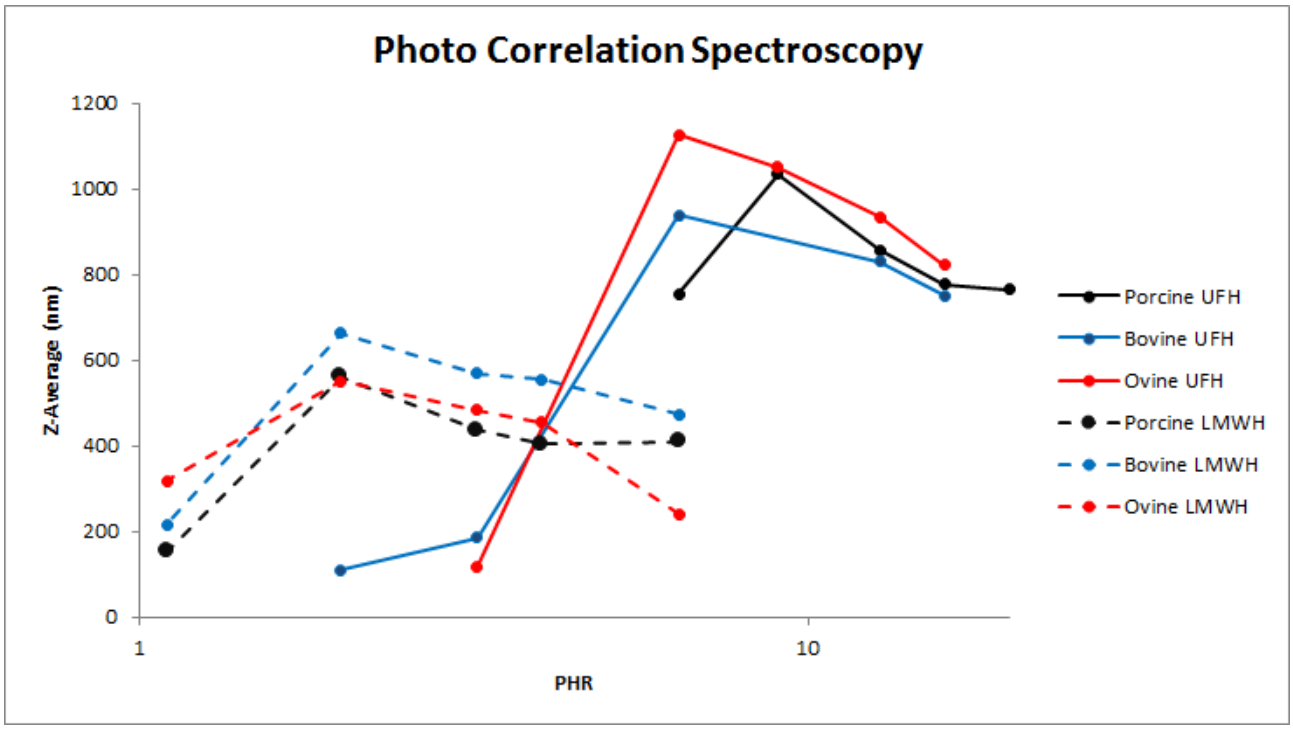


**Figure 4.3.1 PCS titrations results**

**Table 4.3.10 PCS titrations results**

| *Sample* | *Sample type* | *PHR Maximum aggregation* | *Z-average (nm)* |
|---|---|---|---|
| **G9850** | Porcine UFH | 9.0 | 1030 |
| **G11388** | Bovine UFH | 6.4 | 940 |
| **G12301** | Ovine UFH | 6.4 | 1130 |
| **G12292** | Porcine LMWH | 2.0 | 560 |
| **G13152** | Bovine LMWH | 2.0 | 660 |
| **G13168** | Ovine LMWH | 2.0 | 550 |

The size of particles follows a bell-shaped curve with a maximum achieved at different PHR values varying average molecular weight; in particular, 9.0 for G9850, 6.4 for G11388 and G12301, and 2.0 for the three LMWHs were obtained.

Comparing the three UFHs, lower concentrations, so a higher PHR, of porcine UFH are needed to form the large complexes as compared to the other heparins; moreover, ovine heparin forms slightly larger aggregates, a behaviour already observed previously[156]. The three samples showed the formation of the already mentioned ULCs on the surface of platelets, a phenomenon that provides a dynamic structure that facilitates formation of an array of multiple IgG antibodies[134]; the size of the complexes is quite similar, although the molecular weight is significantly different, and this fact is probably due to the higher DS of G11388 (2.8) and G12301 (2.7) in respect to G9850 (2.4). Anyway, the higher PHR of maximum aggregation reached with G9850 is consistent with its higher Mw, and in fact G11388 and G12301 titrations are more like that reported by Bertini et al for porcine heparin fraction with a Mw of 14.7 kDa; the similarity is not only about the PHR max, but also in the size of the complex reached[156].

Instead, the three LMWHs resulted with very similar both titration curves and size of the complexes reached at the PHR of maximum aggregation (2.0); very slightly higher the G13152 size, but we can consider it not significantly different, since under these conditions the measurement is more instable due to the several equilibria that are present among the different structures in solution whose increase the polydispersity index of the measurement, already reported[159].

Another important observation is that LMWHs did not form ULCs, confirming literature data[134], and reached the maximum of aggregation only at much lower PF4-heparin ratios in respect of UFHs, so these sample would be predicted to be less likely to provoke antibody formation.

#### 4.3.3.2. Zeta Potential titrations results

The Zp of complexes was measured using conditions analogous to those of the PCS experiments, whereby increasing amounts of heparin were incubated with a fixed concentration of hPF4. The only significant difference is in the solvent used for solutions preparation; the choice of water instead of HBSS was mainly due to exclude any interference of the salt on Zp evaluation, and in fact it was studied previously that analysing PF4 at higher HBSS concentrations than 5 %, different Zp were obtained[156].

A sigmoidal equation was fitted to the Zp versus the logarithm of PHR data to obtain the PHR value of the curve that corresponds to the neutral state of the complex (Zp = 0). The PHR values at which Zp =0 mV for each heparin, are reported in Table 4.3.11, while the fitted curves are shown in Figure 4.3.2.

As well as for PCS technique, the Zp measurement method employed was already optimized for PF4/heparin interaction in our laboratory, with very good results[156], and further improved, in particular in terms of method validation[158].

**Table 4.3.11 Zp titrations results**

| ***Sample*** | ***Sample type*** | ***PHR for Zp=0*** |
|---|---|---|
| **G9850** | Porcine UFH | 12.9 |
| **G11388** | Bovine UFH | 9.0 |
| **G12301** | Ovine UFH | 10.0 |
| **G12292** | Porcine LMWH | 3.6 |
| **G13152** | Bovine LMWH | 3.4 |
| **G13168** | Ovine LMWH | 3.0 |

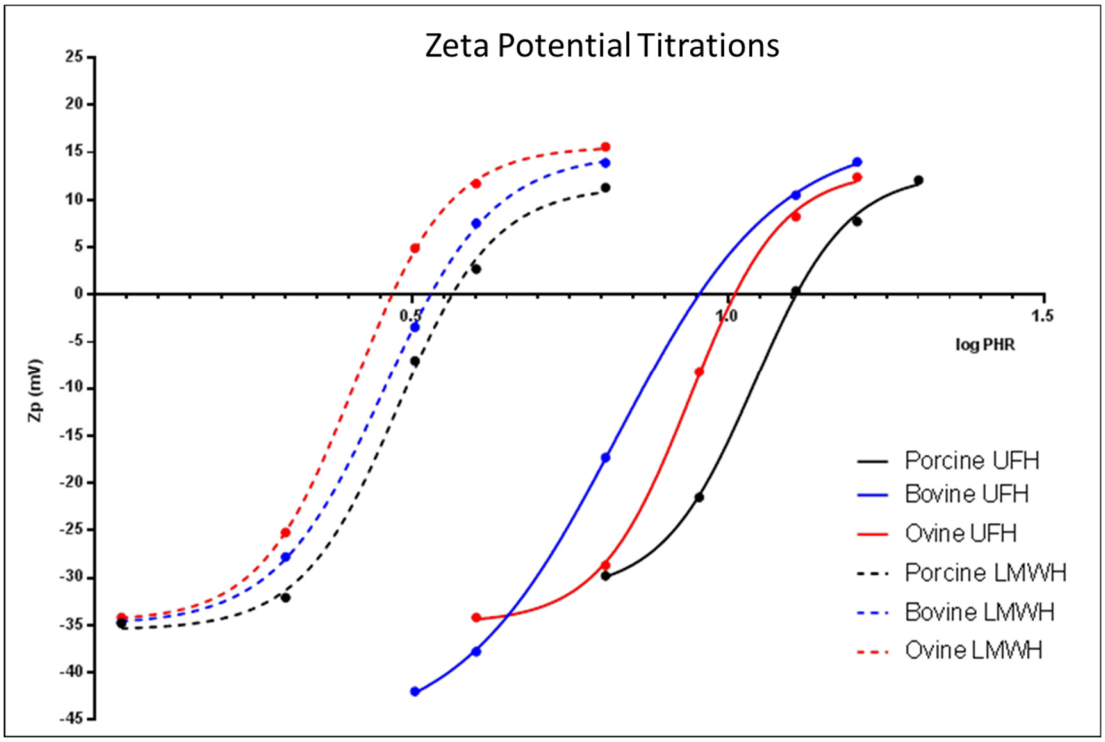


**Figure 4.3.2 Zeta Potential Titrations results**

Comparing the UFHs, in accordance with the PCS result, G9850 exhibited the higher PHR of maximum aggregation (approximately 13), confirming that molecular weight is an important parameter in determining hPF4/heparin complex formation. G11388 differs from porcine and ovine samples in terms of the higher concentration required to obtain the neutrality of charge (PHR = 9.0), even though its maximum complex size was the lower. The only parameter significantly different is the DS, which is lower for the porcine than the then the others (again, 2.4 for the porcine G9850, 2.8 for the bovine G11388 and 2.7 for the ovine G12301), but anyway for all samples the Zp=0 are reached at PHR at least not so different, taking into account that the standard deviation calculated on the Zp=0 obtained by titrating five times the same porcine UFH is ± 4.2[158], confirming that also the sulfate groups play an important role in the PF4/heparin interaction.

Going on with the LMWHs, very slight differences were observed with Zp=0 PHR values, that resulted in a range between 3.6 (porcine heparin) and 3.0 (ovine heparin). Considering that the heparin pattern is not linear, it is obvious to suppose that these variances are due to equilibria phenomena between different species in solutions charged in different manner, an observation already done for the PCS measurement; the declared DS reported in Table 4.3.1 (respectively 2.5 for the porcine G12292 and the bovine G13152 and 2.7 for the ovine G13168), in fact, is an average value,

so it is highly probable to obtain scattered results. Anyway, we can consider the variances not significant, since the standard deviation calculated on the Zp=0 obtained by titrating five times the same porcine LMWH is ± 4.2[158].

An overall consideration on Zp analysis is that this technique is suitable for discerning between UFHs and LMWHs, as already reported by Bertini et al previously[156].

#### 4.3.3.3. Isothermal Titration Calorimetry results

To assess the thermodynamics of PF4 interaction with UFHs and LMWHs of different sources, ITC analysis, which directly measures changes in heat that occur during complex formation, was performed. In particular, a microITC instrument was employed in this work, which has the great advantages of a low protein amount need and a high sensitivity to low heat released, a condition very common for non-specific interactions.

As well as for PCS and Zeta Potential evaluations techniques described above, the ITC method for PF4/heparin interaction was optimized starting from some literature data[157]; in particular, we first evaluated the better analysis conditions, in terms of both protein and samples concentrations using the two porcine samples, then, we assessed if also with this technique it is possible to discriminate between high and low molecular weight heparins, and finally we perform the measurements on all the different sources samples.

<u>Samples concentrations optimization</u>

An important aspect of an ITC experiment is to choose the correct concentration of the ligand. This parameter depends on the "c" value, expressed as

$$c = \frac{nP_t}{K_d}$$

where n is the number of sites per protein molecule, $P_t$ is the concentration of the titrated protein, and $K_d$ the dissociation constant. On the c value depends the shape of the isothermal curve, and its optimal range should be between 20 and 100, in order to obtain a sigmoidal shape and consequently a good fit to correctly estimate the thermodynamic parameters[149].

The experimentation started with the optimization of LMWH analysis; G12292 was analysed at three different concentrations, while the protein was maintained at 3.75 μM (concentration loaded in the instrument sample cell), as reported in Table 4.3.12.

At this stage, we did not modify the protein concentration in order to prevent precipitation phenomena of the two samples, knowing that high concentrations of heparin are needed.

**Table 4.3.12: G12292 ITC experiments conditions.**

| Experiment | [Heparin] (μM) | [PF4] (μM) |
|---|---|---|
| 1 | 30 | 3.75 |
| 2 | 75 | 3.75 |
| 3 | 150 | 3.75 |

The obtained titration curves are reported in Figure 4.3.3, where the raw heat released in function of the time (upper graphs, DP μcal/s) and the integrated heats as a function of the molar ratio of heparin/PF4 (lower graphs, ΔH kcal/mol) for each experiment are shown.

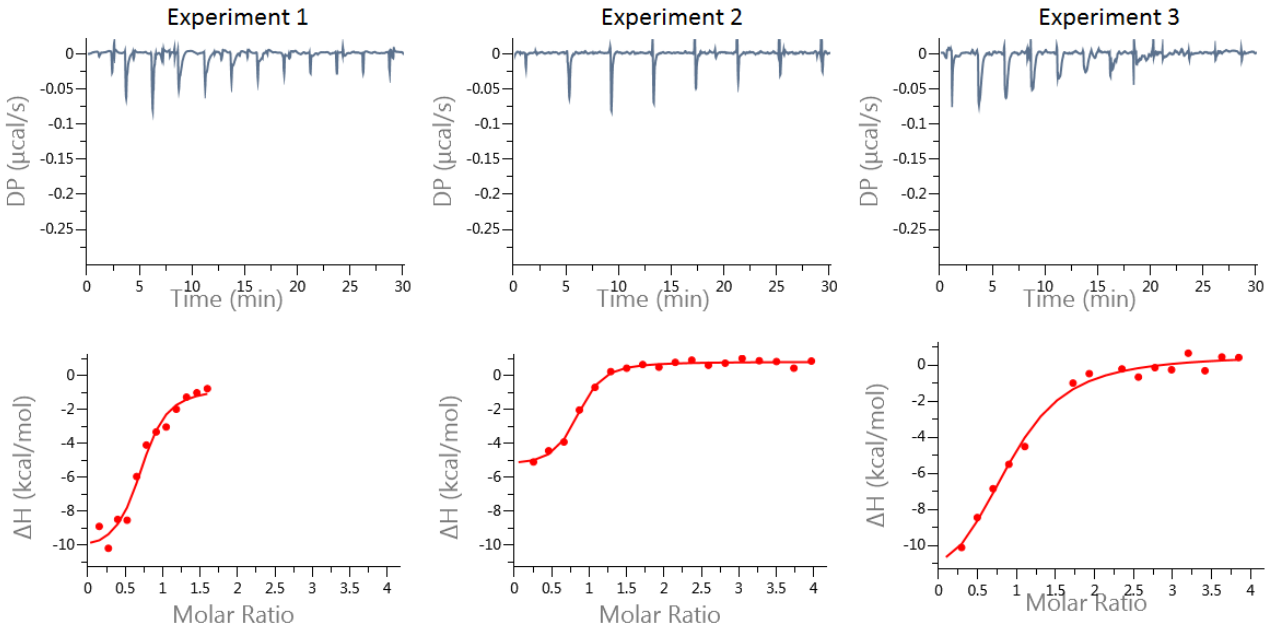


**Figure 4.3.3 G12292 conditions set up results**

In Table 4.3.13, the c values calculated for the three experiments, with the related n sites and $K_d$ (M) are reported; moreover, the ΔH (kcal/mol) of the interaction is reported.

**Table 4.3.13 G12292 concentration optimization results**

| Experiment | $K_d$ (M) | n sites | ΔH (kcal/mol) | c value |
|---|---|---|---|---|
| 1 | 1.72E-07 | 0.69 | -9.8 | 14.9 |
| 2 | 1.32E-07 | 0.77 | -6.2 | 21.9 |
| 3 | 2.29E-07 | 0.86 | -10.6 | 14.0 |

G12292 interacted exothermically with the PF4, although the heat released was very low (about -10 kcal/mol). The experiment 1 titration curve resulted at least poor in molar ratio points after the flex, while the experiment 3 resulted poor in molar ratio points before the flex; anyway, both the dissociation constant and the number of active sites resulted very similar, but looking at the c value calculated, only experiment 2 in inside the declared acceptable range, and in fact its curve has a good fitting both before and after the flex, so a LMWH concentration of 75 μM was choose for different sources comparison.

Then, the UFH concentration was optimized, using G9850 sample; in Table 4.3.14, the tested concentrations are reported, while in Figure 4.3.4, the titration curves are shown, in terms of raw heat released in function of the time (panel A graphs, DP μcal/s) and the integrated heats as a function of the molar ratio of heparin/PF4 (panel B graphs, ΔH kcal/mol) for each experiment.

**Table 4.3.14 G9850 ITC experiments conditions**

| Experiment | [Heparin] (μM) | [PF4] (μM) |
|---|---|---|
| 1 | 37.5 | 3.75 |
| 2 | 75.0 | 3.75 |
| 3 | 37.5 | 10.0 |
| 4 | 50.0 | 10.0 |

As for G12292 experiments, the G9850 titrations results are reported in Table 4.3.15.

**Table 4.3.15 G9850 concentration optimization results**

| Experiment | $K_d$ (M) | n sites | ΔH (kcal/mol) | c value |
|---|---|---|---|---|
| 1 | 0.50E-08 | 0.09 | -30.0 | 66.8 |
| 2 | 8.77E-08 | 0.14 | -57.1 | 5.9 |
| 3 | 1.52E-08 | 0.05 | -27.7 | 34.2 |
| 4 | 1.76E-08 | 0.05 | -52.9 | 26.1 |

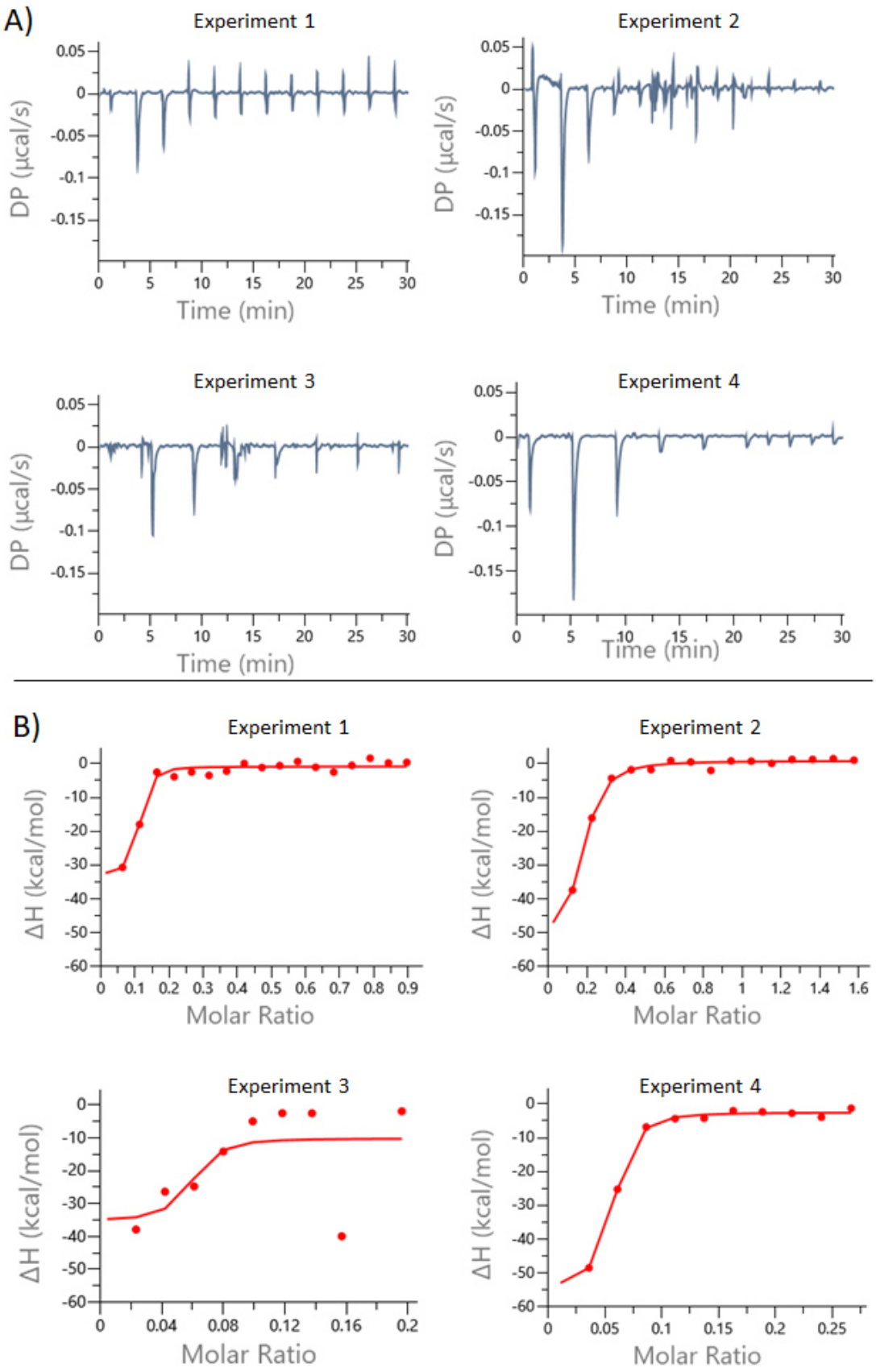


**Figure 4.3.4 G9850 conditions set up results**

Two different PF4 concentrations were tested, 3.75 μM, the same concentration used for LMWH, and 10 μM; with the lower amount of protein high molar heparin/PF4 ratios were achieved after the very first injections, a problem that leads to the loss of points in the flex part of the curve with the consequently error calculations of the dissociations constants and the N sites. Moreover, in experiment 2, a high noise after injections was observed (see Figure 4.3.4, panel A) probably due to precipitation of PF4/heparin complexes (phenomenon owed to the too much high concentration of heparin). So, for UFH, the increase of the protein concentration leads to obtain more stable titrations that resulted with more similar $K_D$ and N sites values.

Looking at the c values obtained, with the very exception of experiment 2, perfectly in range results were obtained, in particular an interesting 66.8 was obtained for experiment 1, that was anyway discharged for the reasons mentioned above. Comparing experiments 3 and 4, the c values are quite similar, but in 4, higher ΔH values are reached, so at least the 4 conditions were selected for continuing the study.

UFH vs LMWH comparison

At this point of the experimentation, the capability in discriminating between a high and a low molecular weight heparin as PCS and Zp techniques was evaluated, so the selected experiments 2 and 4 for respectively G12292 and G9850 (see Tables Table 4.3.12 and Table 4.3.14) were compared. The titration curves overlay, again in terms of integrated heats as a function of the molar ratio of heparin/PF4 (ΔH kcal/mol) are showed in Figure 4.3.5, while the thermodynamic parameters obtained are reported in Table 4.3.16.

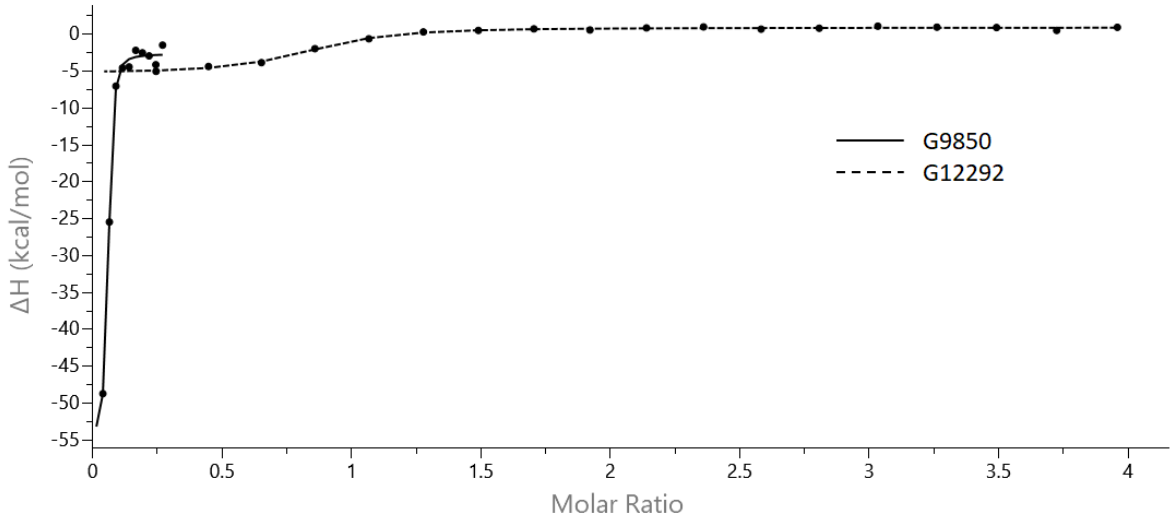


**Figure 4.3.5 G12292 and G9850 ITC integrated heat titration curves overlay**

**Table 4.3.16 Comparison of G9850 and G12292 thermodynamic parameters**

| Sample | N sites | $K_D$ (M) | ΔH (kcal/mol) | ΔG (kcal/mol) | -TΔS (kcal/mol) |
|---|---|---|---|---|---|
| G9850 | 0.05 | 1.76E-8 | -52.9 | -10.6 | 42.4 |
| G12292 | 0.77 | 1.32E-7 | -6.2 | -9.4 | -3.2 |

The first observation made by looking at Figure 4.3.5 is that the flex of the G9850 (UFH sample) titration curve is reached at lower heparin/PF4 molar ratios, leading also to a lower N sites value, so of course this sample has a higher affinity to PF4, and this is confirmed by the lower $K_D$ obtained; moreover, converting the N sites into PHR (calculated as 1/N), respectively 22 and 1.3 for G9850 and G12292 are obtained and these results are on line with the Zp evaluation method.

Another important observation is that for the UFH the interaction is more exothermic than the LMWH one, so a more favourable binding is achieved, a result consistent with literature[160]; moreover, a UFH has longer chain length so it is reasonable to say that a larger quantity of hydrogen bonds can be formed. Anyway, for both samples, negative values of ΔG were reached so as expected the interaction is spontaneous.

Finally, the -TΔS, of course, resulted different, in particular for G9850 is strongly positive, so apparently the conformational changes are unfavourable; on the contrary, G12292 seems to favour these changes in the protein.

Comparison of different sources UFHs and LMWHs

After having assessed the suitability of the optimized ITC method in discriminating between a high and a low molecular weight heparin, the next and final step was to compare the PF4/heparin interaction thermodynamic parameters of the different sources' samples, as already done with PCS and Zp techniques. To better keep in mind the conditions used and the sample in analysis, in Table 4.3.17 the concentrations of both protein and heparin are reported, as well as the type of sample.

**Table 4.3.17 Summary of samples and conditions used for ITC comparison analysis**

| Sample | Sample Type | [Heparin] (μM) | [PF4] (μM) |
|---|---|---|---|
| **G9850** | Porcine UFH | 50 | 10 |
| **G11388** | Bovine UFH | 50 | 10 |
| **G12301** | Ovine UFH | 50 | 10 |
| **G12292** | Porcine LMWH | 75 | 3.75 |
| **G13152** | Bovine LMWH | 75 | 3.75 |
| **G13168** | Ovine LMWH | 75 | 3.75 |

In Table 4.3.18, the titrations results are reported, in terms of thermodynamic parameters ($\Delta H$, $\Delta G$ and $-T\Delta S$, kcal/mol), dissociation constant and number of interactions sites; instead, the titration curves are reported in Figure 4.3.6, the UFHs ones, and in Figure 4.3.7, the LMWHs ones.

**Table 4.3.18 ITC results**

| Sample | Source | N sites | $K_D$ (M) | ΔH (kcal/mol) | ΔG (kcal/mol) | -TΔS (kcal/mol) |
|---|---|---|---|---|---|---|
| **G9850** | Porcine UFH | 0.05 | 1.80E-08 | -52.9 | -10.6 | 42.4 |
| **G11388** | Bovine UFH | 0.07 | 1.07E-07 | -63.0 | -9.5 | 53.5 |
| **G12301** | Ovine UFH | 0.08 | 7.10E-08 | -45.5 | -9.8 | 35.7 |
| **G12292** | Porcine LMWH | 0.77 | 1.32E-07 | -6.2 | -9.4 | -3.2 |
| **G13152** | Bovine LMWH | 0.98 | 1.12E-07 | -10.8 | -9.5 | 1.3 |
| **G13168** | Ovine LMWH | 0.88 | 1.24E-07 | -13.2 | -9.4 | 3.7 |

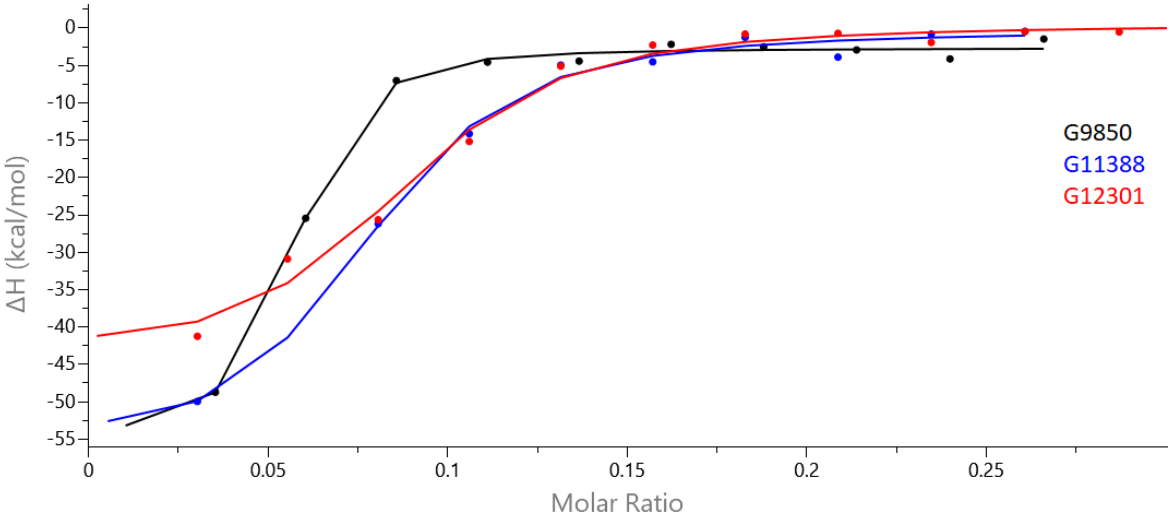


**Figure 4.3.6 UFH titration curves results**

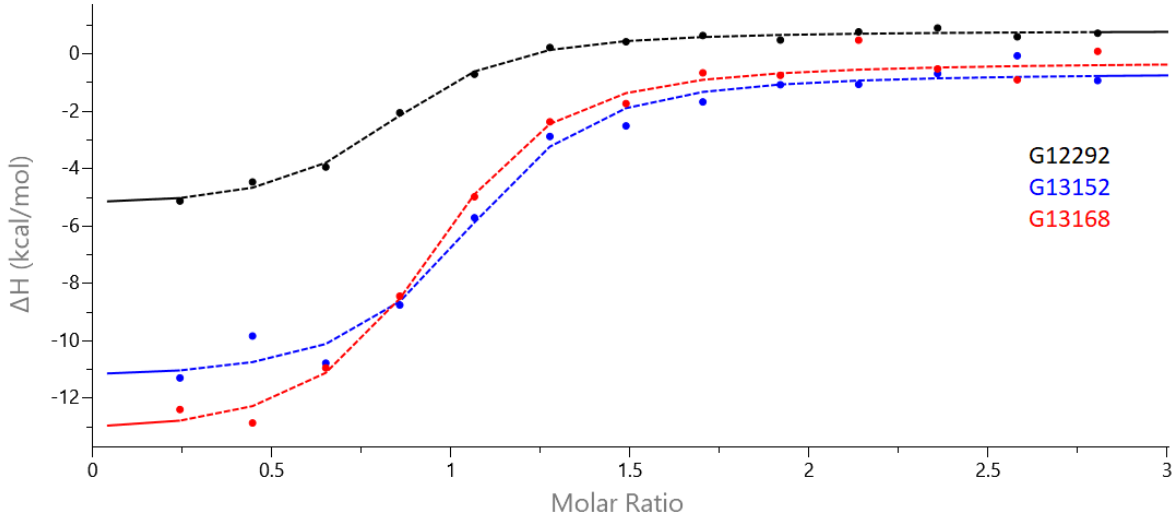


**Figure 4.3.7 LMWH titration curves results**

Starting with the three UFHs, the porcine one showed both the lower $K_D$ constant and the lower number of interaction sites, so it seems that its interaction with the protein is stronger than the other two, although the $\Delta G$ developed is only slightly higher than the other two; again, converting the number of sites into PHR (again, as 1/N), values of 22.0, 14.3 and 12.0 for respectively porcine, bovine and ovine heparins were obtained, so we can confirm that smaller amount of G9850 are needed to obtain the maximum of interaction.

By the Table 4.3.18, the heat released by G11388 is higher than the other two samples, although it seems to show the lower affinity to PF4; the most probable reason for this behaviour could be found in its higher DS (2.8) and so in its bigger number of sulfate groups, so it is reasonable to say that the hydrogen bond formed increased. Moreover, G12301 shows the less heat released but also the less $\Delta S$ parameter, so it is the sample that seems to favour most the conformational changes of the protein, that is necessary for PF4 to enhance its antigenity[128]; this outcome is in good accordance with the Bertini et al observation for the ovine heparin sample[156], for which larger complexes were obtained by PCS so it could reasonably be assumed that the ability in forming complexes is greater for an ovine UFH sample.

Going on with the LMWHs, again the porcine sample showed the need of a less quantity to reach the maximum of interaction, with a calculated PHR of 1.3 versus the 1.0 and 1.1 values for respectively bovine and ovine samples; on the contrary of the UFHs, in this case, the gap between the LMWHs is smaller, confirming the similarity already showed by PCS and Zp technique. Besides, the released $\Delta G$ is not only negative, indicating a spontaneous process of interaction, but also quite the same for all, and in addition also the dissociation constants are very similar, further confirmations of their same affinity for PF4.

Comparing the other thermodynamic parameters, in this case G12292 released less heat then G13152 and G13168, and it is the only sample for which the entropy contribute is negative; the three samples are all enoxaparin, so were obtain by the same pathway, however some variances in the chain pattern could be obtained, in particular in the disaccharide composition, as reported by Watt et al[161]. Nevertheless, the main parameters that could interfere with the interaction with PF4, are molecular weight distributions and sulfation degrees, that are quite the same for the three samples under investigation. So, to justify the porcine LMWH behaviour, we can hypothesize that there is something that in some way could disturb the interaction, for example a different counterion.

### 4.3.5. Overall discussion and conclusions

The interaction of PF4 and heparin is regulated by a dynamic equilibrium, where the stability of complexes depends, among other things, on the relative concentrations of PF4 and heparin. Complexes of PF4 and heparin can be characterized in terms of their size and, due to the electrostatic nature of interaction, surface charge; besides, the thermodynamic parameters of a ligand-protein interaction can elucidate how strong and favourable is the complex formation process, and due to the poor knowledge in this sense for PF4/heparin interaction, studying them could be very useful. The present study has the goal to analyse and compare by diverse techniques the interaction between PF4 and a variety of heparins obtained by different sources, with diverse molecular weight distributions. To resume, in Table 4.3.19 a summary of the main results of the study is reported.

**Table 4.3.19 Summary of the PF4/heparin interaction study**

| Sample | Mw (Da) | Mw/Mn | DS | *PCS* | | *Zp* |
|---|---|---|---|---|---|---|
| | | | | *PHR max* | *Size nm* | *PHR for Zp=0* |
| **G9850** | 18100 | 1.3 | 2.4 | 9.0 | 1030 | 12.9 |
| **G11388** | 15900 | 1.5 | 2.8 | 6.4 | 940 | 9.0 |
| **G12301** | 15100 | 1.3 | 2.7 | 6.4 | 1130 | 10.0 |
| **G12292** | 4500 | 1.3 | 2.5 | 2.0 | 560 | 3.6 |
| **G13152** | 4600 | 1.3 | 2.5 | 2.0 | 660 | 3.4 |
| **G13168** | 4400 | 1.3 | 2.7 | 2.0 | 550 | 3.0 |

| Sample | *ITC* | | | | | |
|---|---|---|---|---|---|---|
| | *n sites* | *Calculated PHR* | *$K_D$ (M)* | *$\Delta H$ kcal/mol* | *$\Delta G$ kcal/mol* | *$-T\Delta S$ kcal/mol* |
| **G9850** | 0.05 | 22.0 | 1.80E-08 | -52.9 | -10.6 | 42.4 |
| **G11388** | 0.07 | 13.0 | 1.07E-07 | -63.0 | -9.5 | 53.5 |
| **G12301** | 0.08 | 14.0 | 7.10E-08 | -45.5 | -9.8 | 35.7 |
| **G12292** | 0.77 | 1.3 | 1.32E-07 | -6.2 | -9.4 | -3.2 |
| **G13152** | 0.98 | 1.0 | 1.12E-07 | -10.8 | -9.5 | 1.3 |
| **G13168** | 0.88 | 1.1 | 1.24E-07 | -13.2 | -9.4 | 3.7 |

For PCS and Zp techniques, we started from already optimized methods, in which their suitability in discriminating from a high and a low molecular weight heparin was assessed[156]; it is in fact known that a less molar quantity of heparin is needed to reach the maximum complex with PF4 in a inversely proportional manner to the molecular weight. By the way, Mw is not the only parameter

that play a role in the PF4/heparin interaction, also the polydispersion index and the sulfation degree have significant part. On the contrary, ITC method was set up in the present work, with the goals of assessing its ability in discriminate between a low and a high molecular weight heparin and between different sources samples.

G9850, the highest Mw heparin analysed, reached the maximum of aggregation at the bigger PHR with each technique used, so requiring the smaller concentration, but it did not show, in e.g., the highest heat released or the highest complex size; moreover, it's Zp=0 is obtained at a PHR not so different from the other two UFHs, although their Mw is at least the 11 % less, a value that as reported in chapter 3.2.4 means a significant variance. In fact, both G11388 and G12301 has a higher DS, so it is reasonable to say that this parameter can increase the electrostatic interaction with the protein, leading to a less heparin quantity needed for PF4 charges saturation; moreover, G11388 showed the highest heat released, and it's not a case that it also has the biggest DS value.

Similarly, the three LMWHs showed the same PCS calculated maximum of aggregation, also with very similar complexes size, and quite the same null Zp PHR and these results are in accordance with the molecular weight distribution and DS profiles of the samples, but going more deeply in the interaction evaluation, ITC technique revealed a slight difference in the thermodynamics of G12292 compared to the other two samples, in particular in the entropy parameter, but anyway, the variances found for the LMWHs can be considered not significant.

Relating PCS and Zeta Potential evaluation, the largest complexes should occur at the molar ratios that lead to charge neutralization, but discrepancies are observed as the result of the different manner from which the PHR of maximum aggregation is calculated, respectively experimentally and by a mathematical extrapolation, and the PHR obtained from Zp is always higher than the PCS one. PHR at null Zeta potential is the most quantitative parameter, whilst PHR for maximum size is a robust, but semi-quantitative parameter due to the low resolution of the concentration range of the test solutions and the maximum complex size is more qualitative. Nevertheless, all the three parameters are suggested to be necessary to understand the complexation profile of a heparin material with PF4.

ITC measurement has revealed to be suitable in discriminate between high and low molecular weight heparin, in particular by the strong difference of heat released during the process and also by the great gap of number of interaction sites per samples, that is more evident when it is

converted in PHR value; furthermore, there is a good accordance between the PHR obtained by ITC and PCS/Zp techniques. In addition, the samples resulted with different dissociation constants that are lower, as expected, for UFHs than LMWHs. Although these outcomes, considering the Gibbs' free energies released, that is the parameter that mostly determine the affinity of the interaction (the more is negative, the more is affine), at least the six samples interact spontaneously with PF4, but also similarly each other. This final assumption seems to be against all the other results obtained, but taking into account that all the samples are heparins and that the Gibbs' free energy only shows that all sample can bind the same to PF4 without considering all the other parameters (Mw, concentrations and so on), it makes sense, since we always demonstrated an interaction between samples and the protein.

To conclude, it is clear that only one technique is not sufficient for a complete description of the PF4/sample interaction, on the contrary it is more useful to obtain a broader picture by taking into account all the three methods together. In this sense, PCS, Zp evaluation and ITC can be reasonably considered orthogonal methods for PF4/heparin interaction study, in particular for the discrimination between a high and a low molecular weight heparin. Regarding the different sources, only the porcine samples seem to differentiate from the bovine and the ovine, in terms of less concentrations needed to obtain the maximum of aggregation, and this result is supported by all the techniques under consideration. Unfortunately, there are no certain proofs in literature that different sources heparins could bind differently with PF4, on the contrary the panorama is highly confused[162,163]; nevertheless, the outcomes of the present work, could be interesting in understanding such differences.

## 4.4. Characterization of Sulodexide/PF4 interaction by PCS and Zp techniques

### 4.4.1. Introduction

At the beginning of chapter 4 was mentioned that after heparin therapy cessation, clinical management of patients with HIT is with non–heparin anticoagulants. The direct thrombin inhibitors (DTIs) are potent anticoagulants that inhibit the high level of thrombin generation in patients with HIT; this drug family success in HIT management is due to the difference in chemical structure from heparin such that these drugs do not generate HIT antibodies, nor do they interact with preformed HIT antibodies[147]. Examples of DTIs are argatroban, approved by the FDA for anticoagulation of HIT patients during percutaneous coronary interventions[164], bivalirudin, successfully used in HIT management and approved for patients undergoing percutaneous coronary interventions, including those with HIT[165], lepirudin, that has been approved for the treatment of HIT thrombosis by the health authorities of the United States, Canada, and Europe, and danaparoid, that has been used to successfully treat HIT patients over the past 15 years[166].

The antithrombotic drug field is growing with new agents at various stages of approval. As these drugs enter the clinical trial phase, questions often are asked if the new agent can be used as an alternative anticoagulant for the management of HIT thrombosis.

As mentioned before (see chapter 3.3.1) Sulodexide (SLDX) is a well-defined mammalian glycosaminoglycan (GAG) that is composed of 2 distinct fractions, 80% fast moving heparin (Fm-Hep) and 20% dermatan sulfate (DeS)[100–102]. The pharmacological effects of SLDX differ substantially from other GAGs and are mainly characterized by a prolonged half-life (18.7 + 4.1 hour after 50 mg per os and 11.7 + 2.0 h after intravenous injection, clearly very different from the 60 to 90 minutes half-life of UFH[167]) and reduced effect on global coagulation and bleeding parameters[104].

Clinically, SLDX is used for the prophylaxis and treatment of thromboembolic diseases; however, recent research has also demonstrated the beneficial effects of SLDX in animal models of reperfusion injury and the treatment of diabetic nephropathy[168–170]. More recently, SLDX is also used in the anticoagulant management of patients with HIT; its activity is also compared to that of an enoxaparin[171,172].

As reported in the previous chapter (4.3), Photo Correlation Spectroscopy (PCS) and Zeta Potential evaluation (Zp), are techniques that give feedbacks on physical-chemical properties of particles in solution, and that are used with great success in heparin/PF4 complex characterization.

### 4.4.2. Aim of the work

In the context of evaluating new antithrombotic drugs for HIT management, aim of the present study is to assess the ability of an API SLDX sample in interact with PF4, using PCS and Zp techniques. Besides, the interaction between the isolated Fm-Hep and DeS fractions and PF4 will be investigated, as well as three mixtures of a Hep fraction and of a DeS fraction in different proportions, with the intention of studying deeper how the two SLDX components interact with the protein.

We decided not to use the ITC technique in the present study, due to the probable uncertainty in understanding the contribution of the two SLDX components in PF4 interaction thermodynamics.

### 4.4.3. Materials and methods

#### 4.4.3.1. Samples in analysis

For the experimentation, some of the samples already used in chapter 3.3 were used, and the related codes, with sample type and Mw (kDa) are reported in Table 4.4.1; for the exact composition of the three DeS/Hep mixtures, see Table 3.3.7.

**Table 4.4.1 Samples in analysis**

| Ronzoni code | Sample type | Mw (kDa) |
|---|---|---|
| G12512* | SLDX | 13.5 |
| G12824_A | Fm-Hep | 10.9 |
| G12909_Fr1 | DeS | 21.5 |
| G14202** | DeS/Hep mix 1 | 17.5 |
| G14203** | DeS/Hep mix 2 | 15.7 |
| G14204** | DeS/Hep mix 3 | 13.7 |

*From this sample, the single Fm-Hep and DeS components were obtained by enzymatic digestion.

**The Mw reported was calculated by HP-SEC-TDA technique, using the chapter 3.3 polymeric conditions, on the whole peak.

#### 4.4.3.2. PCS and Zp analysis

Analysis were conducted following the same preparation and instrument set up already showed in chapter 4.3.3, below reported.

<u>Protein dissolution</u>

PF4 was purchased from ChromaTec GmbH as 1 mg vials freeze-dried in Hanks' Balanced Salt Solution (HBSS, Sigma Aldrich), and each vial was reconstituted in 1 ml of deionized and filtered $H_2O$,

reaching a final 1 mg/ml concentration, that corresponds to 32 μM concentration. Once solubilized, the protein was left about 2 h under stirring to enhance complete dissolution.

Titration solutions preparation

In order to prepare the different sample solutions, the following scheme was followed:

- 0.2mM each sample (**solution 1**; considering the molecular weight of sample reported in Table 4.3.1)
- 31.6μl solution 1+68.4μl $H_2O$ = 0.0632mM (**solution 2**);
- 31.6μl solution 2+68.4μl $H_2O$ = 0.0200mM (**solution 3**);
- 31.6μl solution 3+68.4μl $H_2O$ = 0.00632mM (**solution 4**);
- 31.6μl solution 4+68.4μl $H_2O$ = 0.00200mM (**solution 5**);

To perform the evaluation of PF4/GAG interaction, titration of protein by the samples was performed at different Protein/GAG Ratio (PGR), calculated as:

$$\mathbf{PGR=\frac{hPF4\ molar\ concentration}{GAG\ molar\ concentration}}$$

At least, five were selected for each titration curve, taking into account samples' molecular weight distribution and each PGR solution was prepare starting with the addition of the proper sample amount to the related $H_2O$/HBSS volumes; then, 4 or 40 μl of PF4 was added and analysis was performed 60 minutes after mixing for PCS analysis, or 10 minutes after mixing for Zeta Potential analysis. PGR solutions preparations for respectively PCS and Zp experiments are reported in the following tables.

**Table 4.4.2 G12512 and G12824_A PCS preparation (final reached volume: 80 μl)**

| ***hPF4 mother solution (32 μM)*** | | ***Sample*** | | ***HBSS added*** | ***PGR*** |
|---|---|---|---|---|---|
| *Added volume* | *Final PF4 concentration* | *Added volume* | *Final sample concentration* | | |
| 4μl | 1.6μM | 5.0μl solution 5 | 0.125μM | 71μl | 12.8 |
| 4μl | 1.6μM | 7.1μl solution 5 | 0.178μM | 69μl | 9.0 |
| 4μl | 1.6μM | 10μl solution 5 | 0.250μM | 66μl | 6.4 |
| 4μl | 1.6μM | 6.3μl solution 4 | 0.500μM | 70μl | 3.2 |
| 4μl | 1.6μM | 10.1μl solution 4 | 0.800μM | 66μl | 2.0 |

**Table 4.4.3 DeS/Hep mixtures and G12909_Fr1 PCS preparation (final reached volume: 80 µl)**

| ***hPF4 mother solution (32 µM)*** | | ***Sample*** | | ***HBSS added*** | ***PGR*** |
|---|---|---|---|---|---|
| *Added volume* | *Final PF4 concentration* | *Added volume* | *Final sample concentration* | | |
| 4µl | 1.6µM | 4.0µl solution 5 | 0.100µM | 72µl | 16.0 |
| 4µl | 1.6µM | 5.0µl solution 5 | 0.125µM | 71µl | 12.8 |
| 4µl | 1.6µM | 7.1µl solution 5 | 0.178µM | 69µl | 9.0 |
| 4µl | 1.6µM | 10µl solution 5 | 0.250µM | 66µl | 6.4 |
| 4µl | 1.6µM | 6.3µl solution 4 | 0.500µM | 70µl | 3.2 |

**Table 4.4.4 G12512 and G12824_A Zeta Potential preparation (final reached volume: 800 µl)**

| ***hPF4 mother solution (32 µM)*** | | ***Sample*** | | ***HBSS added*** | ***PGR*** |
|---|---|---|---|---|---|
| *Added volume* | *Final PF4 concentration* | *Added volume* | *Final sample concentration* | | |
| 40µl | 1.6µM | 5.0µl solution 3 | 0.125µM | 755µl | 12.8 |
| 40µl | 1.6µM | 7.1µl solution 3 | 0.178µM | 753µl | 9.0 |
| 40µl | 1.6µM | 10µl solution 3 | 0.250µM | 750µl | 6.4 |
| 40µl | 1.6µM | 6.3µl solution 2 | 0.500µM | 754µl | 3.2 |
| 40µl | 1.6µM | 10.1µl solution 2 | 0.800µM | 750µl | 2.0 |

**Table 4.4.5 DeS/Hep mixtures and G12909_Fr1 Zeta Potential preparation (final reached volume: 800 µl)**

| ***hPF4 mother solution (32 µM)*** | | ***Sample*** | | ***HBSS added*** | ***PGR*** |
|---|---|---|---|---|---|
| *Added volume* | *Final PF4 concentration* | *Added volume* | *Final sample concentration* | | |
| 40µl | 1.6µM | 4.0µl solution 3 | 0.100µM | 756µl | 16.0 |
| 40µl | 1.6µM | 5.0µl solution 3 | 0.125µM | 755µl | 12.8 |
| 40µl | 1.6µM | 7.1µl solution 3 | 0.178µM | 753µl | 9.0 |
| 40µl | 1.6µM | 10µl solution 3 | 0.250µM | 750µl | 6.4 |
| 40µl | 1.6µM | 6.3µl solution 2 | 0.500µM | 754µl | 3.2 |

Data elaboration

Analysis were acquired using a Zetasizer Nano ZS instrument (Malvern Panalytical, UK) with the related dedicated software Zetasizer version 7.12. Data where then exported in Excel for the Z-Average vs PHR plot creation (PCS titration) or further copied in GraphPad software to fit the PHR vs the Zeta Potential and obtaining the Zp=0 PHR, which represents the maximum of aggregation (Zeta Potential titrations).

Instrument set up

- *Size acquisition parameters*

Material: Protein

Dispersant: deionized water

General options: Use dispersant viscosity as sample viscosity

Temperature: 25°C

Equilibration time: 30 secs

Cell: Disposable micro cuvette, for size measurement, minimum volume 40µL (ZEN0040, Malvern Panalytical Instruments Ltd)

Measurement: Angle: 173° Backscatter

Number of runs: 10 runs

Run duration: 10 secs

Number of measurements: 3

Delay between measurements: 5 secs

Position method: Seek for optimum position

Automatic attenuation selection: Yes

Data processing: General purpose (normal resolution)

To obtain the size of complexes in solution, single exponential fitting of correlation function was applied and mean size in terms of z-average radius was obtained.

- Zeta Potential acquisition parameter

Material: Protein

Dispersant: deionized water

Sample viscosity: Use dispersant viscosity as sample viscosity

Model for F(Ka): Smoluchowsky F(Ka) = 1.50

Temperature: 25°C

Equilibration time: 30 secs

Cell: Disposable folded cuvettes for the measurement of Zeta Potential, minimum volume 800 µl (DTS1070, Malvern Panalytical Instruments Ltd)

Measurement: manual (alternately automatic. with number run between 10 to 100)

Number of runs: 10 for every measurement

Number of measurements: 6

Delay between measurement: 5 secs

Automatic attenuation selection: Yes

Automatic voltage selection: Yes

Data processing: Monomodal

### 4.4.4. Results

The present study was at least divided in two different parts: the first one, the assessing of the reproducibility of the methods already optimized for heparin/PF4 for the analysis of SLDX by analyzing 10 different solutions of the same sample; the second one, to compare all the samples.

#### 4.3.4.1. SLDX/PF4 interaction characterization reproducibility

To assess the reproducibility of the SLDX/PF4 complex formation, at least 10 different solutions of G12512 were prepared and analyzed. Results, respectively of PCS and Zp titrations, are reported in Table 4.4.6 and in Table 4.4.7, while the related titrations curves are showed in Figure 4.4.1 and in Figure 4.4.2.

**Table 4.4.6 PCS G2512 reproducibility results**

| ***PGR*** | ***Z-average (nm) Solution A*** | ***Z-average (nm) Solution B*** | ***Z-average (nm) Solution C*** | ***Z-average (nm) Solution D*** | ***Z-average (nm) Solution E*** |
|---|---|---|---|---|---|
| **12.8** | 450 | 450 | 470 | 520 | 530 |
| **9.0** | 700 | 580 | 540 | 620 | 550 |
| **6.4** | 730 | 610 | 570 | 700 | 600 |
| **3.2** | 190 | 210 | 240 | 390 | 270 |
| **2.0** | 120 | 190 | 270 | 270 | 200 |
| ***PGR*** | ***Z-average (nm) Solution F*** | ***Z-average (nm) Solution G*** | ***Z-average (nm) Solution H*** | ***Z-average (nm) Solution I*** | ***Z-average (nm) Solution J*** |
| **12.8** | 460 | 444 | 430 | 460 | 440 |
| **9.0** | 530 | 510 | 530 | 570 | 530 |
| **6.4** | 620 | 580 | 550 | 580 | 590 |
| **3.2** | 180 | 60 | 60 | 130 | 70 |
| **2.0** | 180 | 80 | 60 | 70 | 60 |

**Table 4.4.7 Zp G12512 reproducibility results**

| *PGR* | *Zp (mV) Solution A* | *Zp (mV) Solution B* | *Zp (mV) Solution C* | *Zp (mV) Solution D* | *Zp (mV) Solution E* |
|---|---|---|---|---|---|
| **12.8** | 12.0 | 14.4 | 14.6 | 14.2 | 15.1 |
| **9.0** | 1.9 | 4.0 | 7.4 | 6.6 | 7.0 |
| **6.4** | -20.8 | -19.7 | -11.7 | -11.1 | -6.6 |
| **3.2** | -34.0 | -34.3 | -36.5 | -34.8 | -34.8 |
| **2.0** | -34.6 | -35.0 | -35.8 | -36.0 | -37.2 |
| ***PGR*** | ***Zp (mV) Solution F*** | ***Zp (mV) Solution G*** | ***Zp (mV) Solution H*** | ***Zp (mV) Solution I*** | ***Zp (mV) Solution J*** |
| **12.8** | 12.4 | 12.1 | 12.5 | 11.9 | 11.8 |
| **9.0** | 0.7 | 3.4 | 3.7 | 1.7 | 4.7 |
| **6.4** | -19.2 | -18.0 | -19.4 | -18.7 | -14.3 |
| **3.2** | -28.8 | -31.3 | -32.4 | -29.8 | -31.3 |
| **2.0** | -30.6 | -31.8 | -32.7 | -31.4 | -31.7 |

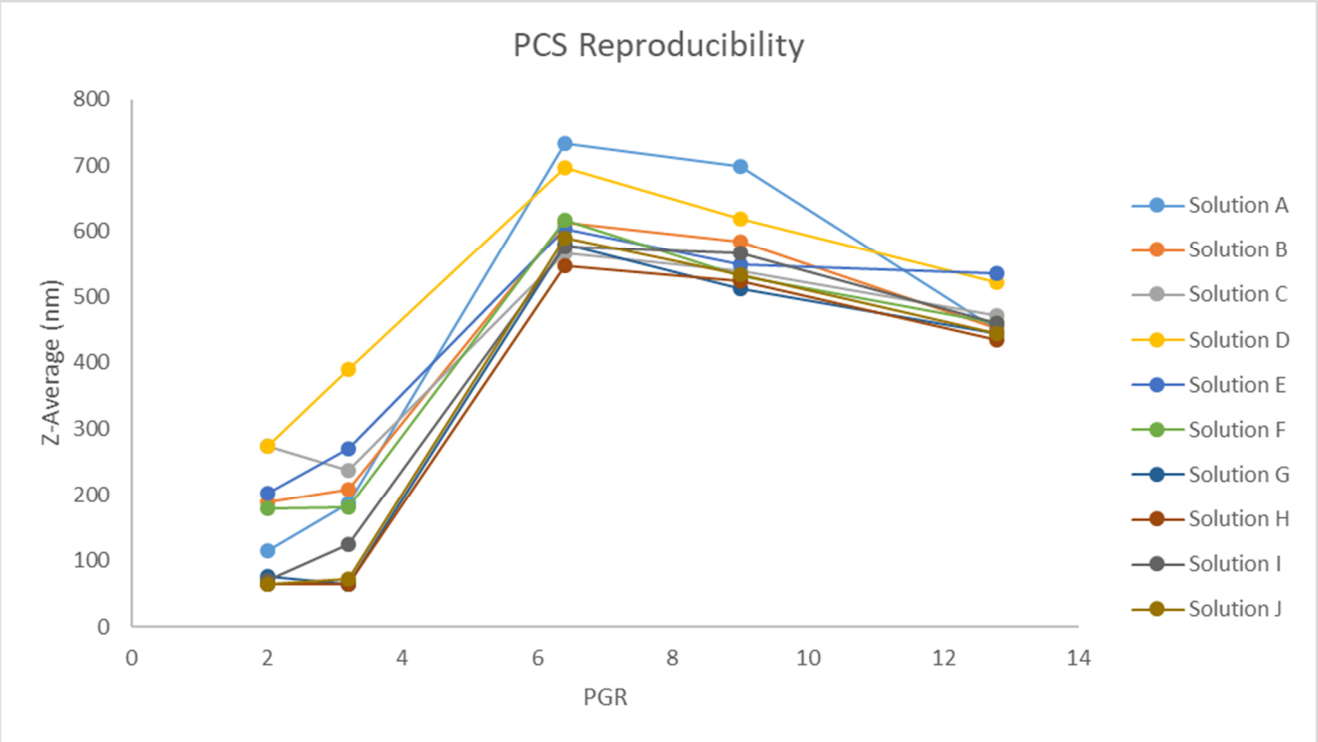


**Figure 4.4.1 SLDX PCS Reproducibility results**

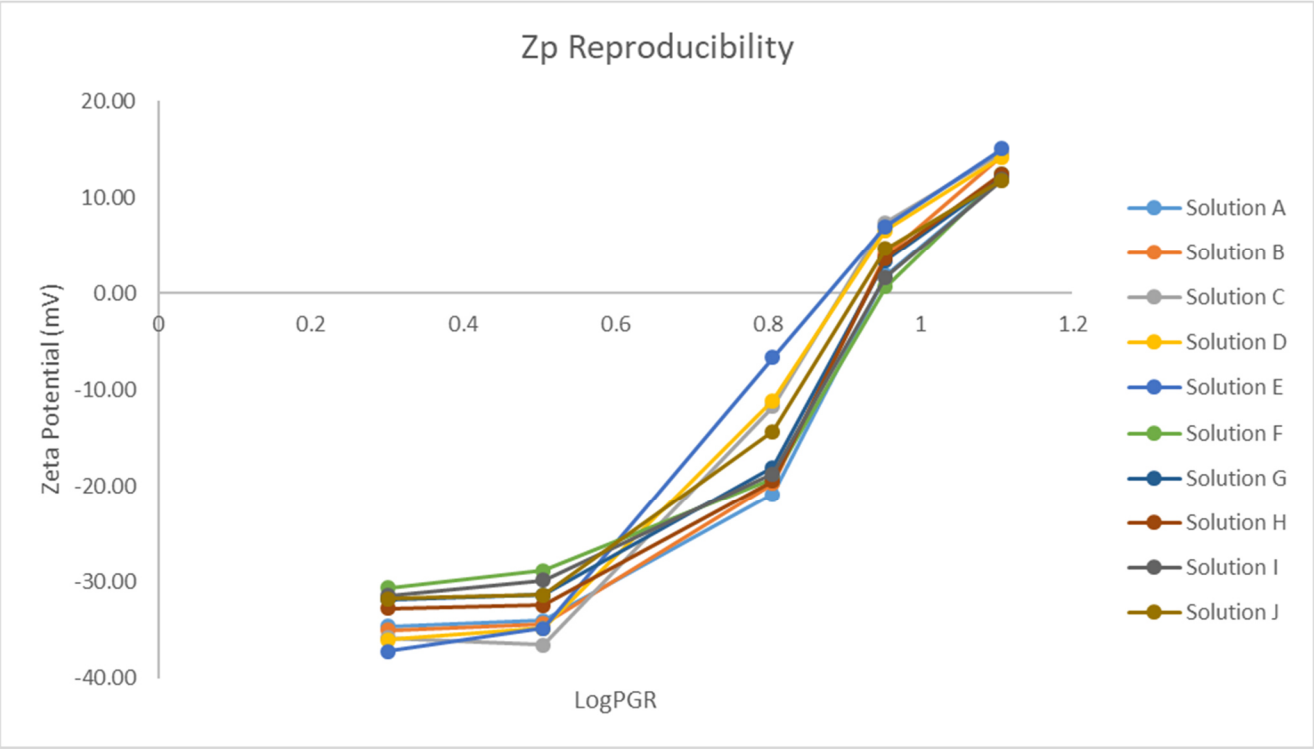


**Figure 4.4.2 SLDX Zp Reproducibility results**

In Table 4.4.8, the resume of the PGR of maximum aggregation and the related Z-average, with the addition of the calculated PGR for null Zp is reported; moreover, the mean and the standard deviation (Std. Dev.) of the ten titrations, with the related coefficient of variation (CV %), are reported.

**Table 4.4.8 Summary of SLDX reproducibility results.**

| | PGR maximum aggregation | Z-Average maximum aggregation (nm) | Zeta Potential = 0 |
|---|---|---|---|
| **Solution A** | 6.4 | 730 | 8.7 |
| **Solution B** | 6.4 | 610 | 8.5 |
| **Solution C** | 6.4 | 570 | 7.6 |
| **Solution D** | 6.4 | 700 | 7.6 |
| **Solution E** | 6.4 | 600 | 7.8 |
| **Solution F** | 6.4 | 620 | 8.9 |
| **Solution G** | 6.4 | 580 | 8.5 |
| **Solution H** | 6.4 | 550 | 8.5 |
| **Solution I** | 6.4 | 580 | 8.7 |
| **Solution J** | 6.4 | 590 | 8.1 |
| **mean** | ***6.4*** | ***610*** | ***8.3*** |
| **Std. Dev.** | - | 59 | 0.5 |
| **CV %** | - | 10 | 5.8 |

As Table 4.4.8 shows, G12512 always reached is maximum of aggregation for a PGR of 6.4 by PCS results, and the size of the complex formed (610 nm, mean value) is more similar to a LMWH than a UFH one, as showed in the previous paragraph for sample G12292 (560 nm); this means that no ultra-large complexes are formed, so although its higher Mw, SLDX would be predicted to be less likely to provoke antibody formation[134]. Nevertheless, the PGR of 6.4 is higher than the porcine LMWH 2.0 one, but of course G12512 also has a longer chain length, and in fact this value is more likely to a heparin fraction with a Mw of approximately 10 kDa[158]; it is not a case that this Mw is highly similar to the Fm-Hep component of G12512 (G12824_A, 10.9 kDa), and this could confirm that is the heparin species that predominantly interact with PF4. The calculated CV % on the size of the maximum complex (expressed as Z-Average, nm) is 10 %, with a gap of approximately 190 nm between the highest and the lowest values. Considering the high instability of the measures due to the several equilibria that are present among the different structures in solution, we can conclude that the PCS method applied on a SLDX sample is reasonably reproducible; such reproducibility is

also appreciable by Figure 4.4.1 in which titration curves are quite well overlaid, with the only exception of solutions A and D ones (only the 20 %).

Zeta Potential reproducibility test on SLDX showed the same high measures instability already observed for PCS analysis, although in this case a less CV % (5.8 %) is reported. The average value at which the Zp is 0 resulted 8.3, much higher than the maximum aggregation PGR obtained by PCS, and if we consider the results for the sample analysed in the previous chapter, this observation was already showed by the UFHs, so in this sense SLDX interacts with PF4 more likely to a UFH than a LMWH; besides, the observed Zp=0 PGR corresponds to a heparin fraction with a molecular weight of approximately 14.7 kDa[156], a Mw value that is similar to the G12512 one. Even if this consideration seems to be in contrast with the PCS one, it has to be considered that Zp evaluation takes into account the charges neutralization, so it is probable that in this case the DeS component plays a role in the interaction. It is in fact known that PF4 can bind with the other GAGs, though with a less affinity (heparin > heparan sulfate > dermatan sulfate > chondroitin 6-sulfate > chondroitin 4-sulfate)[173], so it is reasonable to think that the presence of another sulphated species can increase the heparin interaction with the protein. Nevertheless, the similarity is with a higher Mw heparin fraction, so we can conclude that SLDX interacts less than heparin with PF4.

#### 4.3.4.2. Samples comparison

After the assessment of the method suitability for a GAG mixture, the isolated components were analysed and compared to G12512, from which they were obtained (see chapter 3.3), in order to evaluate their interaction with PF4 when not in mixture; moreover, the three DeS/Hep mixtures analysed for the different chromatographic conditions used for the Mw distribution evaluation were also investigated, this time for trying to better understand of diverse weight quantities of DeS and Hep can influence the PF4/SLDX interaction.

In Table 4.4.9, the PCS and Zeta Potential results, as PGR of maximum aggregation obtained with the related Z-Average value, and PGR for which Zp=0, are reported; in Figure 4.4.3 and in Figure 4.4.4, the titrations curves are showed, respectively PCS and Zeta Potential.

**Table 4.4.9 Samples comparison results.**

| Sample | Type | Mw (kDa) | PGR Max aggregation | Z-Average max aggregation (nm) | Zp = 0 |
|---|---|---|---|---|---|
| **G12512** | SLDX | 13.5 | 6.4 | 620 | 8.1 |
| **G12824_A** | Fm-Hep | 10.9 | 6.4 | 510 | 6.0 |
| **G12909_Fr1** | DeS | 21.5 | 9.0 | 610 | 10.6 |
| **G14202** | MIX 1 | 17.5 | 6.4 | 560 | 11.5 |
| **G14203** | MIX 2 | 15.7 | 6.4 | 630 | 9.8 |
| **G14204** | MIX3 | 13.7 | 6.4 | 550 | 8.5 |

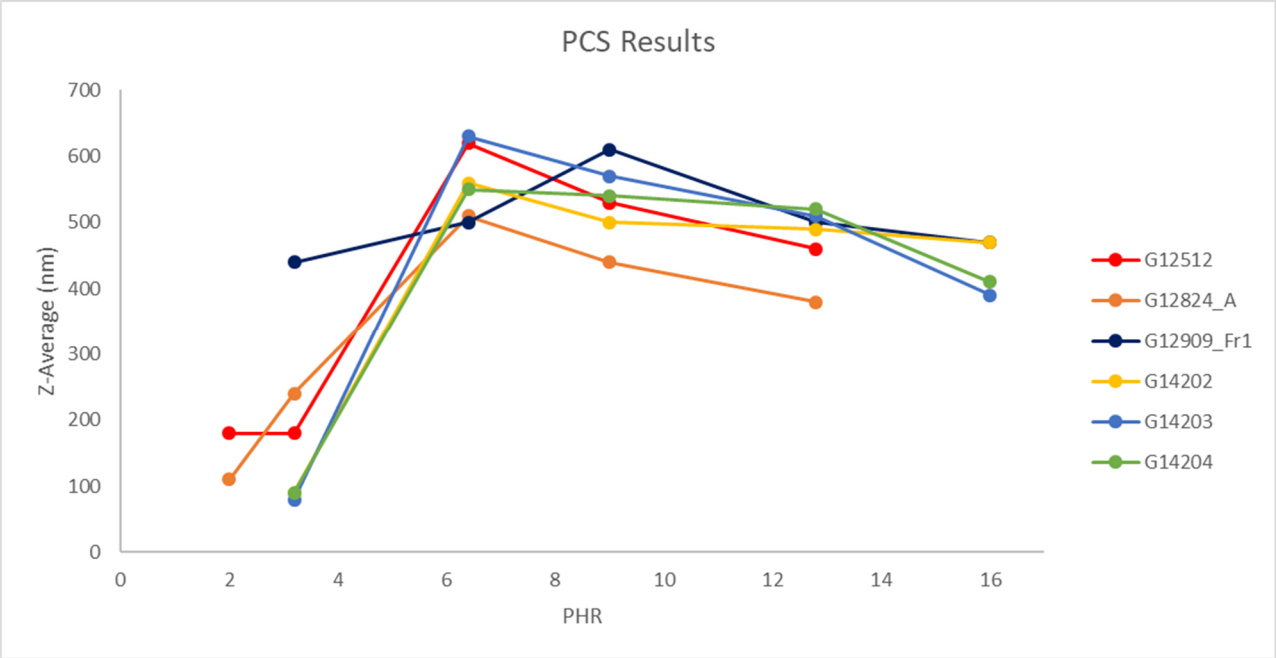


**Figure 4.4.3 PCS samples titrations curves**

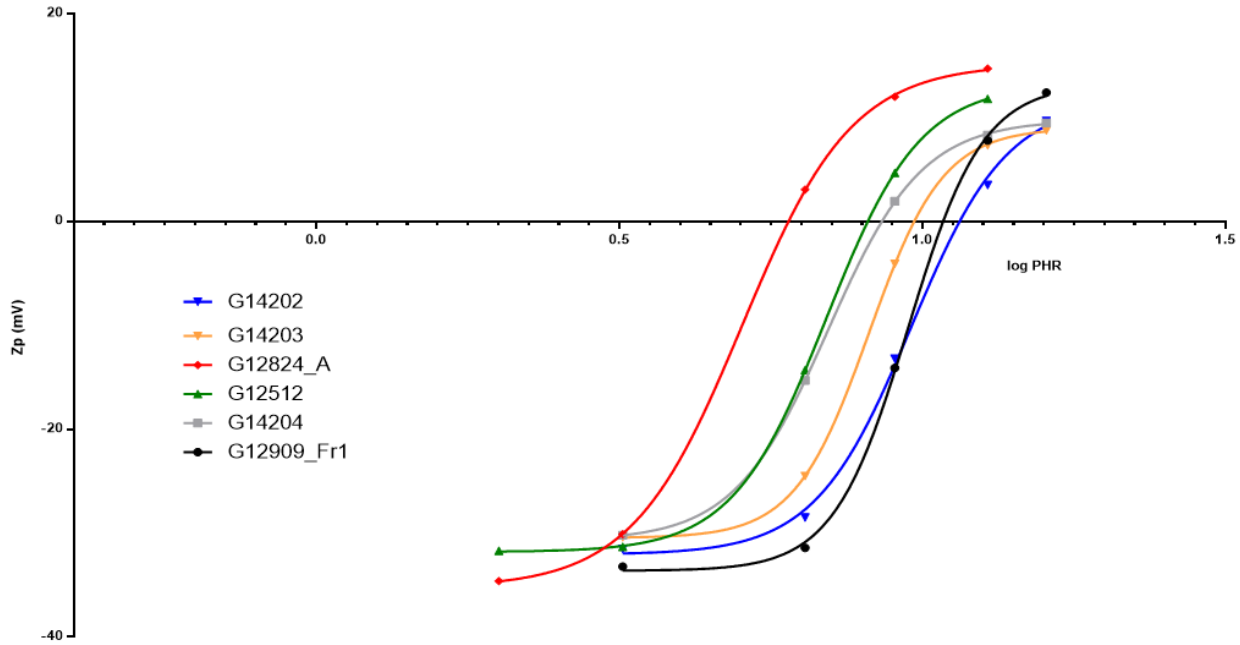


**Figure 4.4.4 Zeta Potential titrations results**

Starting from PCS, the first result that appear from Figure 4.4.3 is that all the curves are very similar each other, no matter what the Mw is; moreover, all the samples maximum PGR is 6.4 with an average size of 600 nm. The only exception is represented from the DeS species (G12909_Fr1), which reaches the maximum aggregation at PGR=9.0; to note, also, is that its titration curve is quite flat and, it does not form the already mentioned ultralarge complexes, as expected from its high Mw (consider as a comparison the value obtained for the porcine UFH G9850 sample analysed in the previous section, for which the maximum of aggregation reached at a PHR of 9.0 is related to a complex size higher than 1000 nm), and this can be considered a confirm of the less interaction of DeS with PF4 as reported in literature[173]. Going back to SLDX sample (G12512) and the three DeS/Hep mixtures, as said before, their titration curves are very similar, but most of all they maintain the same trend of G12824_A, the Fm-Hep species, that is the lowest Mw sample analysed in this section and it is the component with the major interaction for PF4. The only difference is that it reaches in each point lower sizes than the other samples, in particular the complex at the maximum of aggregation is approximately 100 nm lower than G12512 and only 40 nm respect to G14204, which is the mixture with the highest heparin content and the lowest Mw. Comparing the three mixtures, by the significant difference in the Mw and in the components weight percentages, we expected some differences, in particular in the PGR of the maximum aggregation, but, the fact that

all samples interact quite in the same way with PF4 could be explained as the confirm that effectively the heparin component is the one that prevalently interact with the protein.

Different results were achieved from the Zeta Potential evaluation, as appear from Figure 4.4.4, in which a sort of more dispersity in the titration curves is shown. More in detail, the PGR of maximum aggregation tend to increase as the Mw increase, so the sample concentration needed to obtain it decrease, and this behaviour is more "likely" to the typical trend already observed for heparin/PF4 interaction study done in the previous section. More in detail, the PGR for which the Zeta Potential is null starts with the 6.0 of the Fm-Hep sample (G12824_A, 10.9 kDa) and reach about 11.5 for the DeS/Hep mixture sample 1 (G14202, 17.5 kDa). The only exception is G12909_Fr1 (DeS, 21.5 kDa), for which the Zp=0 PGR is 10.6, so slightly lower than G14202, but taking into account the gap between the higher (8.9) and the lower (7.6) PGR values that were obtained for the SLDX repeatability test, we can consider this difference not significant. Moreover, again if compared to the porcine UFH analysed previously (G9850) PHR for which Zp is null (12.9), a major amount of DeS is needed to reach the maximum of aggregation, a further confirm of its less interaction with PF4; it can be also taken into account that probably the presence of the heparin species, which as a greater affinity to the protein, as reported in the Introduction section, can influence the interaction, shifting the achievement of the maximum aggregation to higher amount of sample. The main comment that can be made on Zeta Potential evaluation results is that, if we consider that this titration is based on the positive charge of the protein's saturation, of course the larger is the polysaccharide chain, the higher is the number of charges and so the lower is the amount of sample required for nullify the PF4 charge, and this observation can explain why, for example, the G12512 (13.5 kDa) and G14204 (13.7 kDa) curves are quite the same; nevertheless, the presence of the heparin species has a great influence in the interaction process, as discussed for the comparison between G12909_Fr1 and G14202.

### 4.4.5. Conclusions

The present study has the general aim of assessing the interaction of PF4 with GAGs mixtures, in particular an API SLDX sample, by the already optimized PCS and Zp techniques. Besides, the interaction between the isolated Fm-Hep and DeS fractions and PF4 were investigated, as well as three

mixture of a Hep fraction and of a DeS fraction in different proportions, with the intention of studying deeper how the two SLDX components interacts with the protein.

Firstly, we assessed the suitability of the PCS and Zp methods in analysing polysaccharides' mixtures like the SLDX by repeating ten times the PF4 titration preparing ten different starting 0.2 mM solutions of G12512, and results showed that both techniques are quite reasonably reproducible, obtaining CV % of 10 and 5.8 % for respectively PCS and Zeta Potential methods, values that, considering the high instability of the measures due to the several equilibria that are present among the different structures in solution, are acceptable. As already observed in the previous section, the PGRs for which the maximum of aggregation is reached achieved by the two techniques are quite different, revealing that by PCS G12512 seems to act more likely to a heparin sample with a Mw of approximately 14 kDa[156], whereas by Zeta Potential tends more to a higher Mw heparin sample behaviour. Anyway, discrepancies between the results obtained by the two methods were already observed and commented as the result of a different maximum of aggregation calculation modality, precisely experimental for PCS and extracted from a fitting of the titration curve for Zp.

Going on with the results gained on the isolated DeS and Fm-Hep species (G12909_Fr1 and G12824_A) and on the three different GAGs mixtures, they showed a sort of specificity of interaction for different molecular weights and for different GAG type, as already demonstrated previously by Bertini et al[156], but also show that a description of the interaction requires all the three measured results, maximum size and PHR value at maximum size obtained by PCS and PHR value of null Z-potential from Z-potential measurements. In fact, if by Zeta Potential technique a sort of trend is revealed, for which increasing the Mw means an increasing in the PGR value of PF4 charge neutralization (from 6.0 of the Fm-Hep sample G12824_A to the 11.5 of the mixture sample G14202, respectively of 10.9 and 17.5 kDa), and so a less amount of sample needed, by PCS a different outcome appeared, and in fact all samples reached the maximum aggregation at the same PGR value (6.4) and resulted with quite the same maximum complex size (approximately 600 nm).

Actually, the indeed less interaction of the isolated DeS component, G12909_Fr1, was assessed by both the techniques, for which the flat PCS curve and the not formation of ULC is accomplished with a lower Zp=0 PGR than G14202 sample, the mixture composed of 70 % DeS and 30 % Hep, and in this terms also a role of influence of the heparin species in the mixture is recognized.

# 5. Physical-chemical characterization of Defibrotide and its interaction with PF4

## 5.1. Introduction

Defibrotide (DFT) is a mixture of single and double stranded phosphodiester oligonucleotides derived from the controlled depolymerization of porcine intestinal mucosal DNA[174]; it is approved for the treatment of Veno-Occlusive Disease (VOD), a potentially fatal complication that occurs in ~14 % of haematopoietic stem cell transplantation (HSCT) patients[175–177]. DFT has multiple mechanisms of action, including anti-inflammatory, anti-atherosclerotic, anti-ischemic, and antithrombotic properties[178,179]; in particular, the antithrombotic activity of DFT has been ascribed to the inhibition of cathepsin G serine protease, an enzyme responsible for the cleavage of important extracellular matrix proteins such as elastin, collagen, fibronectin or laminin, causing extensive lung tissue damage[180,181]. Furthermore, the antithrombotic activity of DFT compares favorably to that of heparin, a sulphated polysaccharide belonging to the glycosaminoglycan family and today's most widely used anticoagulant drug[182–185]. Despite widespread use, heparin therapy exhibits several adverse effects mostly related to its potency as an anticoagulant. Additionally, heparin use can lead to Heparin-Induced Thrombocytopenia (HIT), a dangerous drug reaction to UFH or, less commonly, to LMWH that exists in two types. Type-1 HIT is a non-immune disorder that results from the direct effect of heparin on platelet activation and that starts within the first 2 days after exposure to heparin. Type-2 HIT is a drug-induced, immune-mediated thrombocytopenia that typically occurs 4–10 days after exposure to heparin with the development of HIT II antibodies (IgG) that can recognize the complex formed by heparin and Platelet Factor 4 (PF4), a chemokine released by activated platelets. Patients with HIT type 2 are at a considerably increased thrombosis risk[186,187]. Such antibodies can have devastating clinical effects, potentially leading to stroke, cardiac arrest, amputation or even death; consequently, a prompt diagnosis, heparin cessation and the initiation of a non-heparin therapy are important to prevent further complications in HIT. Glycosaminoglycan mixtures (like danaparoid), or synthetic molecules (like fondaparinux) are alternative therapies for HIT management and other types of antithrombotic drugs are under consideration[147,188,189]. In this field, DFT is a valid option, as it was demonstrated that HIT antibodies are not generated after DFT treatment[190]; furthermore, a

clinical case study of HIT management demonstrated DFT effectiveness as an antithrombotic drug[191].

## 5.2. Aim of the work

In the present work, we provide a fine physical-chemical characterization of defibrotide structure and molecular weight distribution, by nuclear magnetic resonance (NMR) and high-performance size exclusion chromatography (HP-SEC)[192]. An in-depth evaluation of the complex formation between DFT and PF4 was investigated using PCS and Zp measurements to monitor the changes in size and surface charge of the DFT-PF4 complexes formed upon titration of the protein with the drug, as already been used to evaluate the heparin-PF4 interaction[156] (see Chapter 4.3). Thermodynamic parameters were investigated using isothermal titration calorimetry, a technique that is widely used for protein-ligand interaction studies. DFT results were compared to a porcine UFH, as previously shown in literature[193,194].

## 5.3. Materials and methods

### 5.3.1. Materials

Three defibrotide API samples manufactured at former Gentium Pharmaceuticals, (P6231, P6232 and P6233), were kindly provided by the Loyola University of Chicago, from prof. Fareed's group. Unfractionated porcine intestinal mucosal heparin was obtained from Techdow Pharmaceuticals (Shenzen, China). Human PF4 (hPF4) was purchased from CromaTec GmbH (Greifswald, Germany), as freeze-dried powder in HBSS, 1 mg per vial. Hank's Balanced Salt Solution (HBSS), sodium nitrate and sodium azide were obtained from Sigma Aldrich. Deioniezd water was obtained using a Culligan water system.

### 5.3.2. Methods

#### 5.3.2.1. NMR characterization

For recording $^{1}H$ NMR spectra, approximately 5 mg of each DFT samples were dissolved in 0.6 ml of $D_2O$ and analyzed by using a Bruker NEO 500 MHz NMR spectrometer (Karlsruhe, Germany),

equipped with 5-mm TCI cryoprobe. The proton spectra were recorded at 323 K, with a pulse delay of 4 s and 128 scans.

An in-depth study of P6231 was performed, and Heteronuclear Correlation NMR spectroscopy (HSQC) spectrum, $^{13}C$ NMR spectrum and $^{31}P$ NMR spectrum of P6231 (20 mg in 0.6 ml deuterated water) were recorded at 323 K on a Bruker HD 500 MHz (Karlsruhe, Germany). For HSQC experiments, water presaturation was applied during each 16 s of relaxation delay and spectra were obtained in phase-sensitive, sensitivity pure-absorption mode with decoupling in the acquisition period (Bruker pulse program hsqcetgpsisp2.2). For recording $^{13}C$ NMR spectrum, a pulse delay of 4 s and 20 K scans were used, while for $^{31}P$ NMR a pulse delay of 4 s and 128 scans were used. Spectra were acquired using TOPSPIN version 3.5 and elaborated using Bruker TOPSPIN 4.0.3 version.

#### 5.3.2.2. Molecular weight distribution evaluation

The evaluation of the molecular weight distribution was performed using High Performance Size Exclusion Chromatography coupled with a multi-detector system (Refractive Index, Light Scattering and Viscometer, HP-SEC-TDA)[78]. The analyses were performed at 40 °C on a Malvern Panalytical system (OmniSEC GPC/SEC System) using TSKG2500PWXL + TSKG3000PWXL columns linked in series (Tosoh Bioscience, 7 μm 7.8x30 cm). The isocratic mobile phase (0.1 M $NaNO_3$ in water containing 0.05 % $NaN_3$ prefiltered using 0.22 μm filter) was used at a flow rate of 0.6 ml/min. DFT samples were injected at concentrations of approximately 2 mg/ml (100 μl volume injection).

DFT dn/dc parameter was experimentally evaluated analyzing different concentrations of P6231, starting from a mother solution of 6.2 mg/ml obtained weighting 31 mg of sample and diluting in 5 ml of mobile phase, using a graduated flask; then the following dilutions were obtained (Table 5.3.1):

**Table 5.3.1 dn/dc calculation solutions**

| Sample solution | Dilution | Concentration (mg/ml) |
|---|---|---|
| **P6231_A (mother solution)** | - | 6.200000 |
| **P6231_B** | 1:2 | 3.100000 |
| **P6231_C** | 1:2 | 1.550000 |
| **P6231_D** | 1:2 | 0.775000 |
| **P6231_E** | 1:2 | 0.387500 |
| **P6231_F** | 1:2 | 0.193750 |
| **P6231_G** | 1:2 | 0.096875 |

Chromatographic profiles were elaborated using OmniSEC software version 4.6.2.

#### 5.3.2.3. PF4-Defibrotide Complex Size and Zeta Potential evaluation

Photon Correlation Spectroscopy (PCS) and Zeta Potential (Zp) measurements were carried out with a Zetasizer Nano ZS instrument (Malvern Panalytical, Worcestershire, United Kingdom) using the same conditions reported in Chapter 4. Data were analyzed using Zetasizer software version 7.11. For Zp experiments, Zp values were plotted against the logarithm of PF4/DFT Ratio (PDR), which is calculated as PF4 molar concentration/DFT molar concentration ratio. A sigmoidal equation was fit to the data using GraphPad Prism software version 6.0 and used to determine the PDR at which Zp= 0 mV, the neutral state of the complex.

#### 5.3.2.4. Isothermal Titration Calorimetry (ITC)

ITC measurement was performed using a MicroCal ITC system (Malvern Panalytical, Worcestershire, United Kingdom). Data were acquired and elaborated using MicroCAL PEAQ-ITC Analysis software version 1.0.0.1259. 280 μl of a 3.0 μM PF4 solution in HBSS buffer was added to the sample cell and a 30.0 μM solution of P6231 sample was loaded into the injection syringe. After 60-second delay, titration was performed by injecting 3 μl of the DFT solution. Fourteen DFT injections were made, spaced 240 seconds apart. The sample cell was maintained at 25°C and the contents were stirred at 1000 rpm during the injections.

#### 5.3.2.5. Anticoagulant activity profile

The anticoagulant activities of the three DFT samples were measured in normal human pool plasma. Each of the individual sample batches was dissolved in normal saline at a concentration of 1.0 mg/ml. Serial dilutions of DFT were made in plasma to obtain concentrations in the range of 0-100 ug/ml. Prothrombin time (PT), partial thromboplastin time (aPTT) and thrombin time (TT) measurements were made on ACL elite using standard reagents. Working heparin solution was prepared at 100 ug/ml. Plasma was supplemented with heparin to obtain 0-10 ug/ml levels. PT, aPTT and TT measurements were performed.

#### 5.3.2.6. HIT antibody screening

HIT mediated platelet aggregation in the presence of DFT and heparins at various concentrations was investigated using a HIT positive serum pool. Platelet rich plasma was prepared from citrated whole blood collected from normal human volunteers by centrifugation at 800 g for 20 mins. Platelet aggregation studies were carried out using a PAP-8 aggregometer (Biodata, Horsham, PA). To investigate the effect of DFT batches, PRP was supplemented at 10, 1.0 and 0.1 ug/ml and mixed well. Following addition of 50 ul of HIT positive serum, platelet aggregation was recorded over a period of 30 minutes. Similar studies were carried out with heparin over the same concentration range.

### 5.3.3. Results

#### 5.3.3.1. DFT NMR spectroscopy analysis

As a derivative of DNA porcine intestinal mucosa depolymerization, DFT consists of repetitive sequences of adenine (A), guanine (G), cytosine (C) and thymine (T) substituted 2''-Deoxy-β-D-Ribose. NMR spectroscopy is a powerful tool for determining the chemical structure, function and dynamics of oligonucleotides in solution. In the present work, $^{1}H$ and $^{13}C$ NMR spectroscopy experiments were performed to confirm the presence of the expected DFT nucleotides; the related spectra of P6231 are reported, in Figure 5.3.1 and Figure 5.3.2, proton and carbon respectively.

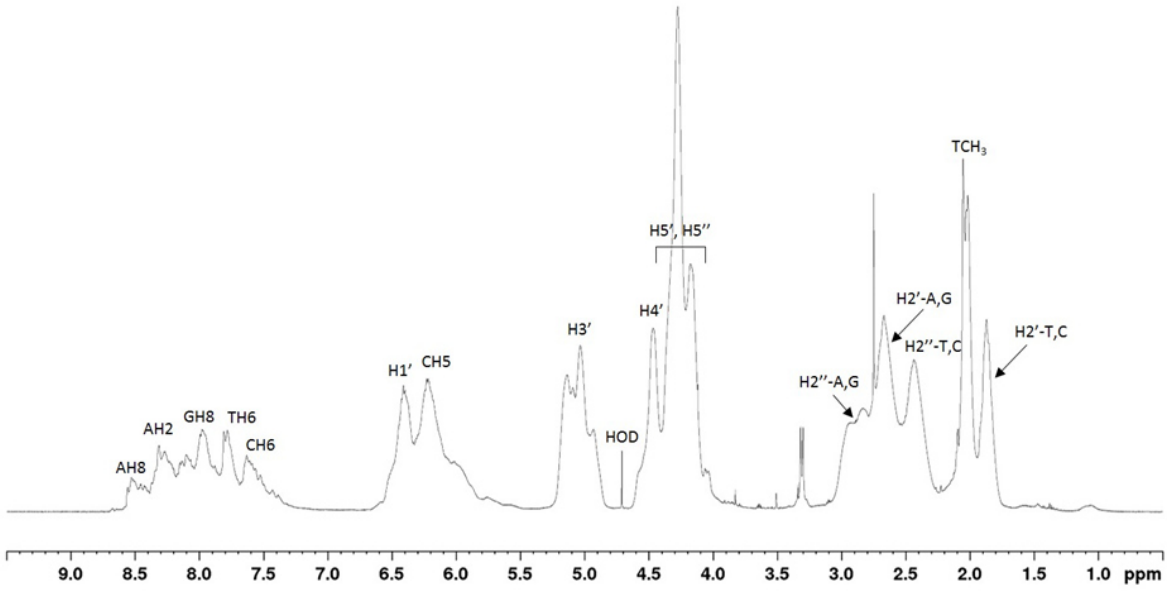


**Figure 5.3.1 $^{1}$H-NMR of P6231 (A=adenine, G=guanidine, T=thymine, C=cytosine)**

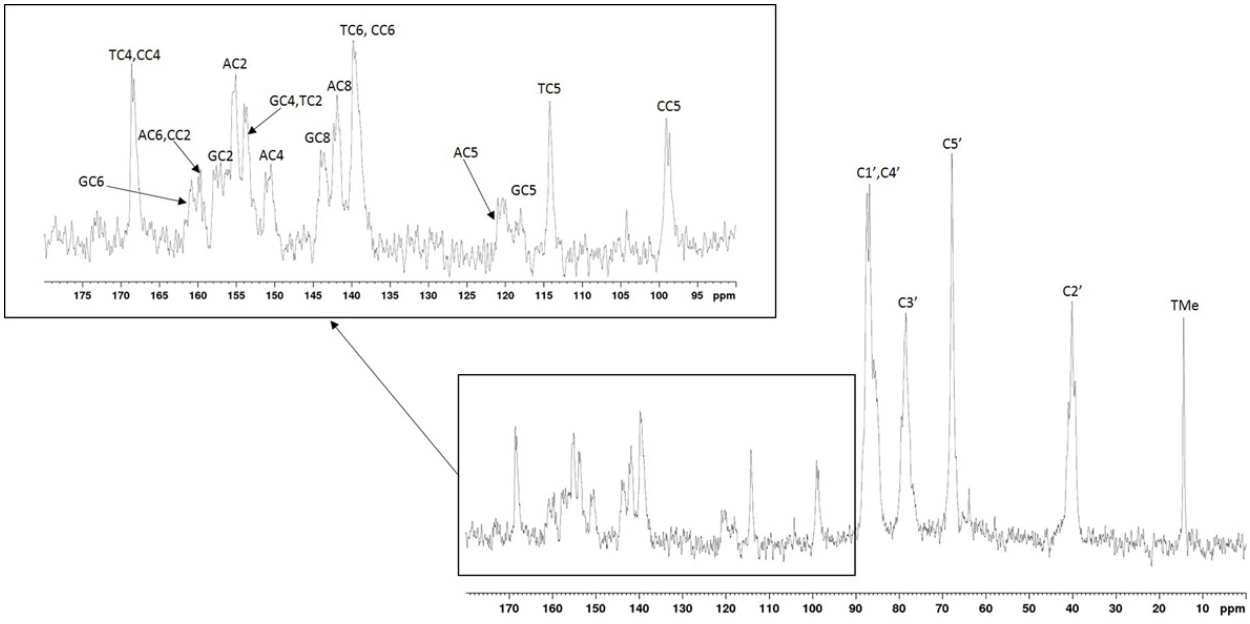


**Figure 5.3.2 $^{13}$C-NMR of P6231 (A=adenine, G=guanidine, T=thymine, C=cytosine)**

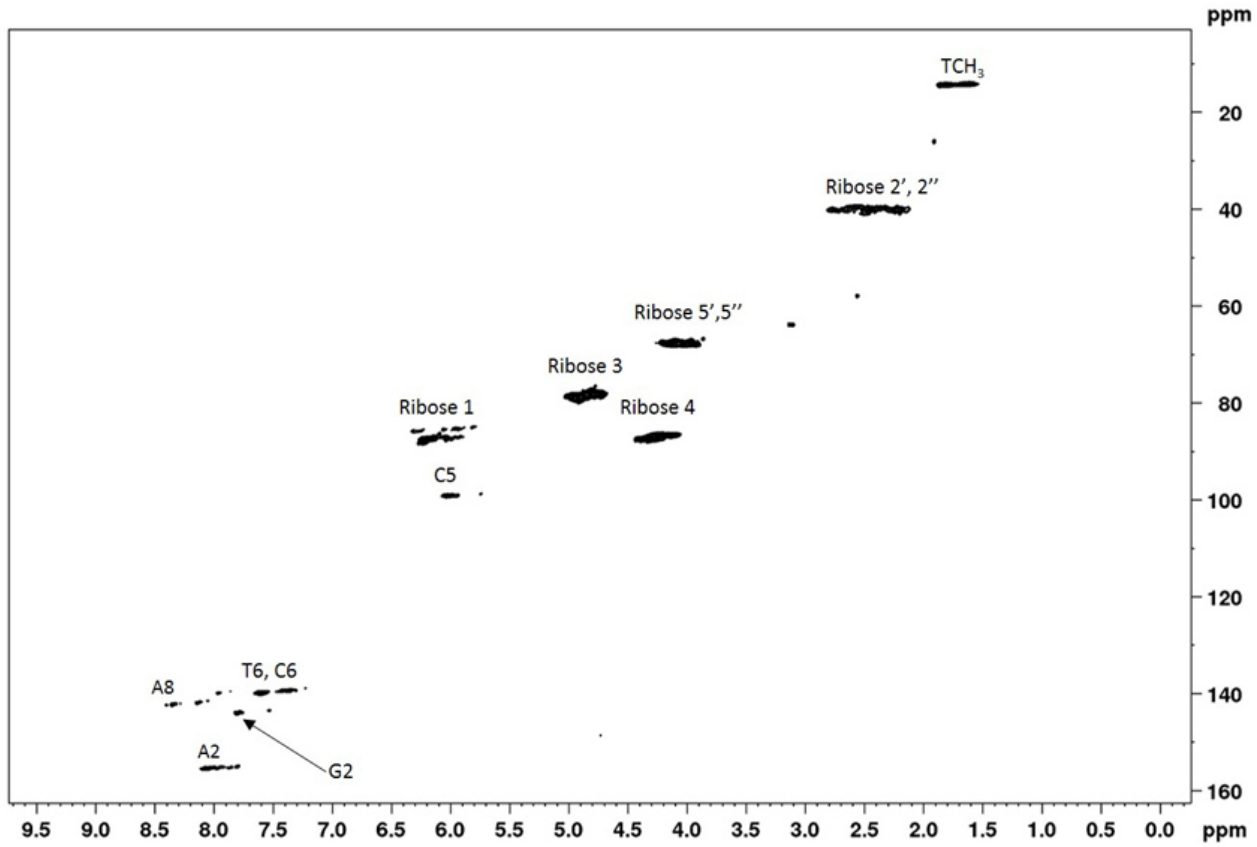


**Figure 5.3.3 HSQC spectrum of P6231 (A=adenine, G=guanidine, T=thymine, C=cytosine)**

Peak assignments were determined based on HSQC study (Figure 5.3.3) and according to literature[195]. From the proton spectrum, it is possible to see that $TCH_3$ protons resonate at ~1.9 ppm. A broad peak is found at ~6.2 ppm, relative to CH5, whereas aromatic base protons (AH8, AH2, GH8, TH6 and CH6) resonate between 8.6 and 7.3 ppm. The H1 ribose signal is shielded to 6.4 ppm, due to the presence of the nitrogenous base. Other signals are found at higher fields, in particular H3 at ~5 ppm, the H4 at ~4.5 ppm followed by the two H5 protons (two broad peaks between 4.4 and 4.0 ppm). Finally, at least four different signals are obtained for the H2 protons, for which the chemical shifts are a function of the base linked to the ribose.

In the $^{13}$C-NMR spectrum the signals for the four bases are clustered in two major groups, the first one in the range 162-149 ppm, where the peaks related to all C2, A and G C6 and A and G C4 are found, and the second one in the range 145-137 ppm, where the A and G C8 and the T and C C6 are found. The T and C C4 resonate at ~168 ppm, while all the C5 signals are at ~ 120 ppm (AC5), 118 ppm (GC5), 114 ppm (TC5) and 99 ppm (CC5); TCH3 signal resonates at ~ 15 ppm. Finally, at least four

peaks were obtained for the ribose, in particular at ~89 ppm (C1 and C4), 79 ppm (C3), 68 ppm (C5) and 40 ppm (C2).

Finally, the $^{31}P$ spectrum (Figure 5.3.4) is compatible with low molecular weight deoxyribonucleic sequences. Together with signals due to diester phosphoric group, between -1.6–1 ppm, signals attributed to end chain monoester groups (linked to C3 and C5 of deoxyribose ring) are observable between 4.1-3 ppm. A trace of inorganic phosphorus is also present (signal at 2.9 ppm).

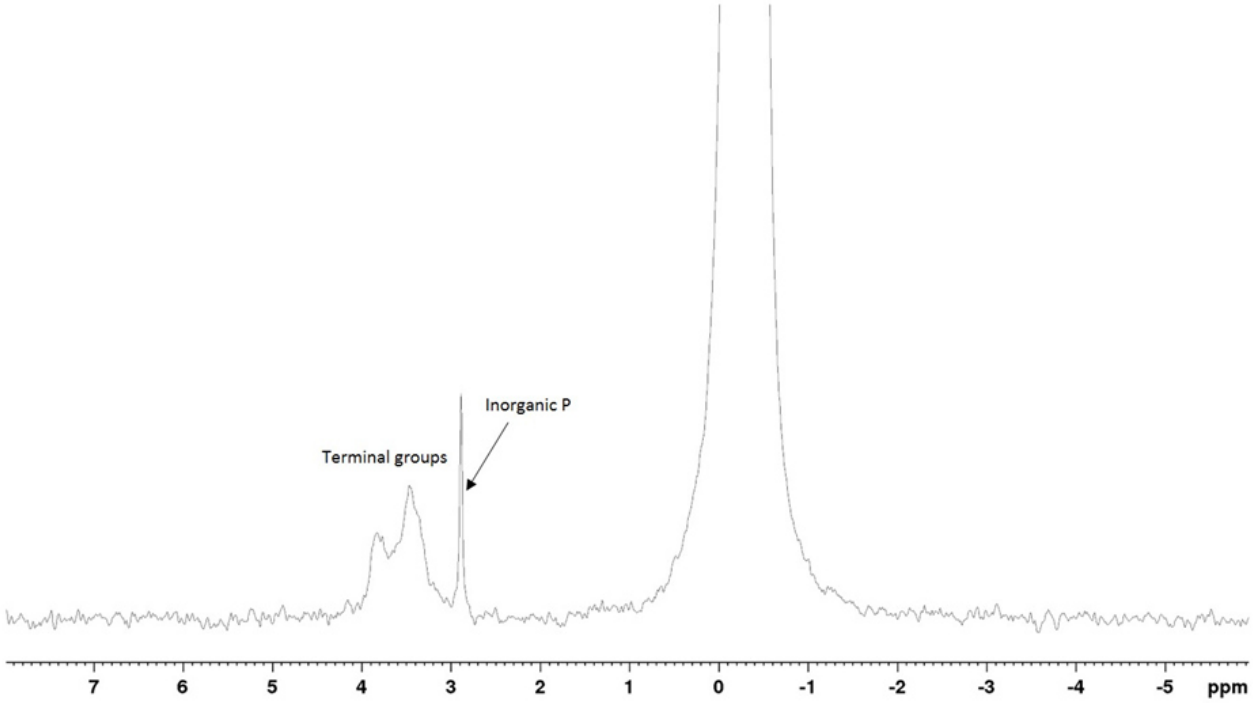


**Figure 5.3.4 $^{31}P$-NMR of P6231**

Comparing the three DFT samples proton spectra (data not shown), a complete overlay was obtained, indicating that the three samples exhibit the same structure.

### 5.3.3.2. Molecular weight distribution evaluation

Analysis of molecular weight distribution was performed using a HP-SEC-TDA technique that does not require any chromatographic calibration and considers the secondary structure of a polymer, either in terms of chain stiffness or conformation[78]. To properly evaluate the molecular weight distribution, the refractive index increment (dn/dc) must be determined. This is an important parameter that describes the refractive index changes due to mobile phase and temperature for a sample

in solution. One of the most accurate methods to obtain the value for dn/dc is to analyze the sample at different concentrations, plot concentration vs RI peak area and extrapolate the value from the slope. For P6231, the solution prepared at the concentrations reported in Table 5.3.1 were injected in twice, and the resulted graph is reported in Figure 5.3.5.

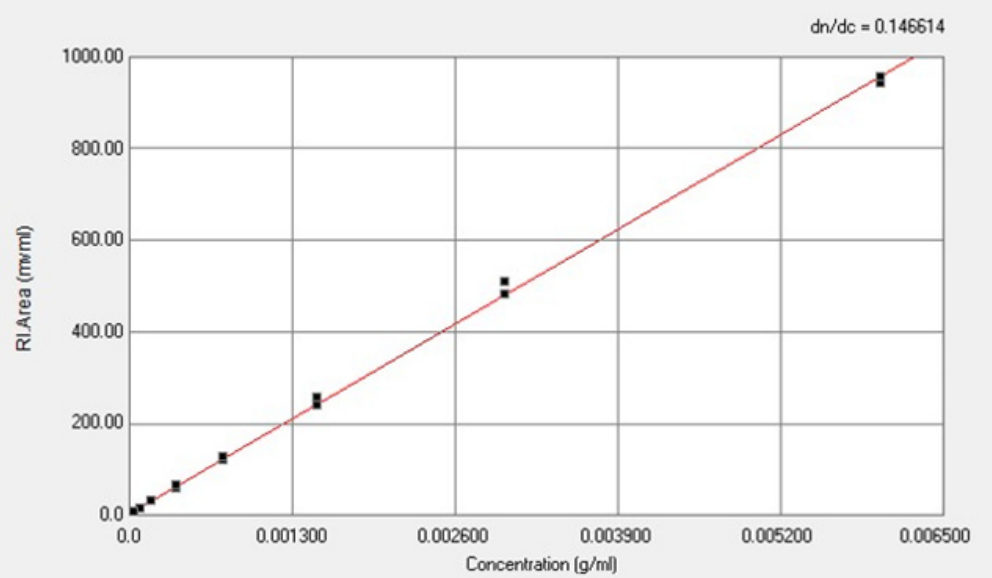


**Figure 5.3.5 Determination of DFT dn/dc parameter**

The curve obtained by RI vs concentration plot, created by a fitting algorithm of the OmniSEC 4.6.2 software, pass through the point (0,0), index that the solution prepared were suitable and correct for the evaluation; moreover, each point of the curve fit quite well, with the only exception of one of the P6231_B injections. The calculated value of dn/dc was 0.147.

Under the chromatographic conditions used, DFT eluted as a bell-shape peak with a retention volume of 11 and 15 ml (Figure 6), with a large shoulder on the high molecular weight side and a smaller one on the lower molecular weight side.

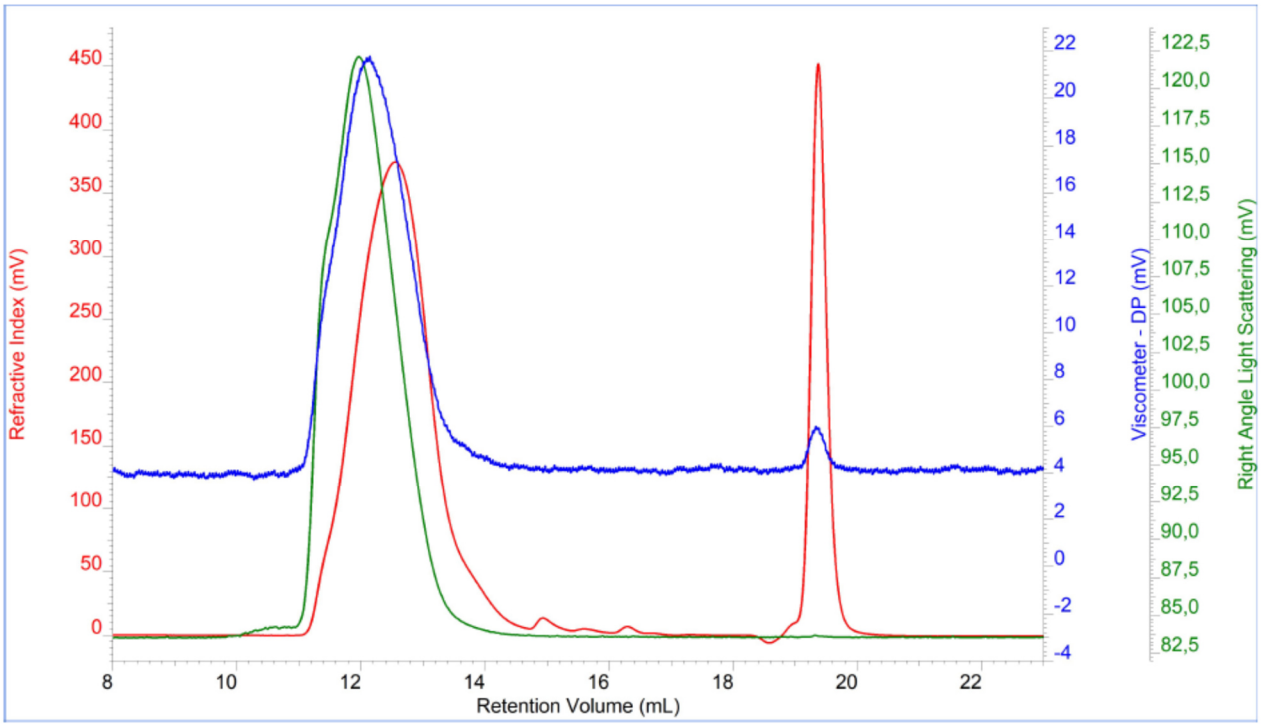


**Figure 5.3.6 Chromatographic profile of P6231. Green profile right angle light scattering, red profile refractive index and blue profile viscometer**

The profile resulted with a very good separation from mobile phase peak (about 19 ml), an index of a proper chromatographic conditions. In, the molecular weight distributions of the three DFT samples, with the addition of G9850 as a comparison sample, are reported, in terms of weight-average molecular weight (Mw, Da), number-average molecular weight (Mn, Da), polydispersion index (Mw/Mn) and hydrodynamic radius (Rh, nm).

**Table 5.3.2 Molecular weight distribution results**

| Sample | Sample type | Mw (Da) | Mn (Da) | Mw/Mn | Rh (nm) |
|---|---|---|---|---|---|
| **P6231** | DFT | 31000 | 15000 | 2.07 | 3.64 |
| **P6232** | DFT | 27400 | 14100 | 1.94 | 3.48 |
| **P6233** | DFT | 23400 | 12800 | 1.83 | 3.24 |
| **G9850** | UFH | 18100 | 13900 | 1.30 | 3.82 |

The molecular weight distributions of the three DFT samples were similar, with average Mw and Mn of 27.4 kDa and 14.0 kDa, respectively; these data are compatible with literature[196,197]. Regarding Mw/Mn, DFT resulted in a quite high average value (~1.9) compared to that of G9850 and is

compatible with the polydisperse chemical nature of DFT's phosphodiester oligonucleotides chains. Despite these results, the DFT samples hydrodynamic radii are very similar to that of porcine heparin.

#### 5.3.3.3. DFT/PF4 complexes size and zeta potential evaluation

The characterization of DFT/PF4 complex formation study is important to assess the potential of using DFT as an alternative therapy for HIT patients. Some good results are already found in literature[190], and in the present work we provide an in depth chemical-physical characterization in terms of size distribution and Zeta Potential evaluation of these complexes, using experimental conditions already used for the evaluation of the heparin/PF4 interaction[156]. Experiments were performed as titrations of the protein by increasing molar amount of DFT, and results in terms of complex size (as hydrodynamic radius, nm) for the PDR at which maximum aggregation occurred, and the PDR for which the Zeta Potential is zero, are reported in Table 5.3.3. The G850 PHR of maximum of aggregation evaluated in the Chapter 4.3 are also reported, as a positive control of PF4/heparin complex formation. In Figure 5.3.7 and in Figure 5.3.8 the titration curves, PCS and Zeta Potential respectively, are also showed, with again the addition of the G9850 ones.

**Table 5.3.3 Characterization of PF4-defibrotide complexes using PCS and Zp.**

| Sample | Z-Average (nm) | PDR max (PCS) | PDR=0 (Zp) |
|---|---|---|---|
| **P6231** | 1070 | 6.4 | 10.0 |
| **P6232** | 1030 | 6.4 | 10.7 |
| **P6233** | 1080 | 6.4 | 10.9 |
| **G9850** | 1030 | 9.0 | 12.9 |

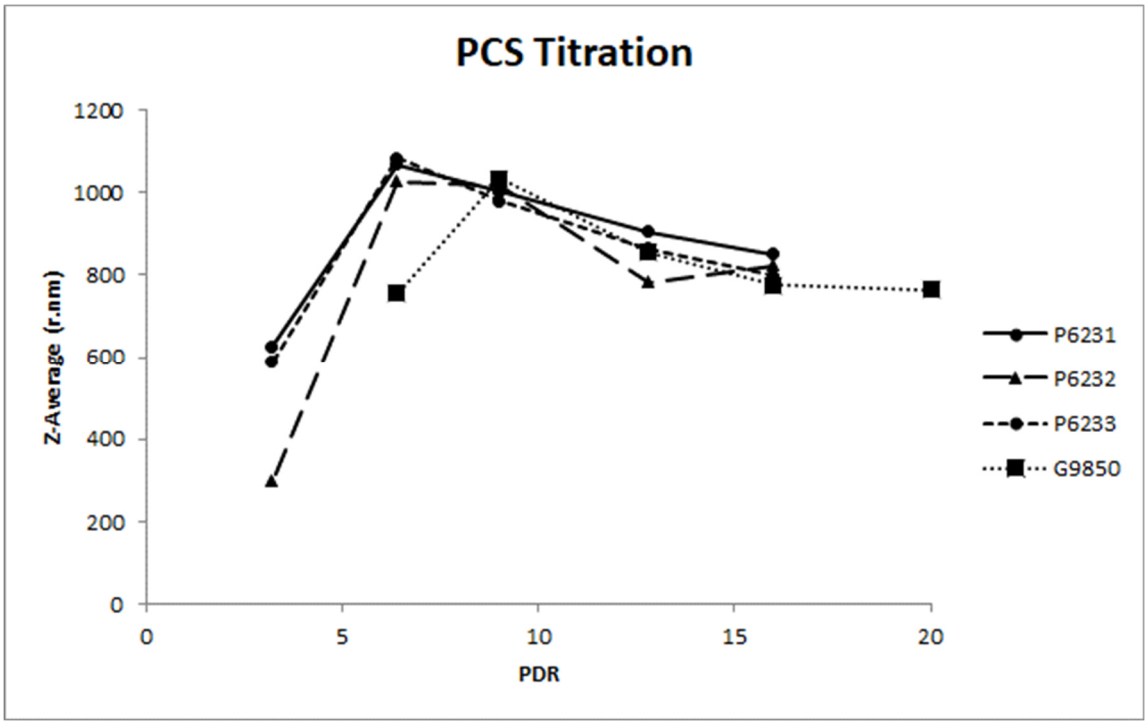


**Figure 5.3.7 PCS Titration results**

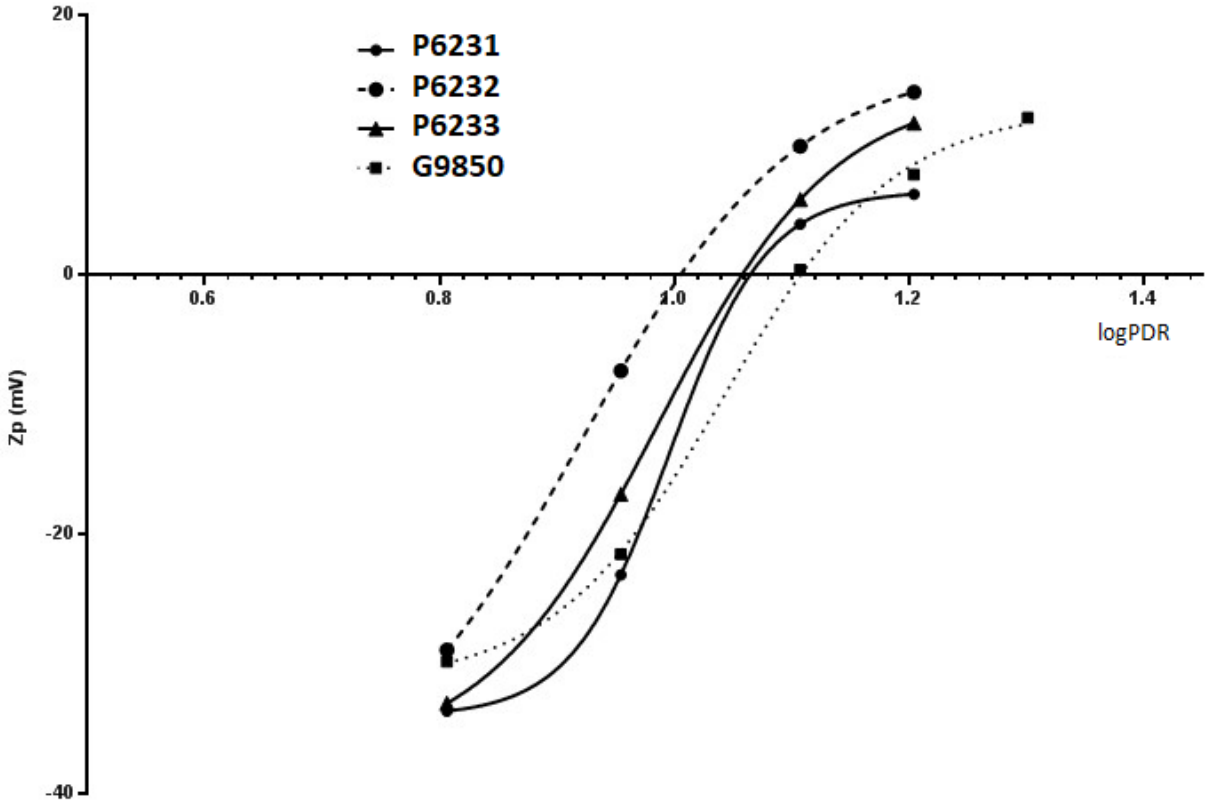


**Figure 5.3.8 Zp measurements Titration results**

By PCS, the maximal aggregation of PF4 with all three DFT samples analysed was observed at a PDR=6.4 with very similar size (about 1000 nm). This repeatability is confirmed by Zp measurements, for which the PDR at which the potential is zero is about 11. Compared to porcine UFH (G9850), DFT's PDR maxima are lower both by PCS and Zp titrations. In particular, by PCS technique, the maximum UFH aggregation is reached at PHR 9.0, and by Zp technique at 13. It is well known in literature that PF4/heparin interaction is not-specific and influenced by the chain length (and so by the molecular weight)[198–202]. Taking into account that DFT needs at least a concentration two times higher than heparin to reach the maximum aggregation even though it has the higher Mw, it can be concluded that defibrotide has less interaction with PF4 then G9850.

#### 5.3.3.4. DFT/PF4 thermodynamic parameters evaluation

ITC technique is widely used to investigate biomolecular interactions, measuring characteristics of molecular complex formation, i.e. heat uptake or release[203]. It can directly measures the energetic characteristics of such interactions, providing thermodynamic parameters such as enthalpy change ($\Delta$H), entropy change ($\Delta$S), Gibbs free energy change ($\Delta$G), reaction stoichiometry (n) and affinity constant (KA) in one experiment[204,205]. The main drawback in ITC use is that a large amount of material is required for accurate measurements, making experiments sometimes impractical[206]. The use of a micro-ITC instrument can be a great advantage, thanks to the very small quantity of both protein and ligand needed to perform the analysis.

Heparin interactions with proteins, in particular antithrombin, were largely studied by ITC methods[117] and in recent years this technique was also applied to studying PF4/Heparin complexes in an effort to understand the causes of HIT[157]. In the present study we evaluated the DFT/PF4 interaction performing a micro-ITC titration of the protein by the DFT-1 sample (P6231). No binding with PF4 was showed by the dedicated software, as reported in Figure 9, in which the released heat ($\Delta$H, kcal/mol) vs DFT/protein Molar Ratio is reported overlapped with the titration of the G9850 one, that was in this case analysed in the same conditions.

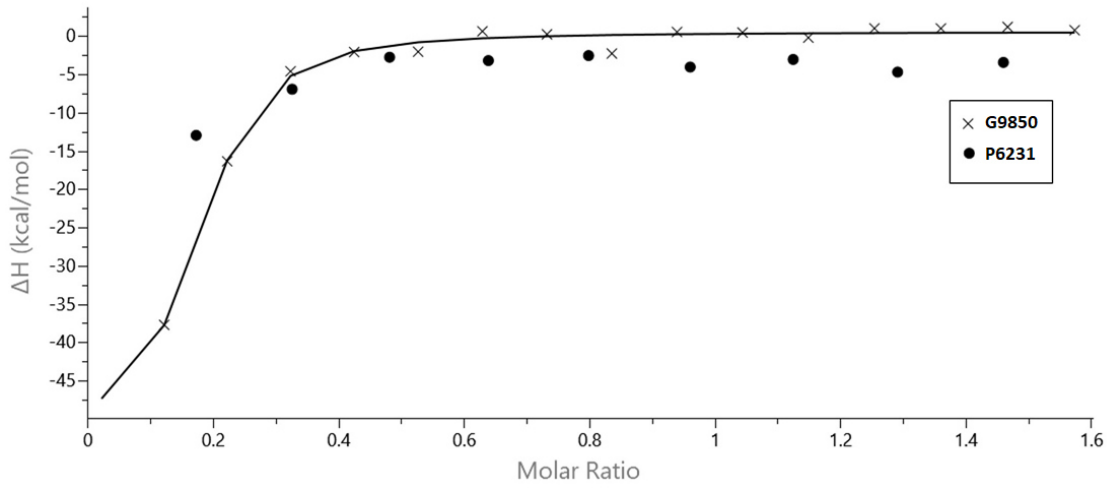


**Figure 5.3.9 ITC measurements titration curves**

The software automatically fits the raw heat released when a binding is recognized, and as can be observed for P6231 no fit curve was obtained, while for G9850, tested as a positive interaction control, the integrated raw heat gave back a fit curve, index of the presence of interaction.

#### 5.3.3.5. Effect of DFT and heparin on clotting parameters and on HIT mediated platelet aggregation

The clotting profile of the plasma supplemented with the three DFT samples, one per time, was studied over a concentration range of 0-100 ug/ml. The clotting profile of G9850 was studied at concentration ranging from 0 to 10 ug/ml, and the comparison of three DFT samples at 100 ug/ml is shown in Table 5.3.4.

**Table 5.3.4 Effect of Defibrotide and Heparin on the Clotting Profiles of Normal Human Plasma (NHP)**

| Sample | PT | aPTT | TT (5 U) |
|---|---|---|---|
| **P6231** | 10.9 | 47.7 | 36.2 |
| **P6232** | 10.8 | 48.5 | 36.4 |
| **P6233** | 10.9 | 47.3 | 39.2 |
| **G9850** | 11.2 | > 300 | > 300 |
| **Saline** | 10.8 | 32.6 | 21.8 |

*** Defibrotide samples were tested at FC = 100 ug/ml. Heparin was tested at a FC = 10 ug/ml**

At the highest concentrations tested, neither DFT nor heparin produced an anticoagulant effect measurable by the prothrombin time. In the aPTT assay, the three batches of DFT produced a mild elevation of aPTT (clotting times of 47.3 – 48.5 secs in comparison to the normal plasma which was 32.6 secs and heparin at 10 ug/ml which produced a greater than 300 seconds response). In the thrombin time assay at 5 U/ml thrombin, the clotting times with DFT ranged from 36.2 – 39.2 secs, whereas heparin produced a greater than 300 sec response in this assay.

The HIT antibody mediated platelet aggregation responses with heparin and DFT were studied at 10ug/ml. The results are shown in Table 5.3.5. At this concentration the batches of DFT produced comparable aggregation responses to the saline control in the range of 9 – 16 % aggregation while heparin supplementation resulted in a response of 63 %.

**Table 5.3.5 Comparative Screening of Defibrotide and Heparin on Heparin - PF4 Antibody Mediated Platelets Aggregation**

| Sample | % Aggregation |
|---|---|
| **P6231** | 16 ± 3 |
| **P6232** | 13 ± 3 |
| **P6233** | 9 ± 4 |
| **G9850** | 63 ± 9 |
| **Saline** | 9 ± 3 |

### 5.3.4. Overall discussion and Conclusions

Defibrotide is a mixture of single and double stranded phosphodiester oligonucleotides derived from porcine intestinal DNA depolymerization that is widely used for VOD treatment. Moreover, within this mixture of oligonucleotides, two aptamers (GGTTGGATTGGTTGG and GGTT-GGATCGGTTGG) that were able to inhibit thrombin were discovered[207]. Defibrotide also has been shown to exhibit antithrombotic activity that compares favorably to heparin[174,182]. Heparin is the most widely used antithrombotic and anticoagulant drug worldwide, but its use is associated with several side effects; in particular, HIT is a prothrombotic adverse reaction due to the interaction of heparin with a chemokine protein called PF4, leading to devastating clinical effects[187]. The use of alternative antithrombotic drugs is vital for preventing further complications in HIT patients, and in

this context DFT has raised interest in the last years, but unfortunately there is still a lack of knowledge about its implication in HIT management. Thus, in the present work we characterize the interaction of DFT with PF4 to assess the potential to use DFT as a substitute therapy to treat HIT patients.

It is well-known that the interaction heparin/PF4 is a result of nonspecific electrostatic forces, mainly due to the presence of sulphated groups[156]. In addition, the polysaccharide chain length plays an important role in the complex formation. It has been shown that with greater chain length, and higher molecular weight, there is a greater interaction with PF4[125]. Because of the lack of knowledge in the characterization of structure and molecular weight distribution of DFT, we first evaluated both the parameters of three different DFT API batches (P6231, P6232 and P6233) by NMR spectroscopy and by HP-SEC. In particular, an in-depth characterization of P6231 structure was performed by proton, carbon and phosphorus NMR analysis, and by $^{1}H/^{13}C$-HSQC study, obtaining spectra according to DNA profiles already reported in literature[195].

HP-SEC coupled with TDA is a technique that combines light scattering (LS), viscometer and refractive index (RI) detectors, and can be applicable to natural molecules, such as proteins or polysaccharides, and synthetic polymers[95]. The major advantage of using this method is that no column calibration is needed, and the molecular size can be related to the secondary structure of a polymer, either in terms of chain stiffness or conformation[78]. After the experimental calculation of the correct dn/dc parameter (0.147), we analysed the three different DFT batches and demonstrated that these samples are considerably similar in terms of their molecular weight distributions. Equating the Mw distribution results of the three DFT with G9850, the UFH was more monodisperse and exhibited a lower Mw in comparison to the average values of the three DFT. Despite these observations, the Rh values were quite similar. These results can be attributed to the different structural conformations: heparin in solution maintains a linear structure due to the repulsive action of the negative charges, while we can propose that DFT, despite the presence of phosphate groups, could tend to fold on itself in solution (data not supported by literature).

PCS and Zp evaluation techniques are very sensitive methods usually employed to analyze particle size and electric potential difference between the dispersion medium and the stationary layer of fluid attached to the dispersed particles respectively. The suitability of these methods for testing polysaccharide/PF4 interactions has been demonstrated[156]. To evaluate DFT/PF4 complex

formation, a titration of the protein with increasing concentrations of the polymer was performed. The main information resulting from PCS and Zp techniques is the evaluation of the PF4/DFT Ratio (PDR) for which the maximal aggregation is obtained; for PCS analysis, this value is experimentally obtained, while for Zp technique, the value is mathematically extrapolated as the PDR at which Zp is zero. The three DFT samples gave analogous titration curves with both the methods, a result consistent with their similar molecular weight distributions. It is known that the interaction with PF4 is purely electrostatic and non-specific for heparin, and that the interaction is greater as the molecular weight and chain length of heparin increases. When similar Mw samples are analysed, similar interaction results are obtained. We expect that complex formation with DFT is also regulated by these forces. Comparing the PDR of maximal aggregation evaluated by PCS (6.4) to the G9850 UFH sample PHR value obtained from a titration curve performed in the same conditions (9.0), a lesser interaction with PF4 was shown, taking into account the higher average DFT Mw, and the same result is obtained by Zp technique, where a lower PDR (about 11) was obtained compared to the UFH's PHR (13). Furthermore, the DFT PDR resulting in maximum aggregation is closer to that of lower molecular weight heparin than the UFH characterized in this work, as showed previously[156], a further confirmation of the lesser interaction with PF4.

For better understand the differences in the anticoagulant and antithrombotic activities of DFT and heparin, we decided to perform PT, aPTT and TT assays. Although DFT is a polyelectrolyte comparable to heparin in molecular weight, its composition differs from heparin. DFT itself did not produced any sizeable effects on coagulation profile of normal plasma as measured by PT, aPTT and TT assays at concentrations of up to 100 ug/ml. However, heparin produced strong anticoagulant effect in aPTT and TT assay at 10 ug/ml. Therefore, in comparison to heparin, DFT is almost a non-anticoagulant agent. In the HIT antibody mediated platelet aggregation assay, DFT did not produce any positive responses at 10 ug/ml, whereas heparin produced a marked aggregation of platelet suggesting strong interaction with HIT antibody. Consequently, DFT is devoid of any positive interactions with HIT antibody in this functional assay and these results are confirmed by ITC analysis, where the analysis of P6231 showed no binding with PF4.

As mentioned above, by ITC measurement the DFT sample analyzed did not bind the protein; on the other hand, as shown by PCS and Zp techniques, DFT can form complexes with PF4 with size very similar to the G9850 one, but needing higher molar concentrations for reaching the maximum of

aggregation, compared to the same heparin. ITC provides thermodynamics of a ligand-protein interaction by measuring the heat released during the complex formation, while the PCS and Zp are techniques that evaluate physical properties of a complex; a reason for not seeing any binding between P6231 and PF4 with ITC could be that the heat released during the titration was under the technique sensitivity threshold, so a very slight interaction between the polymer and the protein exist, but it's very low, and this consideration is on line with PCS and Zp results, which clearly show that a DFT/PF4 complex can be formed.

In the context of finding alternatives for HIT management, in the present work we characterized the interaction between three API DFT samples and the chemokine PF4, by PCS, Surface Charge evaluation and ITC measurements. Results show a low interaction between the polymer and the protein, in particular if compared to a porcine UFH.

# 6. References


1. Gandhi, N. S. & Mancera, R. L. The Structure of Glycosaminoglycans and their Interactions with Proteins. *Chem. Biol. Drug Des.* **72**, 455–482 (2008).
2. McLean, J. The Thromboplastic Action Of Cephalin. *Am. J. Physiol. Content* **41**, 250–257 (1916).
3. Turnbull, J. E. & Gallagher, J. T. Distribution of iduronate 2-sulphate residues in heparan sulphate. Evidence for an ordered polymeric structure. *Biochem. J.* **273**, 553–559 (1991).
4. Carlsson, P. & Kjellen, L. Heparin Biosynthesis. in *Heparin – a century of progress* (eds. Lever, R. & Mulloy, B.) 23–41 (2011).
5. Guerrini, M., Mourier, P. A. J., Torri, G. & Viskov, C. Antithrombin-binding oligosaccharides: structural diversities in a unique function? *Glycoconj. J.* **31**, 409–416 (2014).
6. Huntington, J. A. Mechanisms of glycosaminoglycan activation of the serpins in hemostasis. *J. Thromb. Haemost.* **1**, 1535–1549 (2003).
7. Huntington, J. A., Read, R. J. & Carrell, R. W. Structure of a serpin–protease complex shows inhibition by deformation. *Nature* **407**, 923–926 (2000).
8. Iacomini, M. *et al.* 'Linkage region' sequences of heparins and heparan sulfates: Detection and quantification by nuclear magnetic resonance spectroscopy. *Anal. Biochem.* **274**, 50–58 (1999).
9. Mourier, P., Anger, P., Martinez, C., Herman, F. & Viskov, C. Quantitative compositional analysis of heparin using exhaustive heparinase digestion and strong anion exchange chromatography. *Anal. Chem. Res.* **3**, 46–53 (2015).
10. Kellenbach, E., Sanders, K., Michiels, P. J. A. & Girard, F. C. 1H NMR signal at 2.10 ppm in the spectrum of KMnO4-bleached heparin sodium: identification of the chemical origin using an NMR-only approach. *Anal. Bioanal. Chem.* **399**, 621–628 (2011).
11. Silbert, J. E. Glycosaminoglycan metabolism before molecular biology: reminiscences of our early work. *Glycoconj. J.* **27**, 201–209 (2009).
12. Linhardt, R.J.; Toida, T. Heparin Oligosaccharides: New Analogues Development and Applications. in *Carbohydrates in Drug Design* 277–341 (1997).
13. Oduah, E. I., Linhardt, R. J. & Sharfstein, S. T. Heparin: Past, present, and future.

*Pharmaceuticals* **9**, 1–12 (2016).

14. Lindhal, U., Feingold, D. & Roden, L. Biosynthesis of heparin. *Trends Biochem. Sci.* **11**, 221–225 (1986).
15. Götting, C., Kuhn, J. & Kleesiek, K. Human xylosyltransferases in health and disease. *Cell. Mol. Life Sci.* **64**, 1498–1517 (2007).
16. Bai, X. *et al.* Biosynthesis of the Linkage Region of Glycosaminoglycans. *J. Biol. Chem.* **276**, 48189–48195 (2001).
17. Pinhal, M. A. *et al.* Enzyme interactions in heparan sulfate biosynthesis: uronosyl 5-epimerase and 2-O-sulfotransferase interact in vivo. *Proc. Natl. Acad. Sci. U. S. A.* **98**, 12984–9 (2001).
18. Barrowcliffe, T. W. Heparin - A Century of Progress. **207**, 3–22 (2012).
19. Casu, B., Naggi, A. & Torri, G. Re-visiting the structure of heparin. *Carbohydr. Res.* **403**, 60–68 (2015).
20. Schonberger, L. B. New variant Creutzfeldt-Jakob disease and bovine spongiform encephalopathy. *Infect. Dis. Clin. North Am.* **12**, 111–121 (1998).
21. Keire, D. *et al.* Diversifying the Global Heparin Supply Chain: Reintroduction of Bovine Heparin in the United States? *Pharm. Technol.* **39**, (2015).
22. Casu, B. *et al.* Characterization of Sulfation Patterns of Beef and Pig Mucosal Heparins by Nuclear Magnetic Resonance Spectroscopy. *Arzneimittel- Forsch.* **46**, 472–477 (1996).
23. Fu, L. *et al.* Structural Characterization of Pharmaceutical Heparins Prepared from Different Animal Tissues. *J. Pharm. Sci.* **102**, 1447–1457 (2013).
24. Naggi, A. *et al.* Structural peculiarity and antithrombin binding region profile of mucosal bovine and porcine heparins. *J. Pharm. Biomed. Anal.* **118**, 52–63 (2016).
25. Guerrini, M. *et al.* An unusual antithrombin-binding heparin octasaccharide with an additional 3-O-sulfated glucosamine in the active pentasaccharide sequence. *Biochem. J.* **449**, 343–351 (2013).
26. Guerrini, M. *et al.* Conformational transitions induced in heparin octasaccharides by binding with antithrombin III. *Biochem. J.* **399**, 191–198 (2006).
27. Viskov, C. *et al.* Heparin Dodecasaccharide Containing Two Antithrombin-binding Pentasaccharides. *J. Biol. Chem.* **288**, 25895–25907 (2013).
28. Gray, E., Hogwood, J. & Mulloy, B. The Anticoagulant and Antithrombotic Mechanisms of

Heparin. in *Heparin - A Century of Progress* (eds. Lever, R. & Mulloy, B.) 43–61 (2011).

29. Gettins, P. G. W. Serpin structure, mechanism, and function. *Chem. Rev.* **102**, 4751–4804 (2002).
30. Huntington, J. A. Shape-shifting serpins – advantages of a mobile mechanism. *Trends Biochem. Sci.* **31**, 427–435 (2006).
31. Irving, J. A. *et al.* Evidence That Serpin Architecture Intrinsically Supports Papain-like Cysteine Protease Inhibition: Engineering α1-Antitrypsin To Inhibit Cathepsin Proteases†. *Biochemistry* **41**, 4998–5004 (2002).
32. Craig, P. A., Olson, S. T. & Shore, J. D. Transient kinetics of heparin-catalyzed protease inactivation by antithrombin III. Characterization of assembly, product formation, and heparin dissociation steps in the factor Xa reaction. *J. Biol. Chem.* **264**, 5452–5461 (1989).
33. Gettins, P. G. W. & Olson, S. T. Exosite Determinants of Serpin Specificity. *J. Biol. Chem.* **284**, 20441–20445 (2009).
34. Johnson, D. J. D., Langdown, J. & Huntington, J. A. Molecular basis of factor IXa recognition by heparin-activated antithrombin revealed by a 1.7-A structure of the ternary complex. *Proc. Natl. Acad. Sci.* **107**, 645–650 (2010).
35. Yang, L., Sun, M., Gailani, D. & Rezaie, A. R. Characterization of a Heparin-Binding Site on the Catalytic Domain of Factor XIa: Mechanism of Heparin Acceleration of Factor XIa Inhibition by the Serpins Antithrombin and C1-Inhibitor †. *Biochemistry* **48**, 1517–1524 (2009).
36. Briginshaw, G. F. & Shanberge, J. N. Identification of two distinct heparin cofactors in human plasma: II. Inhibition of thrombin and activated factor X. *Thromb. Res.* **4**, 463–477 (1974).
37. Parker, K. A. & Tollefsen, D. M. The protease specificity of heparin cofactor II. Inhibition of thrombin generated during coagulation. *J. Biol. Chem.* **260**, 3501–5 (1985).
38. Griffith, M. J. Heparin-catalyzed inhibitor/protease reactions: kinetic evidence for a common mechanism of action of heparin. *Proc. Natl. Acad. Sci.* **80**, 5460–5464 (1983).
39. Mosnier, L. O., Zlokovic, B. V. & Griffin, J. H. The cytoprotective protein C pathway. *Blood* **109**, 3161–3172 (2007).
40. Nicolaes, G. A. F. *et al.* Altered inactivation pathway of factor Va by activated protein C in the presence of heparin. *Eur. J. Biochem.* **271**, 2724–2736 (2004).
41. Holroyd, E. W. & Simari, R. D. Interdependent biological systems, multi-functional molecules:

The evolving role of tissue factor pathway inhibitor beyond anti-coagulation. *Thromb. Res.* **125**, S57–S59 (2010).

42. Xu, X. *et al.* Effect of heparin chain length on the interaction with tissue factor pathway inhibitor (TFPI). *Int. J. Biol. Macromol.* **30**, 151–60 (2002).
43. Gray, E., Mulloy, B. & Barrowcliffe, T. W. Heparin and low-molecular-weight heparin. *Thromb. Haemost.* **99**, 807–818 (2008).
44. Fareed, J. *et al.* Differentiation of Low-Molecular-Weight Heparins: Impact on the Future of the Management of Thrombosis. *Semin. Thromb. Hemost.* **30**, 89–104 (2004).
45. Guerrini, M. & Bisio, A. Low-Molecular-Weight Heparins: Differential Characterization/Physical Characterization. in *Heparin - A Century of Progress* **207**, 128–157 (2012).
46. Uzan, A. Sulfated polysaccharides obtained from heparin, preparation process, pharmaceutical composition and use thereof. (1995).
47. Langer, R., Linhardt, R., Cooney, L. & Al, E. Heparinase derived anticoagulants. US Patent #4396762. (1983).
48. Lorneau, J.-C., Petitou, M. & Choay, J. Method for obtaining biologically active mucopolysaccharides of high purity, by controlled depolymerization of heparin. US Patent #5019649.
49. Fussi, F. Process for obtaining low molecular weight heparins. European Patent GB2, 002, 406B. (1982).
50. De-Ambrosi, L., Recchia, W. & Ferrari, G. Process for the controlled preparation of low molecular weight glycosaminoglycans. US Patent #4987222. (1991).
51. Bisio, A. *et al.* Controlled γ-ray irradiation of heparin generates oligosaccharides enriched in highly sulfated sequences. *Carbohydr. Polym.* **55**, 101–112 (2004).
52. Linhardt, R. J. & Gunay, N. S. *Production and chemical processing of low molecular weight heparins. Seminars in Thrombosis and Hemostasis* **25**, 5–16 (1999).
53. Vismara, E. *et al.* Structural Modification Induced in Heparin by a Fenton-Type Depolymerization Process. *Semin. Thromb. Hemost.* **33**, 466–477 (2007).
54. Bianchini, P., Liverani, L., Spelta, F., Mascellani, G. & Parma, B. Variability of Heparins and Heterogeneity of Low Molecular Weight Heparins. *Semin. Thromb. Hemost.* **33**, 496–502 (2007).

55. Mousa, S. A. Heparin and Low Molecular Weight Heparin in Thrombosis and Inflammation: Emerging Links. in *Chemistry and Biology of Heparin and Heparan Sulfate* 571–581 (Elsevier Science, 2005).
56. Emanuele, R. M. & Fareed, J. The effect of molecular weight on the bioavailability of heparin. *Thromb. Res.* **48**, 591–596 (1987).
57. Brieger, D. & Dawes, J. Production Method Affects the Pharmacokinetic and Ex Vivo Biological Properties of Low Molecular Weight Heparins. *Thromb. Haemost.* **77**, 317–322 (1997).
58. Mousa, S. & Mohamed, S. Inhibition of endothelial cell tube formation by the low molecular weight heparin, tinzaparin, is mediated by tissue factor pathway inhibitor. *Thromb. Haemost.* **92**, 627–633 (2004).
59. Mousa, S. & Kaiser, B. Tissue factor pathway inhibitor in thrombosis and beyond: role of heparin. *Drugs Future* **29**, 751–766 (2004).
60. Boneu, B. *et al.* Pharmacokinetic Studies of Standard Unfractionated Heparin, and Low Molecular Weight Heparins in the Rabbit. *Semin. Thromb. Hemost.* **14**, 18–27 (1988).
61. Sutor, A., Massicotte, P., Leaker, M. & Andrew, M. Heparin Therapy in Pediatric Patients. *Semin. Thromb. Hemost.* **23**, 303–319 (1997).
62. Alban, S. Adverse Effects of Heparin. in *Heparin - A Century of Progress* **207**, 211–263 (2012).
63. Alban, S. Natural and synthetic glycosaminoglycans Molecular characteristics as the basis of distinct drug profiles. *Hamostaseologie* **28**, 51–61 (2008).
64. Mulloy, B. The specificity of interactions between proteins and sulfated polysaccharides. *An. Acad. Bras. Cienc.* **77**, 651–664 (2005).
65. Hirsh, J. & Raschke, R. Heparin and Low-Molecular-Weight Heparin: The Seventh ACCP Conference on Antithrombotic and Thrombolytic Therapy. *Chest* **126**, 188S-203S (2004).
66. Eikelboom, J. Nonbleeding complications of unfractionated and low-molecular weight heparins. *Clin. Adv. Hematol. Oncol.* **5**, 871–873 (2007).
67. Warkentin, T. E. & Greinacher, A. Heparin-Induced Thrombocytopenia: Recognition, Treatment, and Prevention: The Seventh ACCP Conference on Antithrombotic and Thrombolytic Therapy. *Chest* **126**, 311S-337S (2004).
68. Christiansen, C. Osteoporosis: diagnosis and management today and tomorrow. *Bone* **17**, 513S-516S (1995).

69. Le Templier, G. & Rodger, M. A. Heparin-induced osteoporosis and pregnancy. *Curr. Opin. Pulm. Med.* **14**, 403–407 (2008).
70. Schindewolf, M. *et al.* Low Allergenic Potential With Fondaparinux: Results of a Prospective Investigation. *Mayo Clin. Proc.* **85**, 913–919 (2010).
71. Hirsh, J. *et al.* Heparin and low-molecular-weight heparin: mechanisms of action, pharmacokinetics, dosing considerations, monitoring, efficacy, and safety. *Chest* **114**, 489S-510S (1998).
72. Gottschalk, A. *Glycoproteins: their composition,structure and function*. (1972).
73. Mitchell, J. *Applied polymer analysis and characterization. Recent developments in techniques, instrumentation, problem solving*. (1987).
74. Harding, S. E., Varum, K. M., Stokke, B. T. & Smidsrod, O. Molecular weight determination of polysaccharides. in *Advances In Carbohydrate Analysis* 63–144 (1991).
75. Lecacheux, D., Mustiere, Y., Panaras, R. & Brigand, G. Molecular weight of scleroglucan and other extracellular microbial polysaccharides by size-exclusion chromatography and low angle laser light scattering. *Carbohydr. Polym.* **6**, 477–492 (1986).
76. Malvern Instruments. Principles of Triple Detection GPC / SEC. 1–19 (2015).
77. Held, D. Tips & Tricks GPC/SEC: UV-vis Detection. *The Column* **14**, 22–26 (2018).
78. Bertini, S., Bisio, A., Torri, G., Bensi, D. & Terbojevich, M. Molecular weight determination of heparin and dermatan sulfate by size exclusion chromatography with a triple detector array. *Biomacromolecules* **6**, 168–173 (2005).
79. Strutt, J. W. XV. On the light from the sky, its polarization and colour. *London, Edinburgh, Dublin Philos. Mag. J. Sci.* **41**, 107–120 (1871).
80. Haney, M. A new differential viscometer. *Am. Lab.* **17**, 116–126 (1985).
81. Striegel, A. M. *Modern size-exclusion liquid chromatography : practice of gel permeation and gel filtration chromatography*. (Wiley, 2009).
82. Grubisic, Z., Rempp, P. & Benoit, H. A universal calibration for gel permeation chromatography. *J. Polym. Sci. Part B Polym. Lett.* **5**, 753–759 (1967).
83. Yau, W. W., Ginnard, C. R. & Kirkland, J. J. Broad-range linear calibration in high-performance size-exclusion chromatography using column packings with bimodal pores. *J. Chromatogr. A* **149**, 465–487 (1978).

84. Mauri, L. *et al.* Combining NMR Spectroscopy and Chemometrics to Monitor Structural Features of Crude Heparin. *Molecules* **22**, (2017).

85. Alf Keire, D. *et al.* Bovine Mucosal Heparins Are Comparable to Porcine Mucosal Heparin at USP Potency Adjusted Levels. *Front. Med.* **1**, 360 (2019).

86. Guerrini, M. *et al.* Oversulfated chondroitin sulfate is a contaminant in heparin associated with adverse clinical events. *Nat. Biotechnol.* **26**, 669–75 (2008).

87. Santos, G. R. C. *et al.* Structural and functional analyses of bovine and porcine intestinal heparins confirm they are different drugs. *Drug Discov. Today* **19**, 1801–1807 (2014).

88. Tovar, A. M. F. *et al.* Structural and haemostatic features of pharmaceutical heparins from different animal sources: challenges to define thresholds separating distinct drugs. *Sci. Rep.* **6**, 35619 (2016).

89. St Ange, K. *et al.* Analysis of Heparins Derived From Bovine Tissues and Comparison to Porcine Intestinal Heparins. *Clin. Appl. Thromb.* **22**, 520–527 (2016).

90. Bianchini, P., Liverani, L., Mascellani, G. & Parma, B. Heterogeneity of Unfractionated Heparins Studied in Connection with Species, Source, and Production Processes. *Semin. Thromb. Hemost.* **23**, 3–10 (1997).

91. Fu, L. *et al.* Enzymatic Generation of Highly Anticoagulant Bovine Intestinal Heparin. *J. Med. Chem.* **60**, 8673–8679 (2017).

92. Mulloy, B. Structure and Physicochemical Characterisation of Heparin. in *Heparin - A Century of Progress* (eds. Lever, R. & Mulloy, B.) **207**, 77–98 (2012).

93. Mulloy, B. *et al.* USP compendial methods for analysis of heparin: chromatographic determination of molecular weight distributions for heparin sodium. *Anal. Bioanal. Chem.* **406**, 4815–4823 (2014).

94. United States Pharmacopeial Convention. USP Heparin Sodium. in *USP Official Monographs USP40-NF35* 4475–4480 (2017).

95. Bertini, S. *et al.* Molecular Weights of Bovine and Porcine Heparin Samples: Comparison of Chromatographic Methods and Results of a Collaborative Survey. *Molecules* **22**, 1214 (2017).

96. Das, T. & Nema, S. Protein particulate issues in biologics development Biotherapeutic Formulation and Stability View project Cytochrome Oxidase structure and function View project Tapan K Das Bristol-Myers Squibb. *Am. Pharm. Rev.* **11**, 52–57 (2007).

97. Štulík, K., Pacáková, V. & Tichá, M. Some potentialities and drawbacks of contemporary size-exclusion chromatography. *J. Biochem. Biophys. Methods* **56**, 1–13 (2003).

98. Mulloy, B., Gray, E. & Barrowcliffe, T. W. Characterization of unfractionated heparin: comparison of materials from the last 50 years. *Thromb. Haemost.* **84**, 1052–6 (2000).

99. Bianchini, P. Method for preparing glucoronyl-glucosamino-glycan sulphates exhibiting antilipasaemic activity. (1974).

100. Casu, B. *et al.* Correlation between structure, fat-clearing and anticoagulant properties of heparins and heparan sulphates. *Arzneimittelforschung.* **33**, 135–142 (1983).

101. Callas, D. D. *et al.* Comparative pharmacologic profile of a glycosaminoglycan mixture, Sulodexide, and a chemically modified heparin derivative, Suleparoide. *Semin. Thromb. Hemost.* **19**, 49–57 (1993).

102. Coccheri, S. & Mannello, F. Development and use of sulodexide in vascular diseases: implications for treatment. *Drug Des. Devel. Ther.* **8**, 49–65 (2014).

103. Silvestro, L. *et al.* Human Pharmacokinetics of Glycosaminoglycans Using Deuterium-Labeled and Unlabeled Substances: Evidence for Oral Absorption. *Semin. Thromb. Hemost.* **20**, 281–292 (1994).

104. Harenberg, J. Review of pharmacodynamics, pharmacokinetics, and therapeutic properties of sulodexide. *Med. Res. Rev.* **18**, 1–20 (1998).

105. Trowbridge, J. M. & Gallo, R. L. Dermatan sulfate: new functions from an old glycosaminoglycan. *Glycobiology* **12**, 117R-125R (2002).

106. Iacoviello, L. *et al.* Antithrombotic activity of dermatan sulphates, heparins and their combination in an animal model of arterial thrombosis. *Thromb. Haemost.* 1102–1107 (1996).

107. Di Carlo, V. *et al.* Dermatan sulphate for the prevention of postoperative venous thromboembolism in patients with cancer. DOS (Dermatan sulphate in Oncologic Surgery) Study Group. *Thromb. Haemost.* **82**, 30–34 (1999).

108. Mannello, F. & Raffetto, J. D. Matrix metalloproteinase activity and glycosaminoglycans in chronic venous disease: the linkage among cell biology, pathology and translational research. *Am. J. Transl. Res.* **3**, 149–158 (2011).

109. Mattana, P., Mannello, F., Ferrari, P. & Agus, G. Vascular pathologies and inflammation: The anti-inflammatory properties of sulodexide | Request PDF. *Ital. J. Vasc. Endovasc. Surg.* **19**,

1–7 (2012).

110. Plichta, J. K. & Radek, K. A. Sugar-Coating Wound Repair. *J. Burn Care Res.* **33**, 299–310 (2012).
111. Cosmi, B. *et al.* Additive thrombin inhibition by fast moving heparin and dermatan sulfate explains the anticoagulant effect of sulodexide, a natural mixture of glycosaminoglycans. *Thromb. Res.* **109**, 333–339 (2003).
112. Andriuoli, G., Mastacchi, R. & Barbanti, M. Antithrombotic activity of a glycosaminoglycan (sulodexide) in rats. *Thromb. Res.* **34**, 81–86 (1984).
113. Broekhuizen, L. N. *et al.* Effect of sulodexide on endothelial glycocalyx and vascular permeability in patients with type 2 diabetes mellitus. *Diabetologia* **53**, 2646–2655 (2010).
114. Radhakrishnamurthy, B. *et al.* Studies of chemical and biologic properties of a fraction of sulodexide, a heparin-like glycosaminoglycan. *Atherosclerosis* **60**, 141–149 (1986).
115. Veraldi, N. *et al.* Fine structural characterization of sulodexide. *J. Pharm. Biomed. Anal.* **156**, 67–79 (2018).
116. Tackx, P. & Bosscher, F. Systematic Deviations due to Random Noise Levels in Size Exclusion Chromatography Coupled With Multi Angle Laser Light Scattering. *Anal. Commun.* **34**, 295–297 (1997).
117. Capila, I. & Linhardt, R. J. Heparin-protein interactions. *Angew. Chem. Int. Ed. Engl.* **41**, 391–412 (2002).
118. Luster, A. D. Chemokines — Chemotactic Cytokines That Mediate Inflammation. *N. Engl. J. Med.* **338**, 436–445 (1998).
119. Wells, T. N., Power, C. A. & Proudfoot, A. E. Definition, function and pathophysiological significance of chemokine receptors. *Trends Pharmacol. Sci.* **19**, 376–380 (1998).
120. Belperio, J. A. *et al.* CXC chemokines in angiogenesis. *J. Leukoc. Biol.* **68**, 1–8 (2000).
121. Witt, D. P. & Lander, A. D. Differential binding of chemokines to glycosaminoglycan subpopulations. *Curr. Biol.* **4**, 394–400 (1994).
122. Middleton, J. *et al.* Transcytosis and surface presentation of IL-8 by venular endothelial cells. *Cell* **91**, 385–395 (1997).
123. Hoogewerf, A. J. *et al.* Glycosaminoglycans Mediate Cell Surface Oligomerization of Chemokines. *Biochemistry* **14**, 13570–13578 (1997).
124. Wang, Z. & Huang, H. Platelet factor-4 (CXCL4/PF-4): An angiostatic chemokine for cancer

therapy. *Cancer Lett.* **331**, 147–153 (2013).

125. Marshall, S. E., Luscombe, M., Pepper, D. S. & Holbrook, J. J. The interaction of platelet factor 4 with heparins of different chain length. *Biochim. Biophys. Acta - Gen. Subj.* **797**, 34–39 (1984).
126. Ibel, K. *et al.* Low-resolution structure of the complex of human blood platelet factor 4 with heparin determined by small-angle neutron scattering. *Biochim. Biophys. Acta - Protein Struct. Mol. Enzymol.* **870**, 58–63 (1986).
127. Zhang, X., Chen, L., Bancrofts, D. P., Lai, C. K. & Maione, T. E. Crystal Structure of Recombinant Human Platelet Factor 4. *Biochemistry* **33**, 8361–8366 (1994).
128. Cai, Z. *et al.* Atomic description of the immune complex involved in heparin-induced thrombocytopenia. *Nat. Commun.* **22**, 8277 (2015).
129. Mayo, K. H. *et al.* NMR solution structure of the 32-kDa platelet factor 4 ELR-motif N-terminal chimera: a symmetric tetramer. *Biochemistry* **34**, 11399–11409 (1995).
130. Mayo, K. H. *et al. Heparin binding to platelet factor-4 An NMR and site-directed mutagenesis study: arginine residues are crucial for binding*. *Biochem. J* **312**, (1995).
131. Ziporen, L. *et al.* Defining an antigenic epitope on platelet factor 4 associated with heparin-induced thrombocytopenia. *Blood* **92**, 3250–3259 (1998).
132. Li, Z. Q. *et al.* Defining a second epitope for heparin-induced thrombocytopenia/thrombosis antibodies using KKO, a murine HIT-like monoclonal antibody. *Blood* **99**, 1230–1236 (2002).
133. Bock, P. E., Luscombe, M., Marshall, S. E., Pepper, D. S. & Holbrook, J. J. The multiple complexes formed by the interaction of platelet factor 4 with heparin. *Biochem. J.* **191**, 769–776 (1980).
134. Rauova, L. *et al.* Ultralarge complexes of PF4 and heparin are central to the pathogenesis of heparin-induced thrombocytopenia. *Blood* **105**, 131–138 (2005).
135. Greinacher, A. *et al.* Close Approximation of Two Platelet Factor 4 Tetramers by Charge Neutralization Forms the Antigens Recognized by HIT Antibodies. *Arterioscler. Thromb. Vasc. Biol.* **26**, 2386–2393 (2006).
136. Suvarna, S. *et al.* Determinants of PF4/heparin immunogenicity. *Blood* **110**, 4253–4260 (2007).
137. Warkentin, T. E. *et al.* Heparin-Induced Thrombocytopenia in Patients Treated with Low-

Molecular-Weight Heparin or Unfractionated Heparin. *N. Engl. J. Med.* **332**, 1330–1336 (1995).

138. Smythe, M. A., Koerber, J. M. & Mattson, J. C. The Incidence of Recognized Heparin-Induced Thrombocytopenia in a Large, Tertiary Care Teaching Hospital. *Chest* **131**, 1644–1649 (2007).
139. Ahmed, I., Majeed, A. & Powell, R. Heparin induced thrombocytopenia: diagnosis and management update. *Postgrad. Med. J.* **83**, 575–582 (2007).
140. Brieger, D. B., Mak, K.-H., Kottke-Marchant, K. & Topol, E. J. Heparin-Induced Thrombocytopenia. *J. Am. Coll. Cardiol.* **31**, 1449–1459 (1998).
141. Alban, S., Krauel, K. & Greinacher, A. The Role of Sulfated Polysaccharides in the Pathogenesis of Heparin-Induced Thrombocytopenia. in *Heparin-Induced Thrombocytopenia* (eds. Warkentin, T. E. & Greinacher, A.) 181–208 (CRC Press, 2012).
142. Mikhailov, D., Young, H. C., Linhardt, R. J. & Mayo, K. H. Heparin Dodecasaccharide Binding to Platelet Factor-4 and Growth-related Protein-α. *J. Biol. Chem.* **274**, 25317–25329 (2002).
143. Brandt, S. *et al.* Characterisation of the conformational changes in platelet factor 4 induced by polyanions: towards in vitro prediction of antigenicity. *Thromb. Haemost.* **112**, 53–64 (2014).
144. Cohen, M. Heparin-induced thrombocytopenia and the clinical use of low molecular weight heparins in acute coronary syndromes. *Semin. Hematol.* **36**, 33–6 (1999).
145. Krauel, K., Hackbarth, C., Fü Rll, B. & Greinacher, A. Heparin-induced thrombocytopenia: in vitro studies on the interaction of dabigatran, rivaroxaban, and low-sulfated heparin, with platelet factor 4 and anti-PF4/heparin antibodies. *Blood* **119**, 1248–1255 (2012).
146. Warkentin, T. E. & Kelton, J. G. Interaction of heparin with platelets, including heparin-induced thrombocytopenia. in *Low-molecular-weight heparins in phrophylaxis and therapy of thromboembolic diseases* (ed. Bounameaux, H.) 75–127 (1994).
147. Prechel, M., Ph, D. & Walenga, J. M. The Laboratory Diagnosis and Clinical Management of Patients with Heparin-Induced Thrombocytopenia: An Update. *Semin. Thromb. Hemost.* **34**, 86–96 (2008).
148. Delcea, M. & Greinacher, A. Biophysical tools to assess the interaction of PF4 with polyanions. *Thromb. Haemost.* **116**, 783–791 (2016).
149. Dutta, A. K., Rösgen, J. & Rajarathnam, K. Using isothermal titration calorimetry to determine

thermodynamic parameters of protein-glycosaminoglycan interactions. *Methods Mol. Biol.* **1229**, 315–324 (2015).

150. Malvern Instruments. Dynamic Light Scattering: An Introduction in 30 Minutes. *Tech. Note MRK656-01* 1–8 (2014).
151. Malvern Instruments. Zeta potential: An Introduction in 30 minutes. *Tech. Note. MRK654-01* **2**, 1–6 (2011).
152. Derjaguin, B. V., Churaev, N. V. & Muller, V. M. The Derjaguin—Landau—Verwey—Overbeek (DLVO) Theory of Stability of Lyophobic Colloids. in *Surface Forces* 293–310 (Springer US, 1987). doi:10.1007/978-1-4757-6639-4_8
153. Pierce, M. M., Raman, C. S. & Nall, B. T. Isothermal Titration Calorimetry of Protein–Protein Interactions. *Methods* **19**, 213–221 (1999).
154. *ImmunogenicityRelated Considerations for Low Molecular Weight Heparin*. (2016).
155. Food and Drugs Administration of America. Generic Enoxaparin Questions and Answers | FDA. Available at: https://www.fda.gov/drugs/postmarket-drug-safety-information-patients-and-providers/generic-enoxaparin-questions-and-answers. (Accessed: 13th September 2019)
156. Bertini, S. *et al.* Characterization of PF4-Heparin Complexes by Photon Correlation Spectroscopy and Zeta Potential. *Clin. Appl. Thromb.* 107602961668543 (2017).
157. Kreimann, M. *et al.* Binding of anti - Platelet factor 4/heparin antibodies depends on the thermodynamics of conformational changes in platelet factor 4. *Blood* **124**, 2442–2449 (2014).
158. Ronzoni Institute. *Validation of the analytical method for PF4/heparin complexes characterization*. (2019).
159. Greinacher, A., Alban, S., Omer-Adam, M. A., Weitschies, W. & Warkentin, T. E. Heparin-induced thrombocytopenia: A stoichiometry-based model to explain the differing immunogenicities of unfractionated heparin, low-molecular-weight heparin, and fondaparinux in different clinical settings. *Thromb. Res.* **122**, 211–220 (2008).
160. Nguyen, T. H. Single-molecule force spectroscopy applied to heparin-induced thrombocytopenia. *J. Mol. Recognit.* **30**, 1–11 (2017).
161. Watt, D. K., Yorke, S. C. & Slimb, G. C. Comparison of ovine , bovine and porcine mucosal

heparins and low molecular weight heparins by disaccharide analyses and 13C NMR. *Carbohydr. Polym.* **33**, 5–11 (1997).

162. Konkle, B. A. *et al.* Heparin-induced thrombocytopenia: bovine versus porcine heparin in cardiopulmonary bypass surgery. *Ann. Thorac. Surg.* **71**, 1920–1924 (2001).
163. Francis, J. L., Palmer, G. J., Moroose, R. & Drexler, A. Comparison of bovine and porcine heparin in heparin antibody formation after cardiac surgery. *Ann. Thorac. Surg.* **75**, 17–22 (2003).
164. Lewis, B. E. *et al.* Argatroban anticoagulation during percutaneous coronary intervention in patients with heparin-induced thrombocytopenia. *Catheter. Cardiovasc. Interv.* **57**, 177–184 (2002).
165. Mahaffey, K. W. *et al.* The anticoagulant therapy with bivalirudin to assist in the performance of percutaneous coronary intervention in patients with heparin-induced thrombocytopenia (ATBAT) study: main results. *J. Invasive Cardiol.* **15**, 611–616 (2003).
166. Magnani, H. & Gallus, A. Heparin-induced thrombocytopenia (HIT). *Thromb. Haemost.* **95**, 967–981 (2006).
167. Cook, B. W. Anticoagulation management. *Semin. Intervent. Radiol.* **27**, 360–7 (2010).
168. Lauver, D. A., Booth, E. A., White, A. J., Poradosu, E. & Lucchesi, B. R. Sulodexide Attenuates Myocardial Ischemia/Reperfusion Injury and the Deposition of C-Reactive Protein in Areas of Infarction without Affecting Hemostasis. *J. Pharmacol. Exp. Ther.* **312**, 794–800 (2004).
169. Achour, A. *et al.* One year course of oral sulodexide in the management of diabetic nephropathy. *J. Nephrol.* **18**, 568–574 (2005).
170. Gambaro, G. *et al.* Treatment with a glycosaminoglycan formulation ameliorates experimental diabetic nephropathy. *Kidney Int.* **46**, 797–806 (1994).
171. Borawski, J., Zbroch, E., Rydzewska-Rosolowska, A., Pawlak, K. & Mysliwiec, M. Sulodexide for hemodialysis anticoagulation in heparin-induced thrombocytopenia type II. *J. Nephrol.* **20**, 370–372 (2007).
172. Adiguzel, C. *et al.* Comparative Anticoagulant and Platelet Modulatory Effects of Enoxaparin and Sulodexide. *Clin. Appl. Thromb.* **15**, 501–511 (2009).
173. Handin, R. & Cohen, H. Purification and binding properties of human platelet factor four. *J. Biol. Chem.* **251**, 4273–4282 (1976).

174. Corbacioglu, S. *et al.* Defibrotide for prophylaxis of hepatic veno-occlusive disease in paediatric haemopoietic stem-cell transplantation: an open-label, phase 3, randomised controlled trial. *Lancet* **379**, 1301–1309 (2012).
175. Coppell, J. A. *et al.* Hepatic veno-occlusive disease following stem cell transplantation: incidence, clinical course, and outcome. *Biol. Blood Marrow Transplant.* **16**, 157–68 (2010).
176. Fulgenzi, A. & Ferrero, M. E. Defibrotide in the treatment of hepatic veno-occlusive disease. *Hepatic Med. Evid. Res.* **8**, 105–113 (2016).
177. Richardson, P. G. *et al.* Defibrotide sodium for the treatment of hepatic veno-occlusive disease/sinusoidal obstruction syndrome. *Expert Rev. Clin. Pharmacol.* **11**, 113–124 (2018).
178. Hassan, Z. Optimal approach to prevent veno-occlusive disease following hematopoietic stem cell transplantation in children. *Pediatr. Transplant.* **14**, 683–687 (2010).
179. Zhang, L., Wang, Y. & Huang, H. Defibrotide for the prevention of hepatic veno-occlusive disease after hematopoietic stem cell transplantation: a systematic review. *Clin. Transplant.* **26**, 511–519 (2012).
180. Evangelista, V., Piccardoni, P., Gaetano, G. & Cerletti, C. Defibrotide Inhibits Platelet Activation by Cathepsin G Released From Stimulated Polymorphonuclear Leukocytes. *Thromb. Haemost.* **67**, 660–664 (1992).
181. Gatto, B. *et al.* Effective DNA inhibitors of cathepsin g by in vitro selection. *Int. J. Mol. Sci.* **9**, 1008–23 (2008).
182. Belcaro, G. Evolution of superficial vein thrombosis treated with defibrotide: comparison with low dose subcutaneous heparin. *Int. J. tissue React.* **12**, 319–324 (1990).
183. Zanasi, R., Fioretta, G., Ciocia, G. & Bergonzi, M. Prevention of Deep Venous Thrombosis in Orthopedic Surgey: Effects of Defibrotide. *Clin. Ther.* **10**, 350–357 (1988).
184. Buccianti, G. *et al.* Kinetics of anti-Xa activity during combined defibrotide-heparin administration in hemodialysis. *Int. J. Artif. Organs* **13**, 416–420 (1990).
185. Filimberti, E. *et al.* Hemodialysis with defibrotide: effects on coagulation parameters. *Int. J. Artif. Organs* **15**, 590–594 (1992).
186. Fathi, M. Heparin-induced thrombocytopenia (HIT): Identification and treatment pathways. *Glob. Cardiol. Sci. Pract.* **2018**, (2018).
187. Salter, B. S. *et al.* Heparin-Induced Thrombocytopenia: A Comprehensive Clinical Review. *J.*

*Am. Coll. Cardiol.* **67**, 2519–2532 (2016).

188. Chaudhary, R. K., Khanal, N., Giri, S., Pathak, R. & R. Bhatt, V. Emerging Therapy Options in Heparin-Induced Thrombocytopenia. *Cardiovasc. Hematol. Agents Med. Chem.* **12**, 50–59 (2014).
189. Ahmad, S. Heparin-induced thrombocytopenia: Impact of bovine versus porcine heparin in HIT pathogenesis. *Front. Biosci.* **12**, 3312–3320 (2007).
190. Fareed, J., Hoppensteadt, D. A., Iacobelli, M. & Walenga, J. M. Defibrotide Does Not Cross-React with HIT Antibodies. Implications in the Management of HIT. *Blood* **108**, 1054 (2006).
191. Pinto, A. *et al.* Recurrent venous thromboembolism complicated by heparin-induced thrombocytopenia as a first manifestation of an occult cancer: a case report. *Int. J. Immunopathol. Pharmacol.* **21**, 247–250 (2008).
192. Risi, G., Bertini, S., Naggi, A., Hoppensteadt, D. & Fareed, J. Physical-chemical characterization of Defibrotide and evaluation of its interaction with PF4 (Manuscript accepted). *Clin. Appl. Thromb.*
193. Cella, G. *et al.* Tissue Factor Pathway Inhibitor Release Induced by Defibrotide and Heparins. *Clin Appl Thromb Hemost* **7**, 225–228 (2001).
194. Tubaro, M. *et al. Defibrotide Versus Heparin in the Prevention of Coronary Reocclusion After Thrombolysis in Acute Myocardial Infarction*. *Cardiovascular Drugs and Therapy* **7**, (1993).
195. Kearns, D. R. NMR Studies of Conformational States and Dynamics of DNA. *CRC Crit. Rev. Biochem.* **15**, 237–290 (1984).
196. Bianchi, G., Mantovani, M., Prino, G., Salvetti, L. & Barone, D. Possible Agonistic Interaction of Defibrotide, A DNA Derivative, with Adenosine Receptors “In Vitro”. *Nucleosides and Nucleotides* **10**, 1149–1150 (1991).
197. Bilsel, S., Yalçin, A. S., Taga, Y. & Emerk, K. Interaction of 3H-defibrotide with cultured human umbilical vein endothelial cells. *Thromb. Res.* **58**, 455–460 (1990).
198. Lane, D. A., Denton, J., Flynn, A. M., Thunbergt, L. & Lindahlt, U. *Anticoagulant activities of heparin oligosaccharides and their neutralization by platelet factor 4*. *Biochem. J* **218**, (1984).
199. Horne, M. K. Heparin binding to normal and abnormal platelets. *Thromb. Res.* **51**, 135–144 (1988).
200. Horne, M. K. & Chad, E. S. The effect of molecular weight on heparin binding to platelets. *Br.*

*J. Haematol.* **74**, 306–312 (1990).

201. Horne, M. K. & Hutchison, K. J. Simultaneous binding of heparin and platelet factor-4 to platelets: further insights into the mechanism of heparin-induced thrombocytopenia. *Am. J. Hematol.* **58**, 24–30 (1998).
202. Walenga, J. M., Prechel, M., Jeske, W. P. & Bakhos, M. Unfractionated heparin compared with low-molecular-weight heparin as related to heparin-induced thrombocytopenia. *Curr. Opin. Pulm. Med.* **11**, 385–391 (2005).
203. Vuignier, K., Schappler, J., Veuthey, J.-L., Carrupt, P.-A. & Martel, S. Drug-protein binding: a critical review of analytical tools. *Anal Bioanal Chem* **398**, 53–66 (2010).
204. Perozzo, R., Folkers, G. & Scapozza, L. Thermodynamics of Protein-Ligand Interactions: History, Presence, and Future Aspects. *J. Recept. SIGNAL Transduct.* **24**, 1–52 (2004).
205. Barbosa, S., Taboada, P. & Mosquera, V. Analysis of the interactions between human serum albumin/amphiphilic penicillin in different aqueous media: an isothermal titration calorimetry and dynamic light scattering study. *Chem. Phys.* **310**, 51–58 (2005).
206. Bjelić, S. & Jelesarov, I. A survey of the year 2007 literature on applications of isothermal titration calorimetry. *J. Mol. Recognit.* **21**, 289–312 (2008).
207. Bracht, F. & Schror, K. Isolation and Identification of Aptamers from Defibrotide That Act as Thrombin Antagonists in Vitro. *Biochem. Biophys. Res. Commun.* **200**, 933–937 (1994).

# 7. Acknowledgments

I would like to thank the Prof. Giuseppe Zanoni for having accepted to be my PhD tutor and Dr. Annamaria Naggi for all the support during my thesis work. But most of all, a big thank goes to Dr. Sabrina Bertini, my mentor, simply for having believed in me during all these three years, and for having contributed in making me the researcher I am today.

Naturally, the second part of my acknowledgments goes to Andrea, to my parents and to my family, that were my biggest fans, and that has supported me, beared me and spurred me in doing always all my best.

A big big thank goes, then, to all the Ronzoni/CAT/Chemi group (oh yes, I'm extremely politically correct), awesome people with which I've spent almost five fantastic years, and that was really hard for me to leave.

Last but not least, all of my friends, first the "Fracitani" group, that after more than ten years and although the great physical distance has remained together and united, and second my theater group, the "G74", that has always brought cheerfulness and much fun in my life.